coatings

MDPI

*Review*

# Film Deposition of Electrochromic Metal Oxides through Spray Coating: A Descriptive Review

**Anthony Maho [1,*], Suraj Nayak [1], Florian Gillissen [2], Rudi Cloots [2] and Aline Rougier [1]**

[1] Univ. Bordeaux, CNRS, Bx INP, ICMCB, UMR 5026, F-33600 Pessac, France; suraj-surendra.nayak@u-bordeaux.fr (S.N.); aline.rougier@icmcb.cnrs.fr (A.R.)
[2] GREEnMat, CESAM Research Unit, Department of Chemistry, University of Liège, B-4000 Liège, Belgium; fgillissen@uliege.be (F.G.); rcloots@uliege.be (R.C.)
* Correspondence: anthony.maho@icmcb.cnrs.fr

**Abstract:** Electrochromism induces reversible changes of coloration in specific organic and inorganic materials through electrical charge/discharge reactions. When processed into thin films, electrochromic metal oxides can be integrated into glazing applications such as displays, rearview mirrors, goggles and, most notably, smart windows in energy-efficient buildings. Over the years, the use of spray coating as a liquid-based approach has been acknowledged for its cost-efficient, high-throughput samples production with a low volume consumption. It represents an interesting alternative to vacuum processes and to other wet methods, suitably responding to the current limitations of electrochromic thin films production by offering improved control over deposition parameters and capacities of up-scaling, together with lowered energetic and economic costs. The present review summarizes the main theoretical and practical aspects of spray coating, notably distinguishing room-temperature methodologies from pyrolysis-based, under heating protocols. The main families of functional electrochromic metal oxides are then screened and discussed, establishing how spray processing can challengingly lead to higher levels of optical contrast, commutation kinetics, coloration efficiency and cycling durability, and how low-toxic and environment-friendly precursors can be favored while sustaining large deposition areas.

**Keywords:** electrochromism; spray coating; thin films; metal oxides; nanomaterials; smart windows; energy



**Citation:** Maho, A.; Nayak, S.; Gillissen, F.; Cloots, R.; Rougier, A. Film Deposition of Electrochromic Metal Oxides through Spray Coating: A Descriptive Review. *Coatings* **2023**, *13*, 1879. https://doi.org/10.3390/coatings13111879

Academic Editor: Carlos José Macedo Tavares

Received: 24 September 2023
Revised: 27 October 2023
Accepted: 27 October 2023
Published: 1 November 2023



## 1. Electrochromism: Materials, Properties, and Fabrication Methods

Electrochromism consists in the capacity of a material to reversibly change its color aspect and, more generally, its optical characteristics (absorbance, transmittance, reflectance) from the application of an appropriate electric stimulus. Originally observed in the 19th century, it has been properly studied starting from the 1960–1970s, notably through the founding works of J. Platt [1] and S. Deb [2,3] on operating mechanisms and resulting optical behavior. Since then, it has developed into a booming technological field active in both fundamental research and practical applications, covering a.o. fenestration devices for energy-efficient buildings—so-called *smart windows* (conceptualized for the first time by C. Lampert [4] and C. Granqvist [5] in 1984–1985); displays, mirrors, and other glazing devices (goggles, helmets…); labels and stickers; energy storage devices including (super)capacitors and batteries; wearable electronics such as intelligent clothes, electronic skin, or paper; etc. [6–16].

Electrochromic (EC) materials are sorted into three constituting categories: *organics*, with viologens and conductive polymers based on polystyrenes (PEDOT:PSS), polyanilines (PANI), polythiophenes ($P_3HT$), or polypyrroles (PPy)…; *inorganics*, with metal oxides, nitrides and sulfides, polyoxymetalates, and carbon-based materials, such as carbon nanotubes (CNTs), graphene, carbon aerogel, and activated carbon…; and *others*, including

organometallics (metal coordination complexes, metal organic frameworks (MOFs), synthetic pigments such as Prussian blue…) [17–25]. Organic EC materials provide a broader range of colors with faster response times, while inorganic counterparts—especially metal oxides—are more easily processed and show higher mechanical, chemical, and thermal stability together with improved reversibility and durability. EC metal oxides are further divided into *anodic* and *cathodic* materials, depending on how they respond to electrical stimuli: oxides of tungsten ($WO_3$), molybdenum ($MoO_3$), niobium ($Nb_2O_5$), titanium ($TiO_2$), and bismuth ($Bi_2O_3$) are examples of cathodic electrochromic compounds, coloring upon the reduction of the metallic element *M* and ionic *X* (proton $H^+$ or alkali ion $Li^+$, $Na^+$, $K^+$, $Cs^+$…) insertion (Equation (1)), while oxides of nickel (NiO), iridium ($IrO_2$), and manganese ($Mn_3O_4$) constitute anodic electrochromic compounds, coloring upon oxidation and ionic extraction (Equation (1)); in addition, oxides of vanadium ($V_2O_5$) and cobalt ($Co_3O_4$) stand as multichromic compounds coloring differently upon reduction or oxidation.

$$M_xO_y + ne^- + nX^+ \underset{(b)}{\overset{(a)}{\rightleftarrows}} x_nM_xO_y \quad (1)$$

These oxides can be integrated as active EC materials at the working electrode of five-layer architectured devices (Figure 1), being combined with an ion storage or counter-electrode material (which can be of an electrochromic nature as well, complementarily to the working electrode compound—e.g., NiO with $WO_3$) through an electrolyte, ion conducting layer, disposed between two transparent electron-conducting layers covering the two transparent substrates. The latter typically consist of *glass* for a well-known applied use as smart windows and other glazing components, standing notably as energy-saving components of novel efficient buildings for lowering their consumption of heating, air conditioning, and lightening by up to 30%. Meanwhile, EC structures can also deal with *flexible substrates* such as polymers, plastics, or even papers for designing multiple sorts of light-weight smart electronic devices, which are increasingly developing nowadays so as to respond to the constant huger consumption of connected appliances. Specifically, as current electronic objects such as displays, labels, (bio)sensors, and even textiles are regularly lacking multifunctionality and tunability in their operation mode, flexible EC devices have recently emerged as conceptually simple and cost-efficient systems consuming low power, as the transition from one optical state to another demands minimal energy in a matter of seconds or minutes (depending on the substrate size). EC technology can therefore contribute to the reusability and recyclability of these electronic devices, reducing the probability and risk of them ending up in biological environment, either on purpose or accidentally, after too short of a lifecycle [11,13,15,26–29].

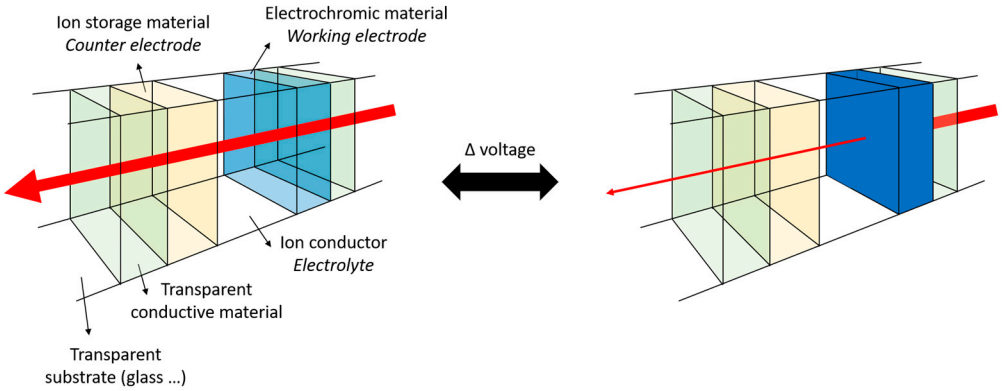


**Figure 1.** Traditional architecture of electrochromic EC devices, responding to applied voltage. Adapted from [9].

Two main approaches may be considered for fabricating EC devices, either through a layer-by-layer continuous deposition process, i.e., a multilayer EC stack (Figure 2A), or by

laminating the two separate working and counter electrodes, i.e., permanently assembling them by the action of pressure, heat, or adhesive strengths, with the intercalated electrolyte layer typically being of a gel polymer nature (Figure 2B).

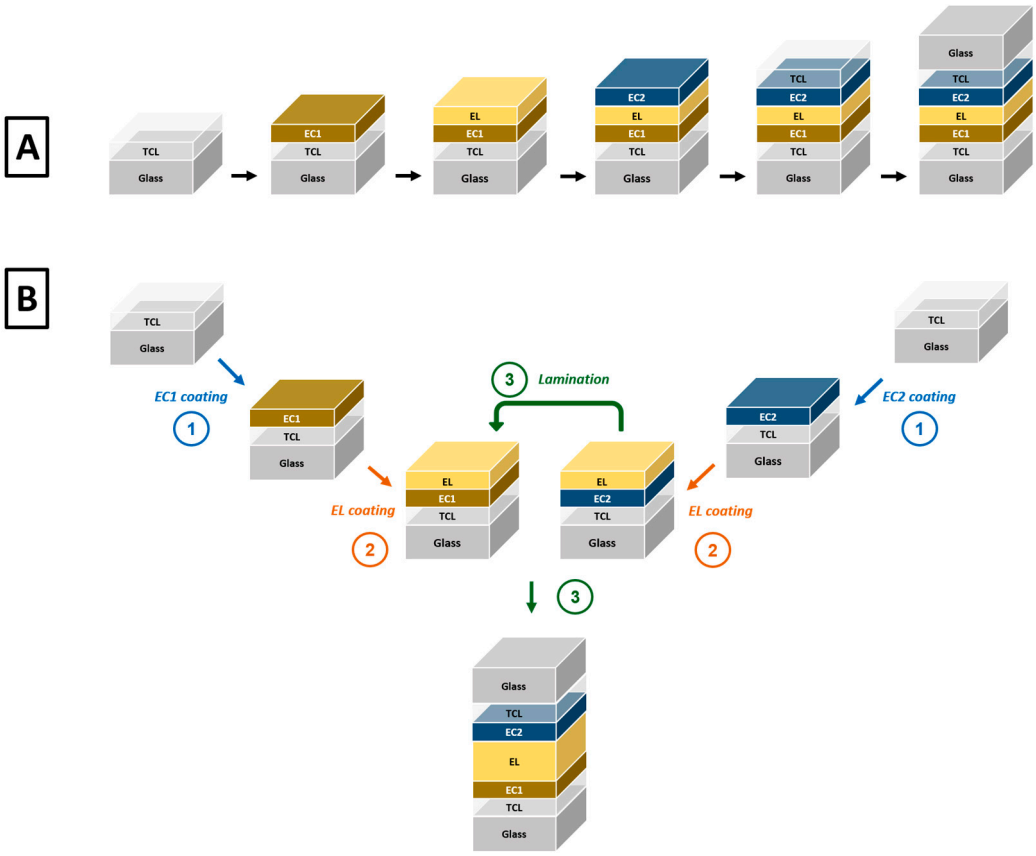


**Figure 2.** Comparison of EC devices' fabrication approaches: (**A**) multilayer stacking vs. (**B**) lamination. TCL stands for "transparent conducting layer", EC1 and EC2 stand for "electrochromic layer 1 or 2", and EL stands for "electrolyte layer".

Most of the currently developed and commercialized EC glazing systems conveniently address the modulation of visible light transmittance. However, the capacity to simultaneously but independently filtrate the infrared radiation, accounting for about half of the incident solar energy, still constitutes an important and critical issue. An ideal EC technology should indeed provide the selective, dynamic control of solar heating (near-infrared NIR range) and daylighting (visible VIS range) so as to better correlate users' needs and preferences depending on locations, climates, and seasons. Hence, there is the recent occurrence of dual-band EC materials and devices, allowing for selectively regulating the NIR and VIS regions of the solar spectrum through suitable, progressive electrical bias that will enable the switching of the EC devices between up to four filtration modes (Figure 3): bright (VIS and NIR transparent), cool (VIS transparent and NIR opaque), warm (VIS opaque and NIR transparent), and dark (VIS and NIR opaque) [9,30–34]. In specific configurations of EC materials and devices, dual-band properties can even be combined with polychromism, leading to multicolored glazing systems providing even more aesthetics and adaptability in daily life [35,36].

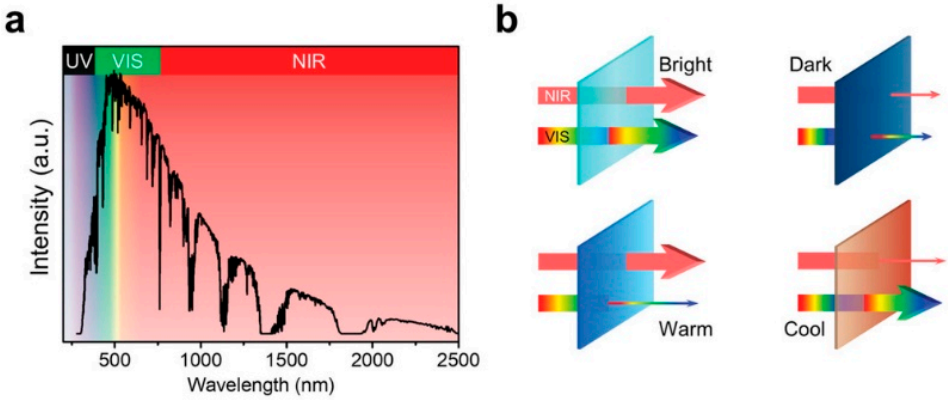


**Figure 3.** Representation of the solar radiation spectrum (**a**) and of the four filtration modes in dual-band EC systems (**b**). Reproduced with permission from [33], Copyright 2023, Wiley.

While the conventional EC mechanism of VIS light modulation consists in combined reduced polaron absorption and in-band transition, the tuning of the NIR region mostly relies on localized surface plasmon resonance LSPR effects, specifically occurring in selected nanocrystals (NCs) of metal oxides doped with hetero-elements and/or oxygen vacancies, including indium-tin oxide ITO, $TiO_{2-x}$, $Nb_2O_{5-x}$, and $WO_{3-x}$ [37–39]. LSPR induces a strongly enhanced light absorption when the frequency of the incident light is resonating with the frequency of collective oscillations of the electrons contained in the (semi)conducting material. The relationship (Equation (2a,b)) between the free carrier concentration $n$ of such doped metal oxide NCs (~$10^{21}$ $cm^{-3}$) and their LSPR frequency $\omega_{LSPR}$ is given by:

$$\omega_{LSPR} = \sqrt{\frac{\omega_P{}^2}{1+2\varepsilon_m} - \gamma^2} \tag{2a}$$

$$\omega_P = \sqrt{\frac{ne^2}{\varepsilon_0 m_e^*}} \tag{2b}$$

With $\omega_P$ being the bulk plasma frequency of electrons, $m_e^*$ being the effective mass of an electron, $\varepsilon_0$ being the permittivity of free space, $\varepsilon_m$ being the dielectric constant of the surrounding environment, and $\gamma$ being the bulk collision frequency. The tuning of $n$ can thus be achieved synthetically by changing the doping type and content, or post-synthetically by varying the applied potential. This consecutively induces the shift of the plasma frequency and of the corresponding LSPR wavelength, and therefore modulates the intensity and range of EC-driven optical absorption throughout NIR and VIS ranges.

The *figures of merits* of EC devices are commonly defined in terms of optical and electrochemical performance criteria [6,12,28,31,34], including:

- the *optical contrast* (i.e., the degree of transmittance modification ΔT% between clear and dark states, recorded at a single wavelength or within a specific wavelength range);
- the *solar AM 1.5 coverage* or *integrated solar transmittance*, defined as Equation (3):

$$T_{sol} = \frac{\int T(\lambda)\psi(\lambda)d\lambda}{\int \psi(\lambda)d\lambda} \tag{3}$$

  with $T(\lambda)$ being the transmittance at λ wavelength and $\psi(\lambda)$ being the incident solar intensity in the AM1.5G spectrum;
- the *apparent color* (regularly quantified in terms of coordinates from the International Commission on Illumination CIE color space with specific chromaticity plots) as well as the *Haze factor* (defined as the ratio between diffuse and total transmittances, which

should be <2% to avoid an undesirable, milky, and troubling aspect in the smart window device);

- the *switching speed* or *response time* (the time required for a specific transmittance change, in terms of coloration $t_{col}$ or bleaching $t_{ble}$, routinely equal to 90% of its full commutation run);
- the *coloration efficiency CE*, expressed in $cm^2/C$, as the change in optical density *OD* at a defined wavelength induced by every unit of charge density *Q* inserted or extracted per unit area, i.e., Equation (4):

$$CE = \frac{\Delta OD}{\Delta Q} \quad (4)$$

- the *memory effect* (i.e., the capacity to maintain a transmittance state without applying an additional charge);
- the *spectral selectivity* (i.e., the ability to selectively control different wavelength ranges of transmittance, typically NIR independently of VIS);
- and the *cycling stability* and *durability*, characterized by the number of switching cycles during which the optical change can be preserved without significant degradation, being influenced by cycling testing conditions—the bias type and duration, electrolyte nature, temperature and pressure, illumination conditions, etc. To this end, the reader could refer to the recent report of J. Padilla et al. [40], presenting a detailed procedure that aims at adequately defining the testing conditions and the analytical description of the evolution of the performance of EC materials through continuous cycling. Their evaluation method relies on three steps: (i) define the reference switching conditions for each material, (ii) define the testing conditions used during the stability test, and (iii) use an analytical description of the contrast vs. the cycling run, like the number of cycles corresponding to an 80% performance retention. Various stability assessments were performed on common EC compounds, including conducting polymers, metal oxides, metallo-supramolecular polymers, and viologens, under a variety of test conditions.

Despite many advances and much progress over the last decades and years, EC systems still suffer from both conceptual and technical issues in the optimization of their formulation and structure, and of the conditions of materials preparation and device assembly towards proper transfer/integration into practical applications. Among key prospective actions, the improvement of device fabrication processes is of crucial importance and interest, as the suitable thin-film processing of their constitutive layers has a critical impact on obtaining EC systems with efficient functionality and performance. Film processing may be achieved by various vacuum- or wet-based methodologies [6,8,11,22,41,42]. Chemical vapor deposition (CVD) with atmospheric pressure (APCVD) and aerosol-assisted (AACVD) conditions, thermal evaporation, and sputtering (DC, RF, magnetron…) are among the vacuum processes commonly exploited to manufacture EC materials, while wet protocols include electrodeposition, sol-gel, inkjet printing, dip coating, spin coating, blade coating, and spray coating. Despite being less controllable, solution-based approaches are considered as simpler and more versatile in terms of deposition conditions and to be of a lower energetic and financial cost. Vacuum technologies present the advantages of a higher purity and precision (with a high degree of control provided on deposition parameters, lowering the contamination rates) but high constraints in terms of vacuum quality and temperature dependence, therefore leading to a higher complexity and increased fabrication costs, especially for large-area substrates.

## 2. Spray Deposition: Principles and Methods

The present contribution proposes to review how the spray deposition approach is precisely exploited for the manufacturing of various sorts of metal oxide-based EC coatings, to be ultimately integrated in functional devices for smart glazing and other (opto)electronic applications.

As an atmospheric pressure technique, spray coating presents a huge potential for producing highly homogeneous films of good adhesion on various substrates—glass, metals and alloys, plastics, polymers, papers, etc., with reduced energy consumption when compared to vacuum processes; it also provides higher upscaling capacities than other lab-level wet routes, therefore being easily transferrable to industrial pilot lines without important production costs. Spray deposition favors the use of low-toxic solvents with efficient precursor utilization, guaranteeing fast and continuous production speeds [8,43–48]. Beyond EC materials, spray coating is widely used in numerous fundamental and applied fields of research and development related to energy, the environment, and health, including semiconductors, solar cells, (bio)sensors, batteries, as well as optical and electronic devices [49–56].

A spray coating setup (Figure 4) generally involves a spray *nozzle*, being an *atomizer* component that converts the precursor fluid feed into a mist of droplets of a specific size and size distribution. These droplets are then conveyed, "sprayed" onto a target substrate, left to stand at room temperature (RT) or heated with a hot plate or in a furnace/oven enclosure, and positioned on a stage at a certain distance of the nozzle. Depending on the setups, either the nozzle or the substrate stage (or both of them) can be moved in the three spatial directions X/Y/Z during the spraying process, following (or not) a pattern of advanced movement control and automation that may be repeated and/or paused on demand. Thanks to its high level of sophistication combined with its practical simplicity, spray deposition may be used for the uniform coverage of uncommon and/or very irregular surfaces, especially flexible substrates such as polymers, plastics, and papers, and/or provide rapid coating conditions leading to stable and adherent functional layers.

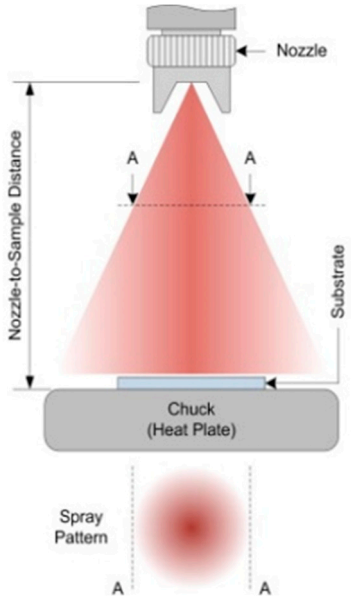


**Figure 4.** Representation of a spray coating setup. Reproduced with permission from [49]. Copyright 2023, Elsevier.

Three types of spray atomization methods are regularly used [44,47,51,54,56]:

- *Air* or *pneumatic spray* (Figure 5a), in which compressed air is used to apply high pressure on the precursor fluid discharged from the nozzle, colliding at a high speed with the remaining air and then being split up and slowed down due to air resistance, before finally turning into a mist of droplets directed towards the target. Because they disperse a large quantity of precursor fluid, air spray setups can cause a significant excess of lost material, i.e., *overspray*.
- *Electrostatic spray* (Figure 5b), in which the precursor fluid is first charged with static electricity by applying a relatively high voltage within the spray nozzle (up to several

thousands of V) and then changed into a droplet mist through electrostatic repulsion; the spray mist is then specifically attracted to the target surface standing on a grounded stage, therefore reducing the overspray quantity. Thanks to the strong electrical field in play, electrospray systems can be used with solutions and suspensions of quite high viscosities as well as with pastes and slurries.

- *Ultrasonic spray* (Figure 5c), in which the nozzle is equipped with a chip (atomization surface) that vibrates upon ultrasonic waves, causing the precursor fluid to spread over the chip and ruffle; when the ultrasonic output becomes higher than the surface tension, the fluid is transformed into a fine droplet mist of a highly uniform size and size distribution (in comparison with other spray modes), being ultimately conveyed onto the substrate surface through a carrier gas of a passive (inert) or active (oxidative, reducing. . .) nature. By controlling the liquid flow and vibration frequency, ultrasonic spray has been shown to produce high-quality coatings with important uniformity, regular thickness, and strong adherence, also involving very limited overspray by producing almost no splashing or avoidable liquid spreading.

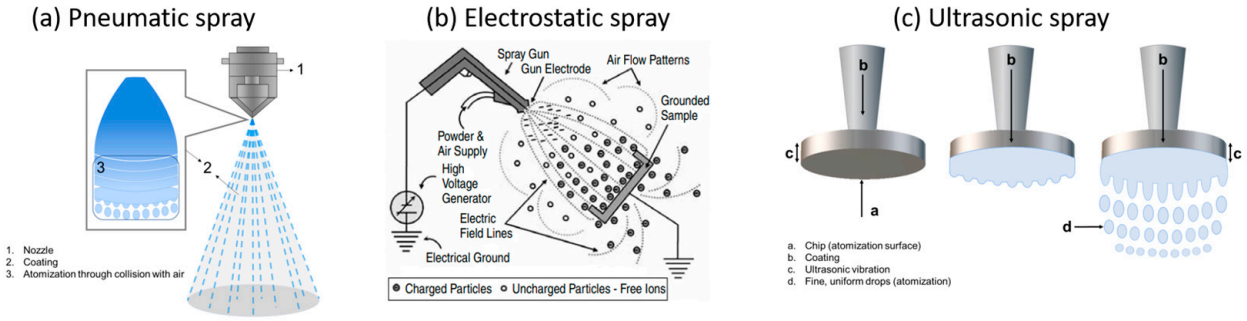


**Figure 5.** Three modes of spray atomization methods: (**a**) pneumatic, (**b**) electrostatic, and (**c**) ultrasonic. Adapted from [47] and reproduced with permission from [57]. Copyright 2023, Elsevier.

Corresponding nozzles can have different dimensions and spray shaping conditions depending on the targeted function and application, particularly where high precision or uniform deposition is needed; shaping can also be adapted to the targeted size area, involving atomizers design favoring either fine or large cones of sprayed droplets as well as tandem/series mounting of spray nozzles.

When substantial heating conditions are applied during the spray protocol, pyrolysis processes (i.e., the thermal decomposition of a material at an elevated temperature, typically metal salts being converted into corresponding oxide(s) formulations) can occur depending on the nature and conditioning of the involved chemical precursors, leading to so-called *spray pyrolysis* deposition [43,44,54,58]. As a function of the substrate temperature or of the initial droplet size, the precursor fluid reaches the substrate surface as a liquid or a precipitate (at a too low temperature or with a too large initial droplet), a vapor (ideal temperature or initial droplet size), or a powder (at a too high temperature or at a too small initial droplet); this is defined according to the Viguié-Spitz [59] and Siefert [60] models (Figure 6) and shown to critically impact the resulting morphological, structural, and functional properties of the obtained films. Other issues must also be considered so to rationalize the basic aspects of the spray process, including (but not limited to): the size, nature, and form of the sprayed materials/particles; the film's structural, kinetic, and topographical characteristics; the chemical bonding and associated structural considerations (including an amorphous or crystalline nature) of the as-deposited layers; and the effects of annealing on the bonding and thickness.

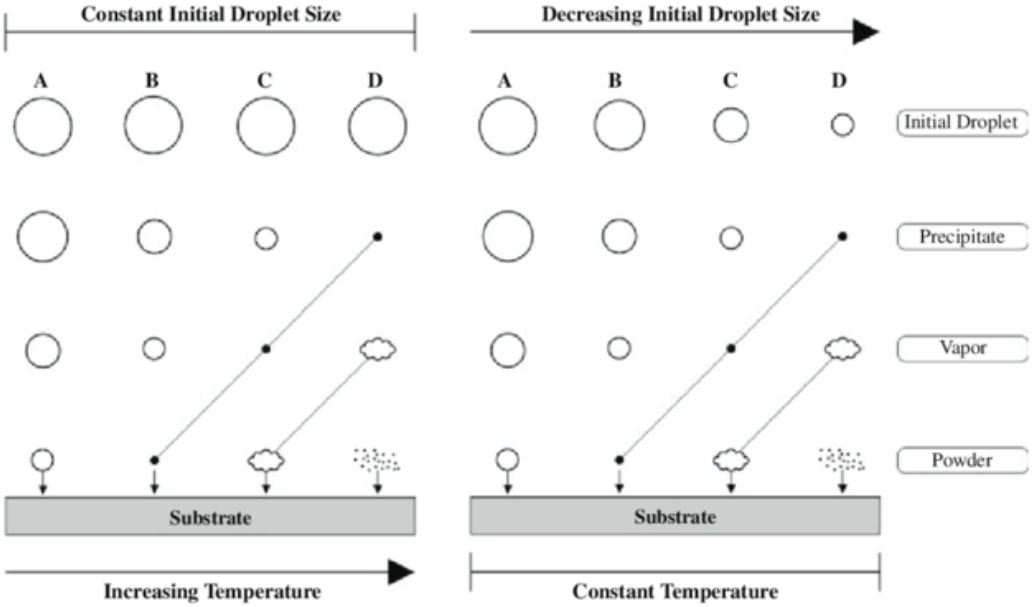


**Figure 6.** Viguié-Spitz and Siefert models, respectively, describing spray pyrolysis as a function of the substrate temperature (increasing from A to D) and constant initial droplet size (**left**), and the constant temperature and variable droplet size (decreasing from A to D) (**right**). Reproduced with permission from [58]. Copyright 2023, Springer.

Spray coating can also be achieved at RT (or under relatively mild heating conditions involving no pyrolysis reaction)—for instance, for the deposition of "pre-formed" functional micro- or nanoparticles as liquid suspensions (Figure 7A) or as dry powders in a so-called *nanoparticle deposition system* (NPDS; Figure 7B) capable of depositing both nano- and micron-sized particles under low vacuum with low-cost compressed air. NPDS has already been reported for the coating of metals, ceramics, or polymer substrates with various metals and ceramics, including Cu, Ni, $TiO_2$, $Al_2O_3$, $WO_3$, NiO, and Sb-doped $SnO_2$ (ATO) [8,61–65].

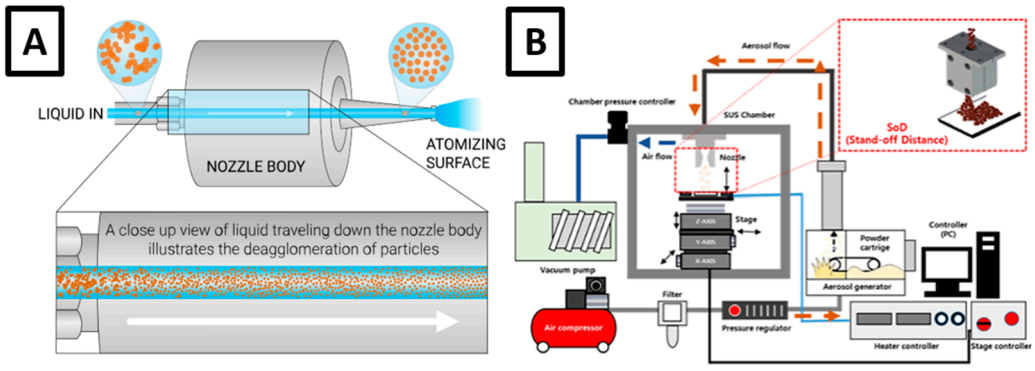


**Figure 7.** Spray deposition of (**A**) liquid suspensions (being ultrasonically deagglomerated here) and (**B**) dry powders of nanoparticles (NPDS). Reproduced with permission from [48] (Copyright 2023, Sono-Tek) and from [64] (Copyright 2023, Springer).

The suitable selection of the spraying conditions, and the corresponding impact on the film's functional properties, are very often reported to be critical and of high importance for all sorts of precursor compounds and formulations. Factors influencing spray deposition can be sorted along the material-based parameters, including the precursor's nature, the solvent, the solution/suspension concentration, the effect of incorporated dopants and/or other additives, etc. Setup-related parameters are also shown to impact the deposited layers' properties, including the nozzle-to-substrate distance, the carrier gas nature and

pressure, the liquid feed flow rate, the nozzle and/or substrate movement/pattern, the spray duration (as a single or sequential run), the substrate temperature during deposition together with the heating conditions (hot plate, furnace, oven, microwaves...), and the (possible) consecutive post-treatment of a thermal/chemical/physical nature, etc. This is of course the case for all EC metal oxides being considered for the present review and examined on a case-by-case basis in the following sections.

## 3. Spray Deposition of Electrochromic Metal Oxides

### *3.1. Tungsten Oxide $WO_3$*

The EC behavior of $WO_3$ was first evidenced by S. Deb in 1969 [2], making it one of the most popular EC materials since then. Coloring cathodically upon the reduction of W(+VI) and cationic insertion, its optical state turns from transparent to dark blue. Praised for their high optical modulation and coloration efficiency, strong cycling stability, and low processing cost, $WO_3$ films are well-established materials for the large-scale development of EC devices, despite a quite slow response time (typically of tens of seconds to minutes) and a mitigated response to the life cycle (aging effect). As for other EC metal oxides (see below), their optical and electrochemical performances rely on various morphological and structural factors, being strongly influenced by the selected fabrication technique, including the crystallinity, roughness, porosity, and conductivity; EC properties can also depend on further material design strategies such as nanostructuration, regulation of crystallinity (between crystalline, polycrystalline, amorphous, and hybrid), doping (with hetero-elements and/or oxygen vacancies), incorporation in hybrid and/or composite structures, as well as film's density and electrolyte nature and concentration [14,66–71].

The spray deposition of $WO_3$ films for EC applications has been covered in about 45 publications since 1986, including 25 (14) over the last 10 (5) years (Table 1). Notable initiatory works were conducted by K. Colbow et al. in the late 1980s and early 1990s [72–75], reporting the spray pyrolysis deposition at 400 °C of polycrystalline $WO_3$ layers from solutions of tungsten chloride $WCl_6$ dissolved in ethanol or dimethylformamide DMF, resulting in 250 to 650 nm thick films showing up to 73% (75–2) of optical contrast in VIS and coloration times of 40 to 60 s. New developments in pyrolytic spraying were achieved in the 2000s [76–89], notably by P. Patil and co-workers who addressed multiple compositions of precursor solutions—the combination of $WO_3$ with other oxides ($MoO_3$, $TiO_2$, $Nb_2O_5$), the nature of W salt (mostly tungstates, being less corrosive and toxic than chloride derivatives) and/or the solvent (mostly water), etc.—and of substrate temperatures during and/or after the deposition process (as annealing post-treatments), being between 300 and 525 °C (typically 450 °C). Films of thickness between 200 and 750 nm were consecutively obtained, presenting moderate VIS contrasts $\Delta T$ (up to 50%) but quite fast commutation kinetics ($t_{col}$ and $t_{ble}$ less than 10 s), and tested over 1000 to 2000 cycles; high coloration efficiency *CE* values were particularly noticed for mixed $WO_3$–$MoO_3$ formulations (42–63 $cm^2/C$) [79] and for $WO_3$ layers included with multi-walled carbon nanotubes (43–79 $cm^2/C$) [85]. Other groups further investigated the effect of $WO_3$ doping with various aliovalent compounds, notably Mo [90,91], Sn [92], Ti [93], Sb [94], Ni [95], or Co [95,96], with the most promising performances obtained by P. Sahay et al. with ammonium tungstate $(NH_4)_2WO_4$ precursor solutions mixed with up to 5% at. of molybdenum chloride $MoCl_5$ in DMF and sprayed at 390 °C [91], leading to ~30% VIS $\Delta T$, 25–50 s switching speeds, and 14–43 $cm^2/C$ *CEs*.

**Table 1.** Review of spray-coated $WO_3$ layers in terms of spray conditions, resulting thickness, and EC metrics. N.p. means "not provided"; O.D. means "optical density". $T_{ble}$ and $T_{col}$ data are represented as "highest–lowest" values obtained on all presented datasets in the corresponding references (which can be related to different samples); however, the reported ranges of ΔT are related to common datasets (and so are $t_{ble}$, $t_{col}$, CE, and the number of cycles data). e.g., a reference covers three samples: $T_{ble,1}$ = 95%, $T_{ble,2}$ = 90%, and $T_{ble,3}$ = 85%, and $T_{col,1}$ = 30%, $T_{col,2}$ = 5%, and $T_{col,3}$ = 15%; reported values in the table will be: $T_{ble}$ = 85–95%, $T_{col}$ = 5–30%, and ΔT = 65–85% (and not ΔT = 55–90%, as it would be calculated from the difference in the maximal $T_{ble}$ and minimum $T_{col}$ values). The same terminology is used in the following tables.

| Reference | Spray Conditions (*$T_{dep}$ for Deposition Temperature, t.t. for Thermal Treatment*) | Thickness (nm) | $T_{ble}$ (%) | $T_{col}$ (%) | ΔT (%) | $t_{ble}$ (s) | $t_{col}$ (s) | CE ($cm^2$/C) | Cycling Runs |
|---|---|---|---|---|---|---|---|---|---|
| **Colbow** [72] | $WCl_6$ in ethanol or DMF $T_{dep}$ = 400 °C | *N.p.* | 75 | 2 | 73 | *N.p.* | *N.p.* | *N.p.* | *N.p.* |
| **Colbow** [73] | $WCl_6$ in DMF $T_{dep}$ = 200–400 °C | 250–650 | *N.p.* | *N.p.* | *N.p.* | *N.p.* | 40–120 | *N.p.* | *N.p.* |
| **Colbow** [74] | $WCl_6$ in DMF $T_{dep}$ = 200–400 °C | 450 | *N.p.* | *N.p.* | *N.p.* | *N.p.* | *N.p.* | *N.p.* | *N.p.* |
| **Livage** [75] | Tungstate/$WOCl_4$ in $H_2O$/alcohol $T_{dep}$ = RT with drying at 80 °C | 500 | *N.p.* | *N.p.* | 0.7 (O.D.) | *N.p.* | *N.p.* | *N.p.* | *N.p.* |
| **Estrada** [76] | Ammonium tungstate in $H_2O$ $T_{dep}$ = 430 °C | 1000 | 75 | *35* | 40 | *N.p.* | *N.p.* | *N.p.* | 100 |
| **Regragui** [77] | $WCl_6$ in $H_2O$–ethanol $T_{dep}$ = 200–400 °C with t.t. at 500 °C | 150 | 60–72 | 10–50 | 22–60 | *N.p.* | *N.p.* | *N.p.* | *N.p.* |
| **Regragui** [78] | $WCl_6$ in $H_2O$–ethanol $T_{dep}$ = 300 °C with t.t. at 500 °C | 150 | >80 | <5 | 75 | <5 | <10 | *N.p.* | *N.p.* |
| **Patil** [79] | $NH_4$ tungstate & molybdate in $H_2O$ $T_{dep}$ = 300 °C with t.t. at 400 °C | 600 | *N.p.* | *N.p.* | 0.6–1.3 (O.D.) | 2–3 | 4–5 | 42–63 | *N.p.* |
| **Patil** [80] | $WO_3$ powder and $C_{10}H_{14}O_5Ti$ in $NH_4OH$ and methanol; $T_{dep}$ = 525 °C | *N.p.* | 45–85 | 25–70 | 20–25 | *N.p.* | *N.p.* | 7–13 | *N.p.* |
| **Patil** [81] | $WO_3$ powder and $TiCl_4$ in $NH_4OH/H_2O$ $T_{dep}$ = 450 °C | *N.p.* | 50–73 | 45–67 | 2–10 | 3–6 | 4–5 | 8–26 | *N.p.* |
| **Patil** [82] | $WO_3$ and $Nb_2O_5$ powders in $NH_4OH/H_2O$ $T_{dep}$ = 450 °C | 520–530 | 73–85 | 55–67 | 6–30 | 1–3 | 3–5 | 17–26 | *N.p.* |
| **Patil** [83] | $WO_3$ and $Nb_2O_5$ powders in $NH_4OH/H_2O$ $T_{dep}$ = 450 °C | 510–530 | 65–75 | 52–58 | 10–20 | 6–8 | 5–7 | 13–19 | 1000 |
| **Patil** [84] | Ammonium tungstate in $NH_4OH/H_2O$ $T_{dep}$ = 450 °C | 200 | 70 | 65 | 5 | 3–4 | 5–6 | 25 | 1200 |
| **Patil** [85] | Ammonium tungstate and MWCNTs in $H_2O$; $T_{dep}$ = 450 °C | 250 | 75–80 | 30–50 | 30–45 | 3–6 | 6–8 | 43–79 | *N.p.* |
| **Patil** [86] | Ammonium tungstate in $NH_4OH/H_2O$ $T_{dep}$ = 450 °C | 250–750 | 25–80 | 10–63 | 10–50 | *N.p.* | *N.p.* | 14–43 | 1000 |
| **Sivakumar** [87] | Ammonium tungstate in $NH_4OH/H_2O$ $T_{dep}$ = 250 °C with t.t. at 500 °C | 600 | *N.p.* | *N.p.* | *N.p.* | *N.p.* | *N.p.* | *N.p.* | *N.p.* |
| **Zelazowska** [88] | $WO(C_5H_7O_2)_4$ in acetylacetone and dichloromethane; $T_{dep}$ = 650 °C | 120 | 58 | 6 | 52 | *N.p.* | *N.p.* | *N.p.* | 100 |
| **Sahay** [89] | $WCl_6$ or ammonium tungstate in DMF $T_{dep}$ = up to 400 °C | 450–500 | *N.p.* | *N.p.* | *N.p.* | *N.p.* | *N.p.* | *N.p.* | *N.p.* |
| **Acosta** [90] | $WCl_6$ and $MoO_2Cl_2$ in DMF $T_{dep}$ = 500 °C | 480–520 | *N.p.* | *N.p.* | *N.p.* | *N.p.* | *N.p.* | *N.p.* | 2000 |

**Table 1.** *Cont.*

| Reference | Spray Conditions (*$T_{dep}$ for Deposition Temperature, t.t. for Thermal Treatment*) | Thickness (nm) | $T_{ble}$ (%) | $T_{col}$ (%) | ΔT (%) | $t_{ble}$ (s) | $t_{col}$ (s) | CE ($cm^2$/C) | Cycling Runs |
|---|---|---|---|---|---|---|---|---|---|
| **Sahay** [91] | Ammonium tungstate and $MoCl_5$ in DMF $T_{dep}$ = 390 °C | *N.p.* | 18–48 | 1–18 | 13–30 | 25–50 | 1–25 | 14–43 | 100 |
| **Sahay** [92] | Ammonium tungstate and $SnCl_4$ in $H_2O$ $T_{dep}$ = 400 °C | 500–550 | *N.p.* | *N.p.* | *N.p.* | *N.p.* | *N.p.* | *N.p.* | *N.p.* |
| **Acosta** [93] | $WCl_6$ and $TiCl_3$ in DMF $T_{dep}$ = 500 °C | 480–520 | *N.p.* | *N.p.* | *N.p.* | *N.p.* | *N.p.* | *N.p.* | 3000 |
| **Sahay** [94] | Ammonium tungstate and $SbCl_3$ in $H_2O$ $T_{dep}$ = 400 °C | 450–470 | *N.p.* | *N.p.* | *N.p.* | 3–6 | 3–10 | *N.p.* | 50 |
| **Mohagheghi** [95] | $WO_3$ powder, $NiSO_4$, and $CoCl_2$ in $H_2O$ $T_{dep}$ = 400 °C with t.t. at 500 °C | 250 | *N.p.* | *N.p.* | *N.p.* | *N.p.* | *N.p.* | *N.p.* | *N.p.* |
| **Mohagheghi** [96] | $WO_3$ powder + $CoCl_2$ in $H_2O$ $T_{dep}$ = 400 °C with t.t. at 500 °C | 250 | *N.p.* | *N.p.* | *N.p.* | *N.p.* | *N.p.* | *N.p.* | *N.p.* |
| **Wolden** [97] | $WCl_6$ + ethanol + P123 $T_{dep}$ = RT with t.t. at 300–400 °C | 400 | 70–92 | 14–38 | 35–75 | 6–120+ | 6–20 | 26–51 | 10 |
| **Wolden** [98] | $WCl_6$ + ethanol + P123 $T_{dep}$ = RT with t.t. at 300–400 °C | 400 | 70–80 | 45–50 | 40–75 | 5–24 | 5–9 | 43–50 | 2500 |
| **Wolden** [99] | $WCl_6$ + ethanol + P123 $T_{dep}$ = RT with t.t. at 350 °C | 1000 | 77–100 | 0–30 | 70–100 | 27–67 | 3 | 36–45 | 1000 |
| **Duta** [100] | $WCl_6$ + ethanol $T_{dep}$ = 200–300 °C | 200 | 65–80 | 15–35 | 21–64 | *N.p.* | *N.p.* | 28–35 | *N.p.* |
| **Duta** [101] | $WCl_6$, HTAB, and PEG in ethanol and acetylacetone $T_{dep}$ = 250 °C with t.t. at 410 °C | 350–375 | 65–80 | 45–50 | 13–35 | 47–58 | 13–19 | 10–43 | 50–100 |
| **Cloots** [102] | AMT and PEG in $H_2O$ $T_{dep}$ = 350 °C | 550 | 92 | 9 | 83 | 42 | 72 | 28 | 500 |
| **Cloots** [103] | AMT and PEG in $H_2O$ $T_{dep}$ = 350 °C | 100–120 | 87–92 | 7–9 | 78–85 | 46–51 | 77–91 | 26–31 | 100 |
| **Cloots** [104] | APTA and Brij-56 in $H_2O$ $T_{dep}$ = 190 °C or 100 °C with t.t. at 350 °C | 200 | 55–85 | 20–55 | 10–40 | 35–200 | 60–300 | 6–40 | 20 |
| **Lin** [105] | $WCl_6$ and P123 in ethanol $T_{dep}$ = RT with t.t. at 350 °C | 1000 | 78–95 | 32–38 | 40–55 | 1–3 | 5–7 | *N.p.* | 3000 |
| **Gesheva** [106] | W powders and $H_2O_2$ in ethanol $T_{dep}$ = RT with t.t. at 100–275 °C | 200 | *N.p.* | *N.p.* | 10–70 | *N.p.* | *N.p.* | 12–134 | *N.p.* |
| **P.S. Lee** [107] | $H_2WO_4$ and $MoO_3$ in $H_2O$ and ethylene glycol; $T_{dep}$ = RT with drying | 200 | 80 | 37 | 43 | 8 | 10 | 36 | 2000 |
| **Elezzabi** [108] | Ti–W–Mo oxides NPs in $H_2O$ $T_{dep}$ = RT with drying at 60 °C | *N.p.* | 22–85 | 7–9 | 15–76 | *N.p.* | *N.p.* | *N.p.* | 100 |
| **Elezzabi** [109] | W-Mo NPs + PEDOT:PSS $T_{dep}$ = 60 °C, layer-by-layer process | 900 | 75–85 | 10–30 | 55–65 | 11–14 | 18–22 | 22–53 | 300 |
| **C.S. Lee** [62] | $WO_3$ NPs $T_{dep}$ = 80 °C, NPDS | 400–700 | 60–70 | 5–20 | 44–64 | *N.p.* | *N.p.* | *N.p.* | *N.p.* |
| **C.S. Lee** [63] | $WO_3$ NPs $T_{dep}$ = RT-200 °C, NPDS | 400–700 | 55–65 | 14–35 | 10–42 | *N.p.* | *N.p.* | *N.p.* | *N.p.* |
| **C.S. Lee** [64] | $WO_3$ NPs $T_{dep}$ = 80 °C, NPDS | 400–700 | 2–15 | 55–62 | 43–55 | >40 | 18–30 | 42–77 | *N.p.* |
| **C.S. Lee** [110] | $WO_3$ NPs $T_{dep}$ = RT, NPDS | *N.p.* | 37–65 | 8–47 | 2–50 | *Fixed time* | *Fixed time* | N.p. | 600+ and over 1M |
| **Tsukagoshi** [111] | $WO_3$ NPs in $H_2O$ $T_{dep}$ = 150 to 300 °C | 450 | 79 | 19 | 60 | 2 | 4 | 37 | 80 |

**Table 1.** *Cont.*

| Reference | Spray Conditions (*$T_{dep}$ for Deposition Temperature, t.t. for Thermal Treatment*) | Thickness (nm) | $T_{ble}$ (%) | $T_{col}$ (%) | ΔT (%) | $t_{ble}$ (s) | $t_{col}$ (s) | CE ($cm^2$/C) | Cycling Runs |
|---|---|---|---|---|---|---|---|---|---|
| **Liu [112]** | $WO_3$ and $MoO_3$ NPs in $H_2O$ and ethanol $T_{dep}$ not provided | *N.p.* | 70–75 | 12–36 | 45–60 | 6–11 | 4–9 | 43–80 | 2000 |
| **Choi [113]** | $WO_3$ NPs + $Ti_3C_2T_x$ MXene $T_{dep}$ = RT with t.t. at 100 °C | 200 | 68–72 | 10–57 | 17–58 | 2–3 | 3–7 | 35–127 | 1000 |
| **Pugliese [114]** | $WO_3$ and $TiO_2$ NCs $T_{dep}$ = 100 °C with t.t. at 300 °C | 500 | VIS: 71 NIR: 70 | VIS: 11 NIR: 5 | VIS: 60 NIR: 65 | VIS: 4 NIR: 22 | VIS: 22 NIR: 5 | VIS: 38 NIR: 29 | 500 |

An interesting approach of surfactant-assisted spray (pyrolysis) deposition was then explored and reported starting from the early 2010s [97–105]. Various sorts of surfactants—cationic and anionic, gemini, and non-ionic—could be used to produce $WO_3$ films with a high order and a controlled particle/grain size, porosity, and crystallinity. Different nucleation and growth processes were observed after the addition of the surfactant(s), impacted by the variation in the surface tension in the corresponding sprayed solution. Notably, C. Wolden and co-workers investigated how the incorporation of a poly(ethylene glycol)-block-poly(propylene glycol)-block-poly(ethylene glycol) triblock copolymer (P123) to an ethanol-based solution of $WCl_6$ could provide nanoscale porosity to consecutively sprayed $WO_3$ layers (of a 400 nm thickness). Electrochromic properties were then directly correlated to the annealing conditions following the RT (ultrasonic) spray deposition—namely, between 300 and 450 °C under "fast" (hot plate) or "slow" (oven with a 5 °C/min ramp) thermal post-treatments: Δ*T* in VIS was shown to evolve from 41 to 77%, $t_{col}$ and $t_{ble}$ were shown to evolve from 20/>120 to 6 s each, and *CEs* were shown to evolve from 26 to 51 $cm^2$/C, considering a 1 h fast treatment at 350 °C for removing the polymer additive [97]. A. Duta et al. considered a mix of anionic and non-ionic surfactants, namely, hexadecyltrimethylammonium bromide (HTAB) and polythelyene glycol (PEG), being added to $WCl_6$-ethanol/acetylacetone solutions sprayed at 200 °C; the obtained 350 nm thick films of a high smoothness and homogeneity delivered up to 35% of VIS Δ*T*, 19 and 51 s of $t_{col}$ and $t_{ble}$, and 43 $cm^2$/C of CEs [101]. Finally, R. Cloots et al. proposed a single-step surfactant-assisted ultrasonic spray pyrolysis (USP) process at 350 °C, using aqueous solutions of ammonium metatungstate (AMT) mixed with PEG at a 1:10 mass ratio (Figure 8) [102]. The obtained layers, of a 550 nm thickness and a very high smoothness, showed a very high VIS Δ*T* of 83% (92–9), moderate kinetics (72 s for $t_{col}$ and 42 s for $t_{ble}$), and a good CE (28 $cm^2$/C), together with a charge reversibility maintained between 89 and 99% over a 500-cycles coloration/bleaching run. Such excellent EC performances were attributed to the beneficial consequence of the interactions between the PEG surfactant and the W precursor (via hydrogen bonding), specifically preventing droplet coalescence during spray deposition and particle aggregation during film formation. The same group kept exploring the surfactant-assisted USP processing of EC $WO_3$ layers in two additional studies. The first one addressed the USP deposition of the same solution in similar temperature conditions onto alternative transparent conducting surfaces, namely, glass covered with tin-doped (ITO) or tungsten-doped indium oxide (IWO) instead of fluorine-doped tin oxide (FTO); the levels of VIS Δ*T* (up to 85%), switching kinetics (between 46 and 91 s), and *CEs* (up to 31 $cm^2$/C) were maintained at a high degree of efficiency [103]. The second one considered alternative precursors and surfactants (namely, acetylated peroxotungstic acid APTA and polyethylene glycol hexadecyl ether Brij-56) for adapting the spray conditions down to 190 °C in single-step or to 100 °C with 250 °C post-annealing in multi-step, ultimately leading to 40% VIS Δ*T* and 40 $cm^2$/C CE (Figure 9) [104]. All in all, these studies paved the way for conducting the spray processing of ($WO_3$) EC layers at a much lower energetical cost.

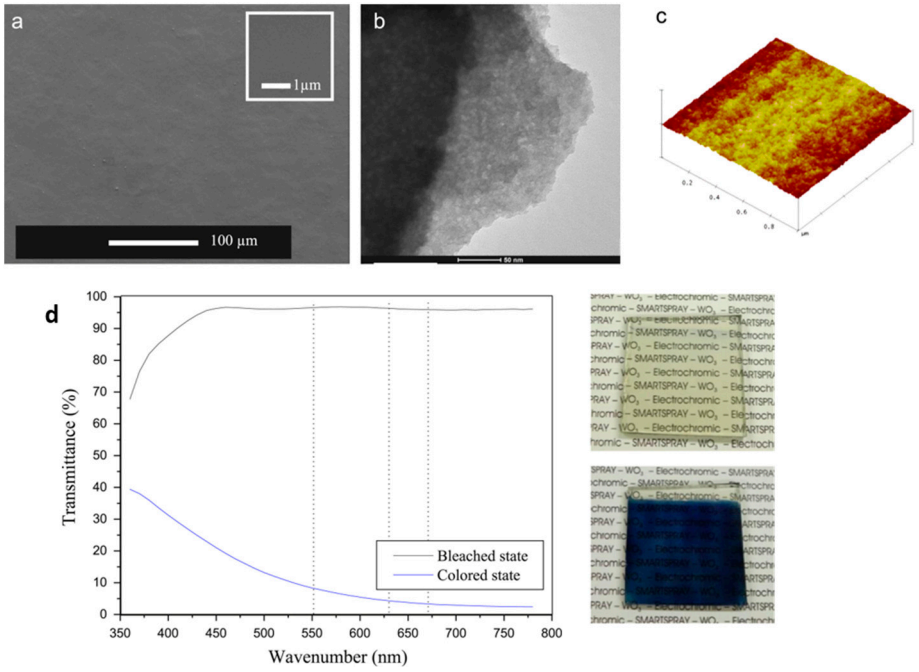


**Figure 8.** $WO_3$ thin films deposited by a surfactant-assisted ultrasonic spray pyrolysis process at 350 °C: scanning (**a**) and transmission (**b**) electron micrographs, AFM image (**c**), UV–visible spectra, and corresponding photography in bleached and colored states (**d**). Reproduced with permission from [102]. Copyright 2023, Elsevier.

The latest works kept investigating this "cooler" trend by considering even lower temperatures for the spray coating processes [62–64,106–114]. Several teams focused on the RT deposition of "pre-formed" $WO_3$ nanoparticles: notably, P.S. Lee et al. discussed the hydrothermal synthesis and consecutive RT spray coating of tungsten molybdenum oxide nanoparticles dispersed in water (Figure 10A) [107], while A. Elezabbi et al. considered colloidally synthesized titanium-substituted molybdenum–tungsten oxide (MTWO) nanoparticles being spray-deposited at RT and then dried in air at 60 °C for 24 h [108], or Mo–W oxide nanoparticles mixed with PEDOT:PSS and sprayed at 60 °C (Figure 10B) [109]. The optical contrasts in VIS reached 43 (Lee) to 65–76% values (Elezzabi), with 10–20 s commutation kinetics (Lee & Elezzabi) and 36 (Lee) to 53 $cm^2/C$ CEs (Elezzabi); the materials were cycled between 100–300 (Elezzabi) and 2000 runs (Lee). C.S. Lee and co-workers developed an original kinetic spray apparatus called a *nanoparticle deposition system* (NPDS; see Section 2), allowing for the low-temperature (from RT to 200 °C) deposition of commercial or lab-synthesized $WO_3$ NPs, achieving maximal EC performances of 64% of VIS $\Delta T$ and 77 $cm^2/C$ of CE [64–66,110]. More recent publications reported the RT deposition of hybrid formulations of $WO_3$ and titanium carbide $Ti_3C_2T_x$ ("MXene"), showing up to 58% of VIS $\Delta T$, <10 s of $t_{col}$ and $t_{ble}$, and 127 $cm^2/C$ of CE (Figure 10C) [113], and of core-shell $TiO_2$@$WO_{3-x}$ colloidal nanocrystals for dual-band EC, sprayed at 100 °C into 500 nm thick films showing 67% of NIR shielding while maintaining 60% of VIS transparency in the "cool mode" and 89% of the screening of both VIS and NIR radiations in the "dark mode" [114].

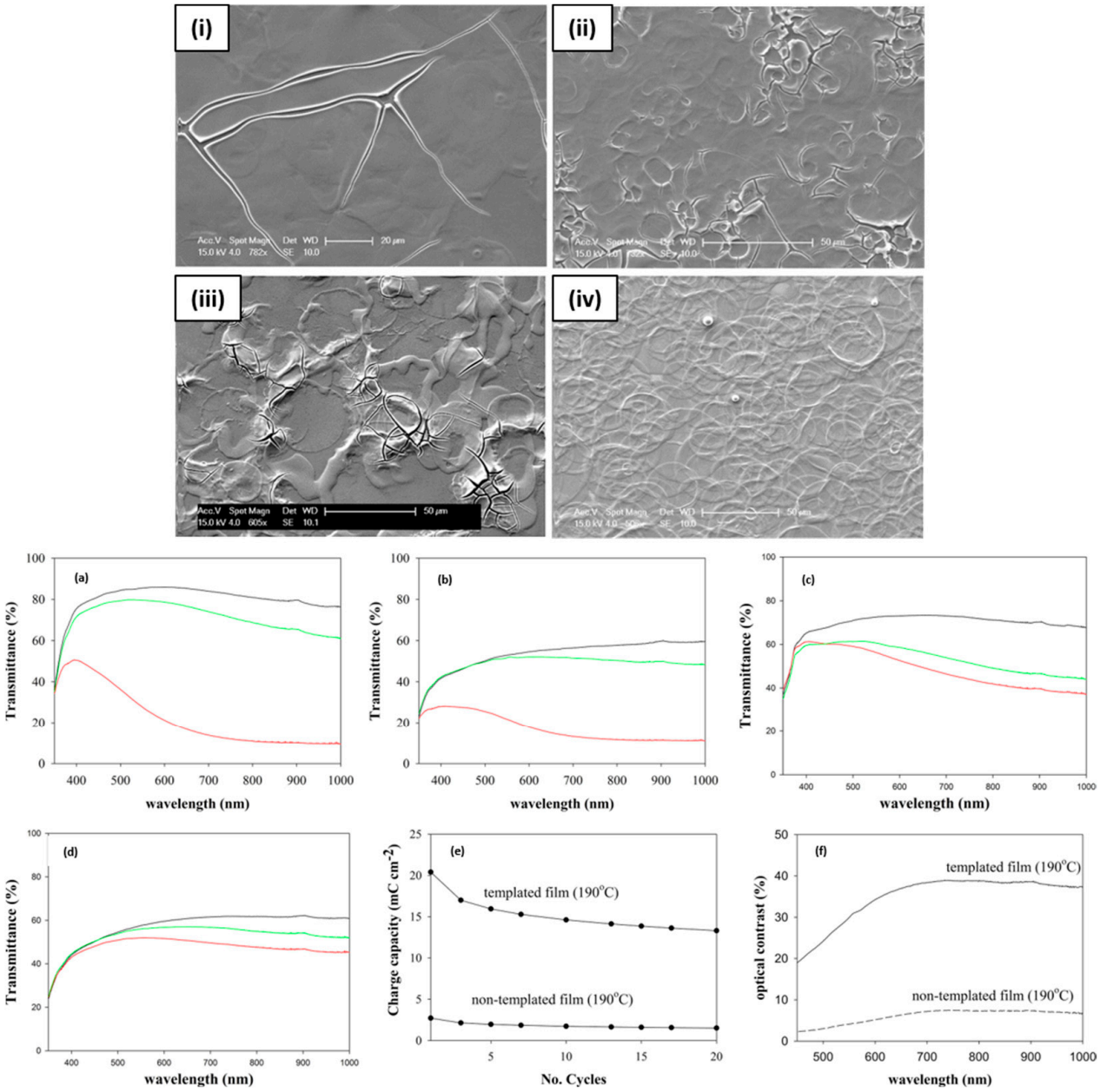


**Figure 9.** $WO_3$ thin films deposited by a surfactant-assisted ultrasonic spray pyrolysis: (**i**–**iv**) SEM micrographs and (**a**–**d**) UV-VIS spectra (green curve: as-deposited state; black curve: bleached state; red curve: colored state) of (**i**,**a**) templated films deposited at 100 °C and post-treated at 350 °C for 2 h; (**ii**,**b**) templated films deposited at 190 °C; (**iii**,**c**) non-templated films deposited at 100 °C and post-treated at 350 °C for 2 h; (**iv**,**d**) non-templated films deposited at 190 °C; (**e**) charge capacity evolution with the cycling of the templated and non-templated films (190 °C); (**f**) optical contrast after the cycling of the templated and non-templated films (190 °C) as a function of the wavelength. Reproduced with permission from [104]. Copyright 2023, Elsevier.

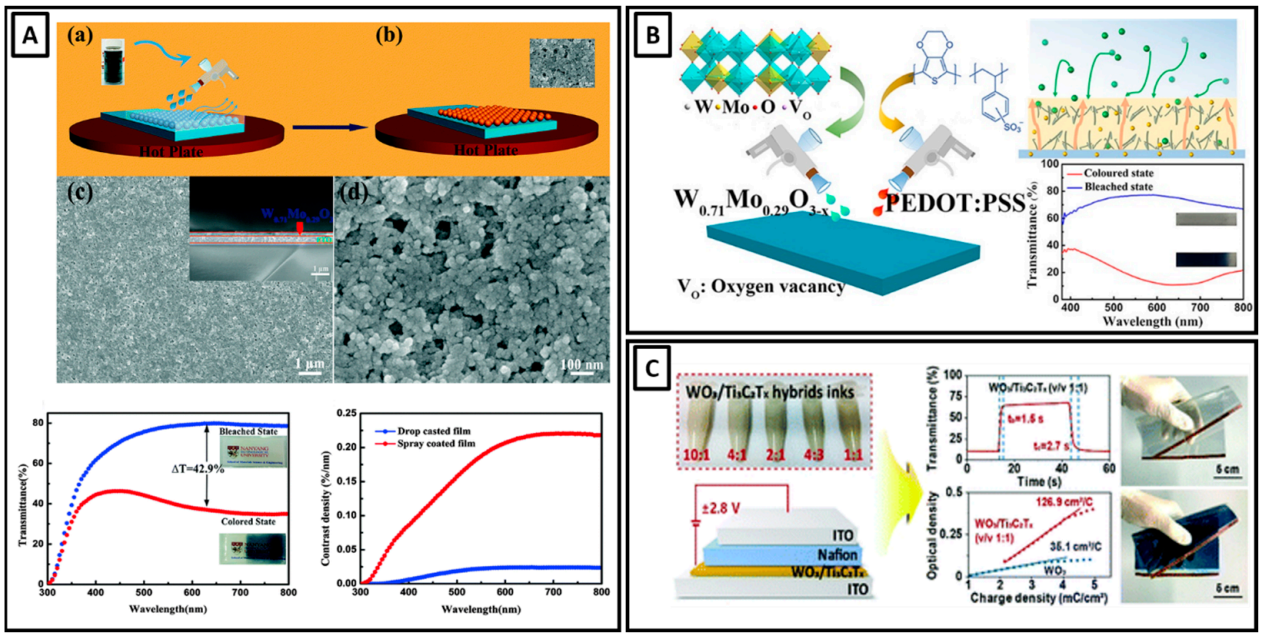


**Figure 10.** (**A**) Spray deposition (a) and drying (b) of $W_{0.71}Mo_{0.29}O_3$ films, with low- (c) and high-magnification (d) SEM images, UV-VIS transmittance spectra in colored and bleached states, and a contrast density of spray-coated and drop-casted films—reproduced with permission from [107] (Copyright 2023, RSC); (**B**) $W_{0.71}Mo_{0.29}O_3$/PEDOT:PSS electrodes prepared by layer-by-layer spray deposition and consecutive spectro-electrochemical measurements—reproduced with permission from [109] (Copyright 2023, ACS); (**C**) EC devices produced from $WO_3/Ti_3C_2T_x$ MXene hybrid inks and consecutive spectro-electrochemical measurements—reproduced with permission from [113] (Copyright 2023, RSC).

### *3.2. Nickel Oxide NiO*

NiO thin films are of high importance for many energy and optoelectronic applications, including semiconductors, sensors and photodetectors, solar cells, and, of course, electrochromic devices. NiO colors anodically by switching from transparent to brownish upon the oxidation of Ni(+II) into Ni(+III) and cation extraction. The presence of free hydroxyl ions and adsorbed water, as well as Ni vacancies inducing additional Ni(+III) content, also play crucial roles in the EC behavior and in the resulting optical and electrochemical properties. Typically used as a complementary counter electrode to $WO_3$, NiO is also praised as an individual EC material of a large dynamic contrast range, high coloration efficiency, good cyclic reversibility, and low material cost; however, its relatively poor stability and low charge capacity vs. $WO_3$ still somehow limit its widespread application in EC technology, and its coloration mechanism remains not fully understood due to the evolution of its chemical nature during the coloration/bleaching processes [43,68,115–118].

More than 35 articles on sprayed EC NiO have been referenced, with 26 (12) of them being published during the last 10 (5) years (Table 2). EC in NiO has been studied starting from the mid-1980s [119] and, specifically, by spray coating since 1995 and the pioneering study of J. Arakaki et al. [120], in which NiO layers were pyrolytically deposited at 400 °C and provided a 35% optical contrast in VIS and a 30 $cm^2/C$ CE. The impact of spray pyrolysis conditions has been screened in multiple following studies, notably in terms of the precursor nature (chlorides, nitrates, acetates), solvent (water, methanol, ethanol, isopropanol), and deposition and/or annealing temperature dependence (from 200 to 500 °C) [121–135]. Selected contributions from P. Patil [121], K. Abdel-Hady [122], S.-H. Lin [125], and C. Ravi Dhas [132] highlighted the maximal VIS $\Delta T$ between 20 and 60%, switching kinetics between 1 and 40 s, CE values of 8 to 44 $cm^2/C$, and cyclability tests performed up to 3000 runs.

**Table 2.** Review of spray-coated NiO layers in terms of spray conditions, resulting thickness, and EC metrics; N.p. means "not provided", O.D. means "optical density", and $T_{asdep}$ means "transmittance of the as-deposited sample".

| Reference | *Spray Conditions ($T_{dep}$ for Deposition Temperature, t.t. for Thermal Treatment)* | Thickness (nm) | $T_{ble}$ (%) | $T_{col}$ (%) | ΔT (%) | $t_{ble}$ (s) | $t_{col}$ (s) | CE ($cm^2$/C) | Cycling Runs |
|---|---|---|---|---|---|---|---|---|---|
| **Arakaki** [120] | $Ni(NO_3)_2$ in $H_2O$ $T_{dep}$ = 220–400 °C | *N.p.* | 50+ | *N.p.* | 35 | *N.p.* | *N.p.* | 30 | 100+ |
| **Patil** [121] | $NiCl_2$ in $H_2O$ $T_{dep}$ = 350 °C | 300 | 80 | 60 | 20 | 40 | 20 | 37 | 500 |
| **Mahmoud** [122] | $NiCl_2$ in $H_2O$ $T_{dep}$ = 350 °C | 50–200 | *N.p.* | *N.p.* | 2–23 | *N.p.* | *N.p.* | *N.p.* | 150 |
| **Wang** [123] | $Ni(NO_3)_2$ in $H_2O$ $T_{dep}$ = 200–400 °C | 4500 | *N.p.* | *N.p.* | *N.p.* | *N.p.* | *N.p.* | *N.p.* | *N.p.* |
| **Abdel-Hady** [124] | $NiCl_2$ in $H_2O$ $T_{dep}$ = 225–425 °C | 50–400 | 50–80 | 5–50 | 30–60 | 13 | 5 | 44 | 150 |
| **Lin** [125] | $Ni(NO_3)_2$ in ethanol $T_{dep}$ = 200 °C with t.t. at 300 °C | 500 | 20–30 | 70–80 | 48–51 | 9–10 | 7–12 | *N.p.* | 3000 |
| **Leinen** [126] | Ni acetate in $H_2O$ $T_{dep}$ = 350–450 °C | 230–840 | 20–70 ($T_{asdep}$) | *N.p.* | *N.p.* | *N.p.* | *N.p.* | *N.p.* | *N.p.* |
| **Ismail** [127] | $NiCl_2$ in $H_2O$ $T_{dep}$ = 280–400 °C | 200–900 | 65–70 ($T_{asdep}$) | *N.p.* | *N.p.* | *N.p.* | *N.p.* | *N.p.* | *N.p.* |
| **Sharma** [128] | $NiCl_2$ in $H_2O$ $T_{dep}$ = 350 °C | 70–110 | 60–90 ($T_{asdep}$) | *N.p.* | *N.p.* | *N.p.* | *N.p.* | *N.p.* | *N.p.* |
| **Sanjeeviraja** [129] | $NiCl_2$ in $H_2O$ $T_{dep}$ = 400 °C | 1100–2700 | 45–95 ($T_{asdep}$) | *N.p.* | *N.p.* | *N.p.* | *N.p.* | *N.p.* | *N.p.* |
| **Benhaoua** [130] | $Ni(NO_3)_2$ in $H_2O$ $T_{dep}$ = 500 °C | 170–200 | 45–85 ($T_{asdep}$) | *N.p.* | *N.p.* | *N.p.* | *N.p.* | *N.p.* | *N.p.* |
| **Gomaa** [131] | $NiCl_2$/$Ni(NO_3)_2$/$Ni(OCOCH_3)_2$ in $H_2O$ $T_{dep}$ = 450 °C | 270–300 | 35–50 ($T_{asdep}$) | *N.p.* | *N.p.* | *N.p.* | *N.p.* | *N.p.* | *N.p.* |
| **Chtouki** [132] | $NiCl_2$ in $H_2O$ $T_{dep}$ = 350 °C with t.t. at 500 °C | 390 | 75 ($T_{asdep}$) | *N.p.* | *N.p.* | *N.p.* | *N.p.* | *N.p.* | *N.p.* |
| **Ravi Dhas** [133] | $Ni(NO_3)_2$ in $H_2O$ $T_{dep}$ = 300 °C with t.t. at 400–550 °C | *N.p.* | *N.p.* | *N.p.* | 6–29 | 0.3–1.1 | 0.5–1.8 | 8–29 | 10 |
| **Obaida** [134] | Ni acetylacetonate in $H_2O$ $T_{dep}$ = 400–500 °C | 190–400 | 20–60 ($T_{asdep}$) | *N.p.* | *N.p.* | *N.p.* | *N.p.* | *N.p.* | 500 |
| **Krunks** [135] | Ni acetate in $H_2O$ and isopropanol $T_{dep}$ = 300–420 °C | 20–430 | 20–85 ($T_{asdep}$) | *N.p.* | *N.p.* | *N.p.* | *N.p.* | *N.p.* | *N.p.* |
| **Ortiz** [136] | Ni and Li acetates in $H_2O$ and methanol $T_{dep}$ = 360–440 °C | 300–1000 | 10–50 ($T_{asdep}$) | *N.p.* | *N.p.* | *N.p.* | *N.p.* | *N.p.* | *N.p.* |
| **Yahia** [137] | $NiCl_2$ + $AgNO_3$ in $H_2O$ $T_{dep}$ = 450 °C | 400–420 | *N.p.* | *N.p.* | *N.p.* | *N.p.* | *N.p.* | *N.p.* | *N.p.* |
| **Naik** [138] | $Ni(NO_3)_2$ + $Co(NO_3)_2$ in $H_2O$ $T_{dep}$ = 400 °C | 700 | 5–20 ($T_{asdep}$) | *N.p.* | *N.p.* | *N.p.* | *N.p.* | *N.p.* | *N.p.* |
| **Garcia-Lobato** [139] | Ni and Co acetates in $H_2O$ and EtOH $T_{dep}$ = 225 °C with t.t. at 300 °C | 310–380 | 50–60 | 4–6 | 46–54 | 13–18 | 18–25 | 27–32 | 65 |
| **Ganesan** [140] | $NiCl_2$ and $CoCl_2$ in $H_2O$ $T_{dep}$ = 300 °C | 350 | 55–85 ($T_{asdep}$) | *N.p.* | *N.p.* | *N.p.* | *N.p.* | *N.p.* | *N.p.* |
| **Ganesan** [141] | $NiCl_2$ and $CuCl_2$ in $H_2O$ $T_{dep}$ = 350 °C | *N.p.* | 35–50 ($T_{asdep}$) | *N.p.* | *N.p.* | *N.p.* | *N.p.* | *N.p.* | *N.p.* |
| **Manickam** [142] | $NiCl_2$ and $CuCl_2$ in $H_2O$ $T_{dep}$ = 450 °C | *N.p.* | 20–45 ($T_{asdep}$) | *N.p.* | *N.p.* | *N.p.* | *N.p.* | *N.p.* | *N.p.* |
| **Anslin Ferby** [143] | $Ni(NO_3)_2$ and $Mn(NO_3)_2$ in $H_2O$ $T_{dep}$ = 300 °C | *N.p.* | 60–75 | 30–45 | 29–37 | 0.2–1 | 0.4–1.1 | 29–105 | *N.p.* |
| **Jbilou** [144] | $NiCl_2$ and $InCl_3$ in $H_2O$ $T_{dep}$ = 450 °C | 120 | 60–70 | 22–47 | 24–38 | *N.p.* | *N.p.* | 31–94 | *N.p.* |

**Table 2.** *Cont.*

| Reference | *Spray Conditions ($T_{dep}$ for Deposition Temperature, t.t. for Thermal Treatment)* | Thickness (nm) | $T_{ble}$ (%) | $T_{col}$ (%) | $\Delta T$ (%) | $t_{ble}$ (s) | $t_{col}$ (s) | CE ($cm^2/C$) | Cycling Runs |
|---|---|---|---|---|---|---|---|---|---|
| **Mrabet** [145] | $NiCl_2$ and $LaCl_3$ in $H_2O$ $T_{dep}$ = 450 °C | *N.p.* | 30–55 ($T_{asdep}$) | *N.p.* | *N.p.* | *N.p.* | *N.p.* | *N.p.* | *N.p.* |
| **Dillon** [146] | $Ni(NO_3)_2$ and $LiNO_3$ in $H_2O$ $T_{dep}$ = 330 °C | *N.p.* | 83 | 33 | 50 | 57 | 29 | 33 | 50 |
| **Sahay** [147] | $Ni(NO_3)_2$ and Li acetate in $H_2O$ $T_{dep}$ = 400 °C with t.t. at 500 °C | *N.p.* | 78–85 | 55–75 | 10–25 | *N.p.* | *N.p.* | 3–35 | *N.p.* |
| **Cloots** [148] | $Ni(NO_3)_2$ + $LiNO_3$ + PEG in $H_2O$ $T_{dep}$ = 350 °C | 300 | 89–97 | 45–58 | 39–43 | 8–17 | 29–115 | 31–41 | 100 |
| **Cloots** [149] | $Ni(NO_3)_2$ + PEG in $H_2O$ $T_{dep}$ = 350 °C with t.t. at 350–600 °C | 200–300 | 70–80 | 65–70 | 5–10 | *N.p.* | *N.p.* | *N.p.* | 10 |
| **Torres-Torres** [150] | Ni acetate in PEG $T_{dep}$ = 250 °C | 110 | 75 | 30 | 45 | *N.p.* | *N.p.* | *N.p.* | *N.p.* |
| **Garcia-Lobato** [151] | $Ni(NO_3)_2$ + MWCNTs in ethanol $T_{dep}$ = 110 °C with t.t. at 350 °C | 110–200 | 80–90 | 10–30 | 40–80 | 2–7 | 4–10 | 26–31 | 5000 |
| **Garcia-Lobato** [152] | $Ni(NO_3)_2$ + MWCNTs in ethanol $T_{dep}$ = 110 °C | 20–245 | 80–95 | 35–40 | 45–55 | *N.p.* | *N.p.* | 25–30 | 5000 |
| **C.S. Lee** [63] | NiO powder $T_{dep}$ = RT-200 °C, NPDS | 400 | 75–80 ($T_{asdep}$) | *N.p.* | *55–65 (device)* | *N.p.* | *N.p.* | *N.p.* | *N.p.* |
| **Cai** [153] | NiO NPs in ethanol $T_{dep}$ not provided | 330–1600 | 90 | 10 | 83 | *N.p.* | *N.p.* | 76 | *N.p.* |
| **Dini** [154] | NiO NPs in alcohol $T_{dep}$ = RT with t.t. at 450 °C | 200–4000 | *N.p.* | *N.p.* | *N.p.* | *N.p.* | *N.p.* | *N.p.* | *N.p.* |
| **Dini** [155] | NiO NPs in methanol $T_{dep}$ = RT with t.t. at 450 °C | 200–3500 | *N.p.* | *N.p.* | *N.p.* | *N.p.* | *N.p.* | *N.p.* | 100 |

Doping strategies were attempted in several studies with Li [136], Ag [137], Co [138–140], Cu [141,142], Mn [143], In [144], and La [145] elements. In particular, Co doping led to interestingly high contrasts of 46%–54% [139], while increased CE values were reported with Mn (105 $cm^2/C$) [143] and In dopants (94 $cm^2/C$) [144]. Li doping was also shown to be successful for improving EC performances, notably by the teams of A. Dillon [146] and P. Sahay [147]. R. Cloots et al. also considered the Li doping of NiO layers [148], reporting a VIS $\Delta T$ enhanced from 39 to 44% and CE values from 31 to 41 $cm^2/C$, while the switching kinetics were slightly slowed down (from 2 to 12 s of $t_{col}$, and 8 to 17 s of $t_{ble}$); films of 300 nm thickness were ultrasonically sprayed at 350 °C without further post-treatment, using precursor solutions of $Ni(NO_3)_2$ and 5% $LiNO_3$ mixed with a PEG surfactant in a 3:1 mass ratio with Ni salt (Figure 11). The same PEG-assisted USP protocol was used in another study to generate undoped NiO layers whose Ni/O stoichiometry could be straightforwardly predicted from optical and electrochemical (impedance analysis) measurements [149].

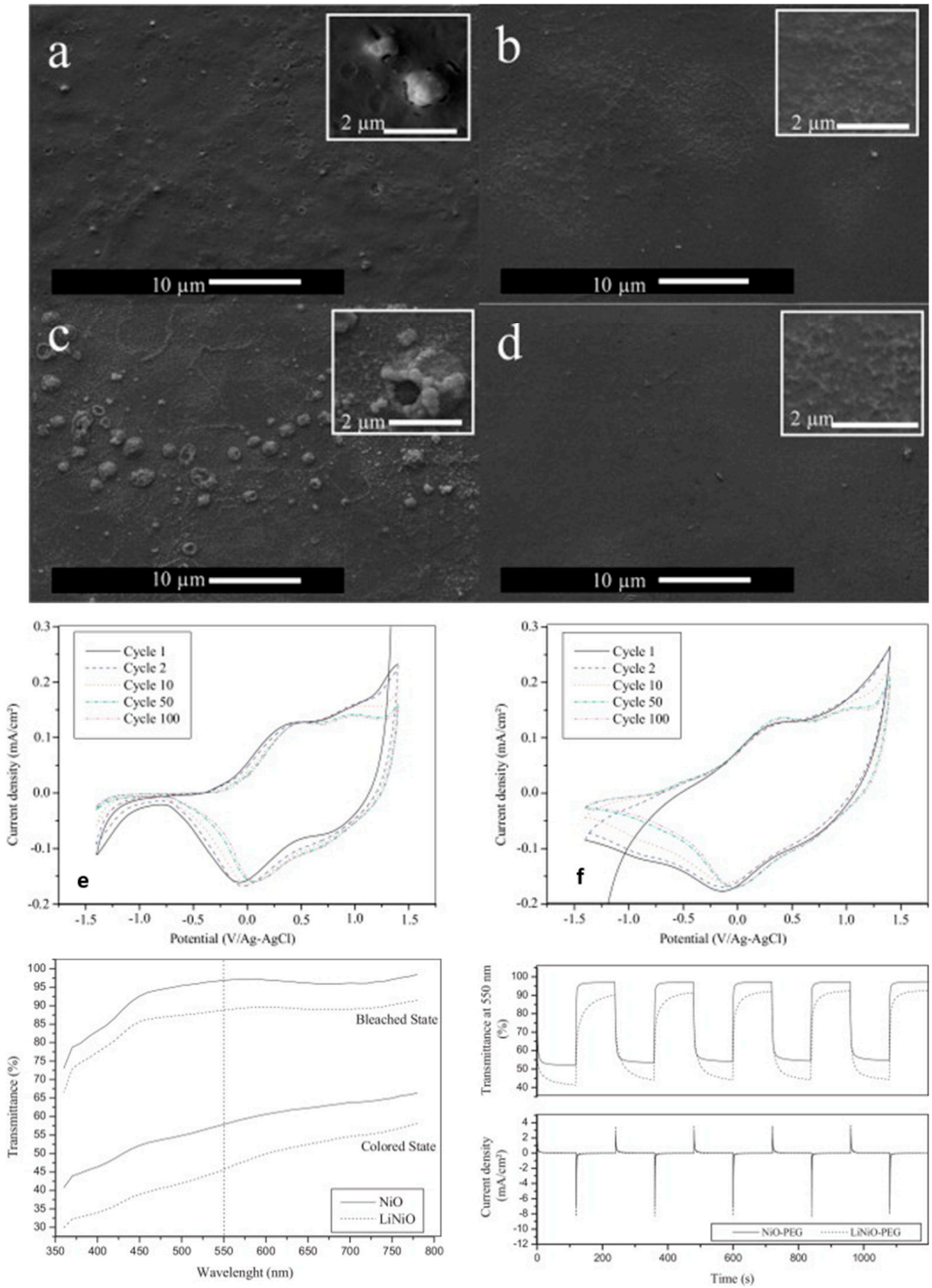


**Figure 11.** Top: scanning electron micrographs of (**a**) NiO, (**b**) NiO–PEG, (**c**) LiNiO, and (**d**) LiNiO–PEG thin films. Middle: cyclic voltammetry of (**e**) NiO–PEG and (**f**) LiNiO–PEG films. Bottom-left: UV–visible spectra of NiO–PEG and LiNiO–PEG thin films, both on their bleached and colored states. Bottom-right: spectroelectrochemical analysis (550 nm, chronoamperometry) of NiO–PEG and LiNiO–PEG films. Reproduced with permission from [148]. Copyright 2023, Elsevier.

Other teams further explored the impact of incorporating additives in the sprayed liquid fluid, including D. Torres-Torres et al., who used Ni acetate as a precursor and PEG as a solvent and surfactant, obtaining 110 nm thick films at a deposition temperature of

250 °C, showing a VIS Δ*T* of 45% (75–30) [150]. Also, M. Garcia-Lobato et al. showed the very promising effect of adding CNTs into a precursor $Ni(NO_3)_2$/ethanol solution being electrostatically sprayed at 110 °C into 20 to 250 nm thick films, obtaining high contrasts (up to 80%) and good CE values (up to 30 $cm^2$/C) after a quick thermal annealing of 1 min at 350 °C (Figure 12) [151,152].

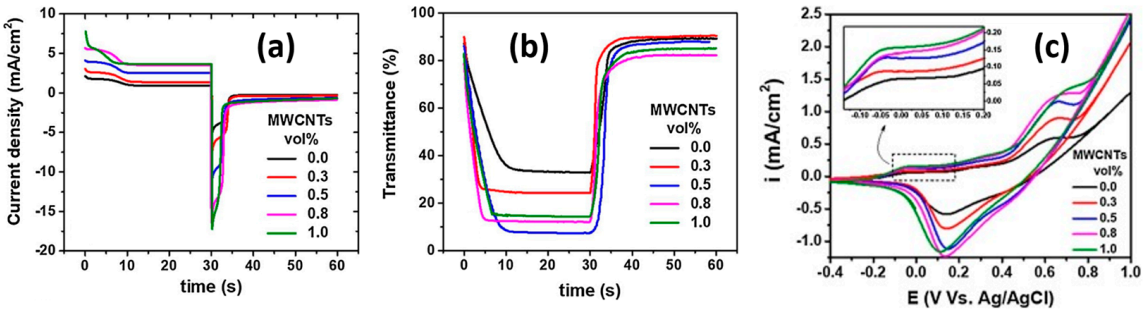


**Figure 12.** Chronoamperometry (**a**), in situ transmittance (**b**), and cyclic voltammetry curves (**c**) of NiO films containing different vol% values of MWCNTs. Reproduced with permission from [151]. Copyright 2023, Elsevier.

Similar to $WO_3$ formulations, the RT deposition of "pre-formed" NiO NPs was also considered quite recently for the "low energetical cost" spray fabrication of corresponding EC layers [63,153–155]. C.S. Lee et al. used their acknowledged kinetic spray approach (previously described) to design 400 nm thick films from different-sized NiO powders, showing diameters from 1–2 µm down to 20 nm; EC devices made by assembling these NiO counter-electrode materials with $WO_3$ counterparts presented 56%–65% VIS Δ*T* [63]. G. Cai et al. (Figure 13) considered an electrostatic spray deposition process with solvothermally synthesized NiO NPs dispersed in ethanol, leading to 330 to 1600 nm thick films, allowing for an extremely high optical contrast (more than 83%) and CE values (up to 76 $cm^2$/C) [153].

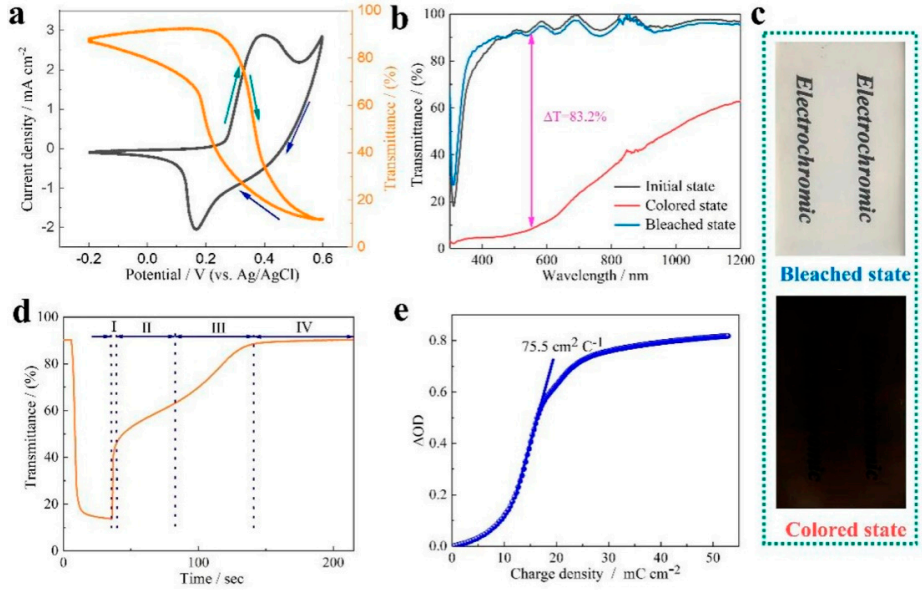


**Figure 13.** Electrochromic characteristics of NiO NPs-based thin films: (**a**) CV curve at 20 mV $s^{-1}$ (with green and blue arrows showing the oxidative and reducing waves, respectively) and in situ dynamic transmittance spectrum at 550 nm; (**b**) transmittance spectra in three optical states: the initial, coloration at +0.6 V, and bleaching at −0.2 V; (**c**) digital photographs in bleached and colored states; (**d**) in situ dynamic transmittance spectrum by coloring (30 s) and bleaching (180 s) at 550 nm; (**e**) optical density with a changed charge density at 550 nm. Reproduced with permission from [153]. Copyright 2023, ACS.

### *3.3. Vanadium Pentoxide $V_2O_5$*

The vanadium element exists in several oxidation states, namely, V(+III), V(+IV), and V(+V), involving multiple stoichiometries and phases that are often difficult to control. The $VO_2$ formulation is an acknowledged thermochromic material of great interest, as it exhibits a transition temperature at 68 °C (not too far from RT) combined with a conversion from a monoclinic to rutile crystal structure, and the $V_2O_3$ phase presents a phase transition coupled with a magnetic disordering varying with the temperature. The $V_2O_5$ stoichiometry, the most stable one, is well known as a performant battery material thanks to its layered structure, and also as a multicolor material exhibiting both anodic (coloring from green to orange–yellow) and cathodic EC (coloring into blue) as a result of the occurrence of various oxidation states associated with different colors; however, it generally suffers from low conductivity and instability during cycling [156–160].

Sprayed films of EC $V_2O_5$ have been reported in about 30 articles, among which 20 (13) were published over the last 10 (5) years (Table 3). Initiatory studies go back to the early 2000s with a.o. A. Bouzidi et al., who pyrolytically sprayed $V_2O_5$ layers at 250 °C from vanadium trichloride $VCl_3$ aqueous solutions [161], and C. Mathieu et al., who could lower the deposition temperature to 150 °C from similar precursor fluids [162]. P. Patil and co-workers followed with new protocols [163–166] mainly involving $VCl_3$ methanolic solutions sprayed between 300 and 450 °C (potentially with further annealing at 400 °C for 2 h), obtaining ~120 nm thick layers with up to 20% (50–30) of VIS $\Delta T$ between clear (oxidized) and dark (reduced) states and a CE of 10 to 15 $cm^2/C$ [163]. The same group then developed ~300 nm thick mixed layers of $V_2O_5$ and $MoO_3$ [164] or $WO_3$ [166] being (pulsed) spray pyrolyzed at 400 °C from $VCl_3$ solutions, leading to VIS contrasts of 7 to 25%, switching times of ~10 s, and CE values of 15 to 35 $cm^2/C$ ($V_2O_5$-$MoO_3$) or 49 $cm^2/C$ ($V_2O_5$-$WO_3$), being stable up to 1000 cycles (Figure 14). Other teams considered similar strategies [167–177] as well as doping approaches with aliovalent elements such as S [178], F [179], Li [180], In [181], and Mo [182]; in the latter case, the incorporation of 4% at. $MoCl_6$ powder into the $VCl_3$ aqueous precursor solution led to noticeably high values of VIS $\Delta T$ (67%) and CE (80 $cm^2/C$) in comparison with undoped and other doped (2, 6% at.) formulations [182]. More recently, $V_2O_5$ formulations hybridized with carbon-based materials led to interesting EC properties [183–186], in some cases being significantly enhanced with respect to the state-of-the-art: these notably involved metal-organic-frameworks (MOFs) containing vanadium (V) sprayed at RT to 50 °C, resulting in highly functional layers with a VIS $\Delta T$ of 46 to 55%, a mean response time of 1 to 3 s, a CE of 89 to 109 $cm^2/C$, and 81 to 96% of optical retention after several thousands of cycles [184,185]. Mixes of $V_2O_5$ with MXenes, especially $V_2C_2T_x$ formulations, led to even more increased figures of merits, with the VIS $\Delta T$ improved from 5 (pristine $V_2O_5$) to 54% ($V_2O_5$-MXene), the switching times reduced from 21–25 to 5–7 s, and the CE values raised from 5 to 91 $cm^2/C$ (Figure 15) [186].

**Table 3.** Review of spray-coated $V_2O_5$ layers in terms of the spray conditions, resulting thickness, and EC metrics; *N.p.* means "not provided", O.D. means "optical density", and $T_{asdep}$ means "transmittance of the as-deposited sample".

| Reference | *Spray Conditions ($T_{dep}$ for Deposition Temperature, t.t. for Thermal Treatment)* | Thickness (nm) | $T_{ble}$ (%) | $T_{col}$ (%) | $\Delta T$ (%) | $t_{ble}$ (s) | $t_{col}$ (s) | CE ($cm^2/C$) | Cycling Runs |
|---|---|---|---|---|---|---|---|---|---|
| **Bouzidi [161]** | $VCl_3$ in $H_2O$ $T_{dep}$ = 250 °C | *N.p.* | *N.p.* | *N.p.* | *N.p.* | *N.p.* | *N.p.* | *N.p.* | *N.p.* |
| **Mathieu [162]** | $VCl_3$ in $H_2O$ $T_{dep}$ = 150 °C | *N.p.* | 40 ($T_{asdep}$) | *N.p.* | *N.p.* | *N.p.* | *N.p.* | *N.p.* | *N.p.* |
| **Patil [163]** | $VCl_3$ in methanol $T_{dep}$ = 300 °C with t.t. at 400 °C | 120 | 49 | 32 | 17 | *N.p.* | *N.p.* | 13 | *N.p.* |
| **Patil [164]** | $VCl_3$ and $MoO_3$ in methanol $T_{dep}$ = 400 °C + t.t. at 400 °C | 130–370 | 45–61 | 23–44 | 13–24 | 9–11 | 9–11 | 15–35 | *N.p.* |

**Table 3.** *Cont.*

| Reference | *Spray Conditions ($T_{dep}$ for Deposition Temperature, t.t. for Thermal Treatment)* | Thickness (nm) | $T_{ble}$ (%) | $T_{col}$ (%) | $\Delta T$ (%) | $t_{ble}$ (s) | $t_{col}$ (s) | CE ($cm^2/C$) | Cycling Runs |
|---|---|---|---|---|---|---|---|---|---|
| **Patil** [165] | $VCl_3$ in methanol $T_{dep}$ = 300–500 °C | *N.p.* | 36–61 | 23–44 | 8–17 | *N.p.* | *N.p.* | 10–15 | *N.p.* |
| **Patil** [166] | $VCl_3$ and ammonium tungstate $T_{dep}$ = 400 °C | 300–370 | 48–61 | 27–44 | 7–22 | 10–20 | 9–23 | 15–49 | 1000 |
| **Kim** [167] | V tri-isopropoxide in ethanol $T_{dep}$ = 200 °C with t.t. at 200 °C | *N.p.* | 75 ($T_{asdep}$) | *N.p.* | *N.p.* | *N.p.* | *N.p.* | *N.p.* | *N.p.* |
| **Wei** [168] | $V_2O_5$ NPs in $H_2O$ $T_{dep}$ = RT with drying at 110 °C | 30–120 | 70–85 ($T_{asdep}$) | *N.p.* | *N.p.* | *N.p.* | *N.p.* | *N.p.* | *N.p.* |
| **Mohammad** [169] | $VCl_3$ in $H_2O$ $T_{dep}$ = 350 °C | *N.p.* | 75–80 ($T_{asdep}$) | *N.p.* | *N.p.* | *N.p.* | *N.p.* | *N.p.* | *N.p.* |
| **Ramamurthi** [170] | $NH_4VO_3$ in $H_2O$ $T_{dep}$ = 300–400 °C | *N.p.* | 62–78 ($T_{asdep}$) | *N.p.* | *N.p.* | *N.p.* | *N.p.* | *N.p.* | *N.p.* |
| **Eshghi** [171] | $VCl_3$ in $H_2O$ $T_{dep}$ not provided with t.t. at 200 °C | 600–2000 | 35–50 ($T_{asdep}$) | *N.p.* | *N.p.* | *N.p.* | *N.p.* | *N.p.* | *N.p.* |
| **Mouratis** [172] | $NH_4VO_3$ in $H_2O$ $T_{dep}$ = 250 °C with t.t. at 400 °C | 1000 | 18–26 | 6–8 | 10–20 | 16–34 | 10–35 | *N.p.* | *N.p.* |
| **Mouratis** [173] | $NH_4VO_3$ in $H_2O$ $T_{dep}$ = 250 °C with t.t. at 400 °C | N.p. | 40–43 | 31–32 | 8–12 | 15 | 10 | 4–6 | *N.p.* |
| **Chen** [174] | $V_2O_5$ powders $T_{dep}$ = RT with drying at 70 °C | 690–800 | 80–36 | 33–39 | 4–42 | 4–9 | 1–7 | 8–83 | 1000 |
| **Mahmoud** [175] | $V(NO_3)_5$ in $H_2O$ $T_{dep}$ = 350 °C with t.t. at 400–550 °C | 120–140 | 45–70 ($T_{asdep}$) | *N.p.* | *N.p.* | *N.p.* | *N.p.* | *N.p.* | *N.p.* |
| **Unalan** [176] | $VO(acac)_2$ and $V_2O_5$ in methanol $T_{dep}$ = 100 °C with t.t. at 450–550 °C | 60–80 | 75–94 | 64–94 | 0–18 | *N.p.* | *N.p.* | *N.p.* | 25 (1000 in devices) |
| **Suchea** [177] | $NH_4VO_3$ in $H_2O$ $T_{dep}$ = 250 °C with t.t. at 400 °C | 100–800 | 12–65 | 1–60 | 5–11 | 2–34 | 2–35 | *N.p.* | *N.p.* |
| **Mousavi** [178] | $VCl_3$ and $(NH_2)_2CS$ in $H_2O$ $T_{dep}$ = 400–450 °C | 110–270 | *N.p.* | *N.p.* | *N.p.* | *N.p.* | *N.p.* | *N.p.* | *N.p.* |
| **Abyazisani** [179] | $VCl_3$ and $NH_4F$ in $H_2O$ $T_{dep}$ = 450 °C | *N.p.* | *N.p.* | *N.p.* | *N.p.* | *N.p.* | *N.p.* | *N.p.* | *N.p.* |
| **Kovendhan** [180] | $VCl_3$ and LiCl in $H_2O$ $T_{dep}$ = 450 °C | 50–1400 | *N.p.* | *N.p.* | *N.p.* | *N.p.* | *N.p.* | *N.p.* | *N.p.* |
| **Tabatabai** [181] | $VCl_3$ and $InCl_3$ in $H_2O$ $T_{dep}$ = 430 °C | *N.p.* | *N.p.* | *N.p.* | *N.p.* | *N.p.* | *N.p.* | *N.p.* | *N.p.* |
| **Mrigal** [182] | $VCl_3$ and $MoCl_6$ in $H_2O$ $T_{dep}$ = 500 °C with t.t. at 400 °C | *N.p.* | 50–77 | 10–43 | 29–67 | *N.p.* | *N.p.* | 42–80 | *N.p.* |
| **Sreelatha** [183] | $NH_4VO_3$ and Triton-X 100 surfactant in $H_2O$; $T_{dep}$ = 300 °C with t.t. at 350–450 °C | 250 | 15–30 ($T_{asdep}$) | *N.p.* | *N.p.* | *N.p.* | *N.p.* | *N.p.* | *N.p.* |
| **Hsiao** [184] | $VCl_3$ and PEDOT:PSS $T_{dep}$ = RT with t.t. at 120 °C | *N.p.* | 68 | 14–42 | 20–46 | 3–7 | 4–8 | 39–89 | 10000 |
| **Wang** [185] | $VCl_3$ and 1,4-benzendicarboxylic acid and HTAB in $H_2O$/ethanol $T_{dep}$ = 50 °C with t.t. at 50 °C | *N.p.* | 29–73 | 22–49 | 20–55 | 1–2 | 1–3 | 20–109 | 2000 |
| **Kim** [186] | $V_2CT_x$ in $H_2O$ $T_{dep}$ = 70 °C with t.t. at 350 °C | 600–1500 | 49–59 | 5–44 | 5–54 | 5–25 | 7–21 | 5–91 | 200 |

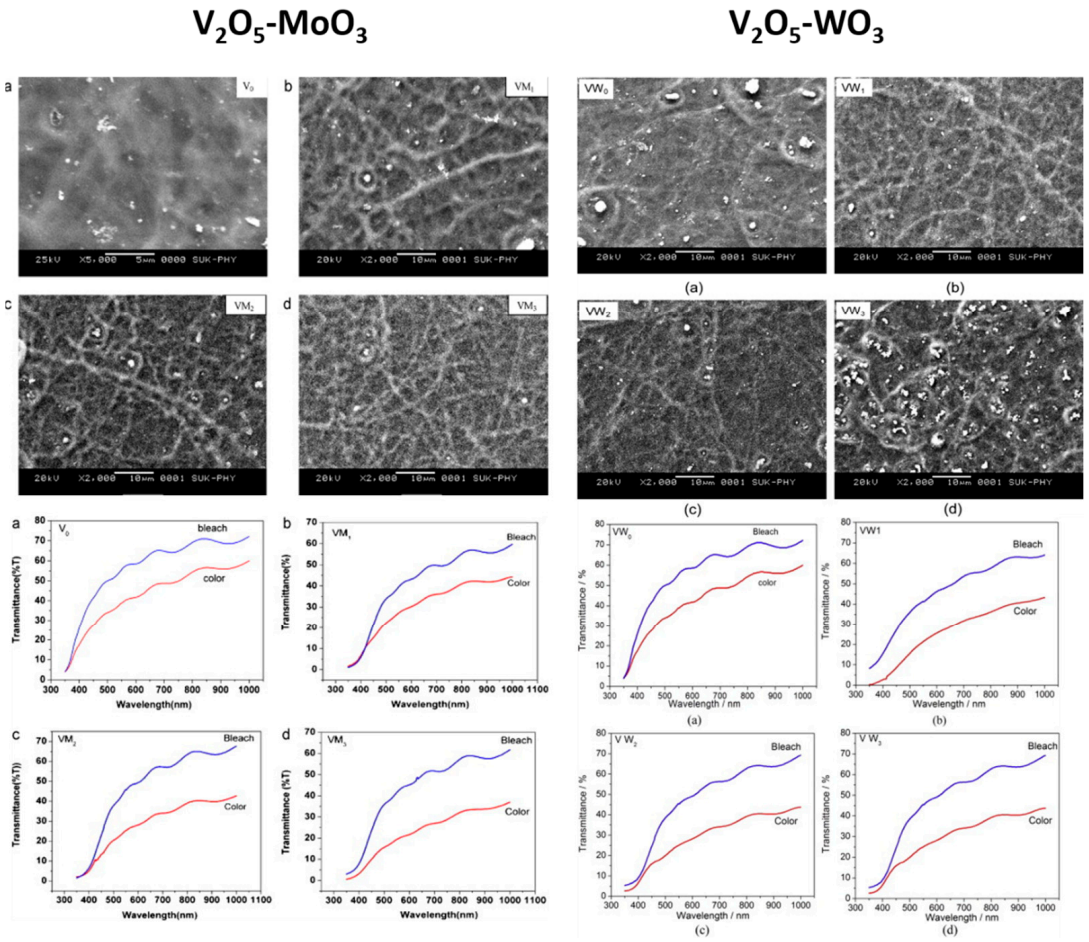


**Figure 14.** SEM micrographs and optical spectra of $V_2O_5$ thin films with various $MoO_3$ (**left**; reproduced with permission from [164]; copyright 2023, Elsevier) or $WO_3$ (**right**; reproduced with permission from [166]; copyright 2023, Elsevier) contents: (**a**) 0% ($V_0$/$VW_0$), (**b**) 5% ($VM_1$/$VW_1$), (**c**) 10% ($VM_2$/$VW_2$), and (**d**) 15% ($VM_3$/$VW_3$).

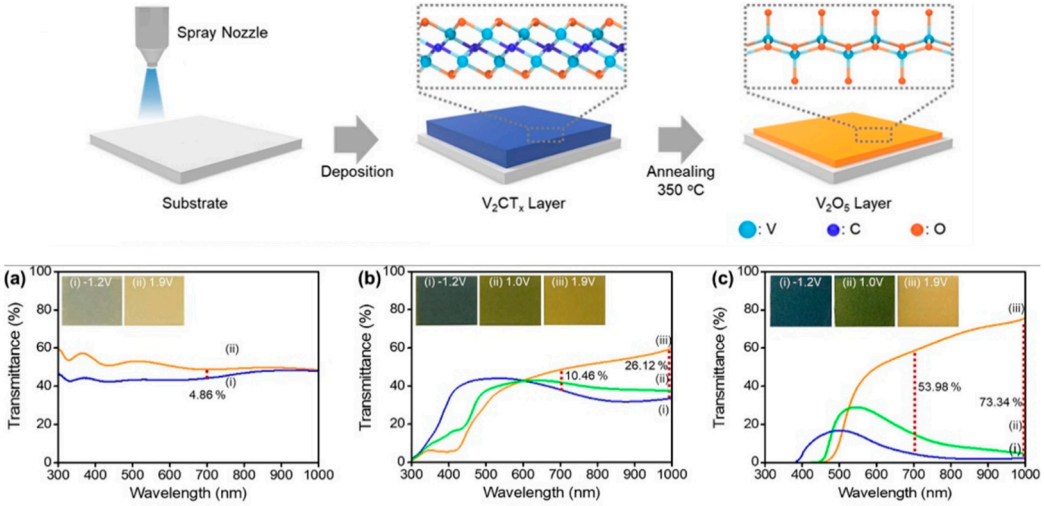


**Figure 15.** Spray-based fabrication of EC devices based on $V_2CT_x$-derived 2D $V_2O_5$ nanosheets. Transmittance spectra at (i) colored (−1.2 V), (ii) intermediate (+1.0 V), and (iii) bleached (+1.9 V) states of (**a**) $V_2O_5$ powder, (**b**) accordion-structured, and (**c**) 2D $V_2O_5$ nanosheet-based ECDs. Reproduced with permission from [186]. Copyright 2023, Elsevier.

### *3.4. Other Oxides*

Other EC oxides were also spray-coated into active EC films over the years, with about 30 related studies reported below (Table 4).

As cathodic EC oxides, one can cite:

- *$MoO_3$*, with works [187–190] reporting deposition protocols at high temperatures (250 to 400 °C), starting from precursor solutions constituting $MoCl_5$ salts or $MoO_3$ pre-formed powders and resulting in 100 to 550 nm thick layers with up to 23% of VIS optical contrast and 37 $cm^2/C$ of CE; further doping with W led to CE values improved up to 168 $cm^2/C$ [189].
- *$TiO_2$*, obtained as 100 to 800 nm thick layers from titanium alkoxide precursors at spray temperatures of 200 to 680 °C and showing VIS $\Delta T$ values as high as 61%, a switching time below 10 s, and CEs of 18 to 101 $cm^2/C$ [191–196]; selected articles investigated the further doping of $TiO_2$ with W [194], Nb [195], and Ni [196], the latter resulting in extremely high CE values of 474 $cm^2/C$ for 46% VIS $\Delta T$. $TiO_2$ layers can also be used as passive counter electrodes in assembled EC devices [191].
- *$Nb_2O_5$*, starting from $NbCl_5$ dissolved in water–ethanol mixes or from $Nb_2O_5$ pre-formed powders combined with tartaric acid, sprayed at 300–500 °C into 400–500 nm thick layers of 15%–40% VIS $\Delta T$, $t_{col}$ and $t_{ble}$ values below 10 s, and 4–26 $cm^2/C$ CEs [197–199].
- *$Bi_2O_3$*, spray-processed at 500 °C from bismuth carbonate aqueous solutions, into 125–450 nm thick films presenting 71% optical contrast and 12–18 $cm^2/C$ [200].
- *$SnO_2$*, for which P. Patil et al. explored various substrate temperatures between 450 and 500 °C for the pyrolytic transformation of tri-*n*-butyl tin acetate solutions into layers of 400–500 nm thickness [201]; a modest EC performance of 13% VIS optical contrast and 14 $cm^2/C$ of CE could be highlighted. In a later study, C.S. Lee and co-workers used pre-formed NPs of *Sb-doped $SnO_2$ (ATO)* for NPDS-based spray coating at RT, leading to a ~35% VIS transmittance change and a CE of 16 $cm^2/C$ [61].

More recently, D. Milliron, A. Maho and co-workers considered *indium-tin oxide (ITO)* nanocrystalline formulations for the spray deposition of VIS-transparent but NIR-modulating EC thin films. Owing to their plasmonic behavior (LSPR) and low carrier concentration (~$10^{20}$–$10^{21}$ $cm^{-3}$), ITO NCs strongly absorb NIR light between 1500 and 2000 nm; from there, their reversible electrochemical doping, when submitted to an external bias, achieves strong blue shifts in absorption intensity and frequency. With such electrochemical charging being capacitive and not faradic/intercalative, films of ITO NCs therefore exhibit unique NIR EC performances, including extremely fast switching kinetics, high CE, and extended cycling stability. Two articles accordingly reported the spray coating of such inks of ITO NCs synthesized either from solvothermal processing or from ligand-tuned Schlenk line colloidal methods. In the first case [202], ITO dispersions were straightforwardly deposited from low-toxic isopropanol media according to a RT procedure implying no harsh chemical or thermal post-treatment—only a mild drying step at 100 °C for 10 min; in situ spectroelectrochemical measurements completed on the films (of 70–415 nm thickness) showed appreciable NIR contrasts (up to 40%) upon electrochemical charge/discharge, together with a >80% VIS transmittance (Figure 16). The other study [203] introduced an original method for producing aqueous ITO inks by refunctionalizing the NCs' surface, previously stripped of their native hydrophobic ligands, with a hydrophilic poly(acrylic acid) polymer featuring a low density of methoxy-terminated poly(ethylene oxide) grafts (PAA-$mPEO_4$). The polymer-wrapped ITO NC thin films did show the fast, stable, and reversible EC modulation of NIR (up to 39%), without the need to remove the polymer after deposition, as long as a wrapping density of ~20% by mass was not overpassed (Figure 17).

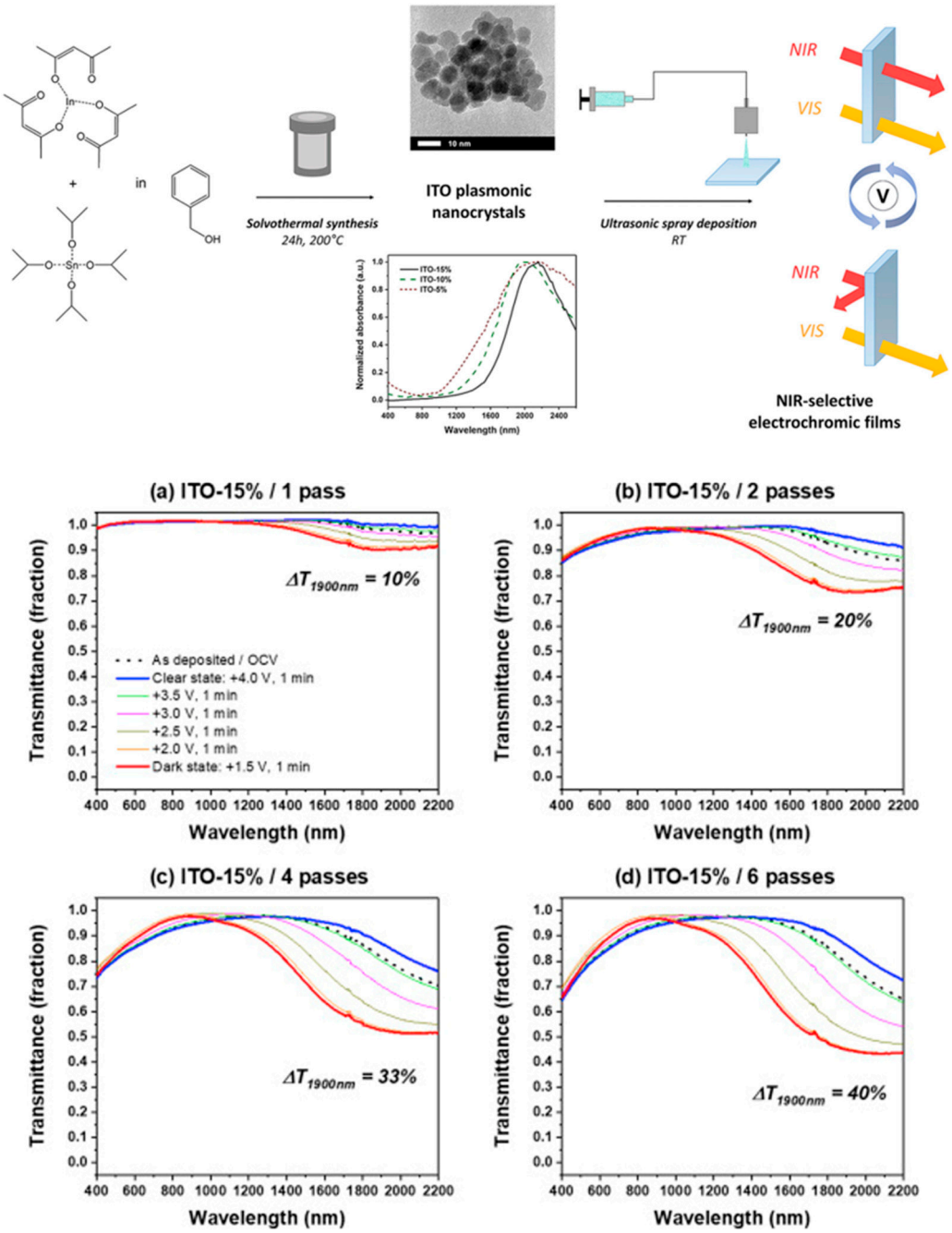


**Figure 16.** Solvothermally-synthesized ITO NCs with 5, 10, and 15% Sn doping (TEM, UV–VIS–NIR) spray-deposited as NIR EC coatings onto glass. Transmission spectra of ITO NCs (15% Sn doping) layers obtained from: (**a**) one pass, (**b**) two passes, (**c**) four passes and (**d**) six passes of the spray nozzle. Reproduced with permission from [202]. Copyright 2023, Elsevier.

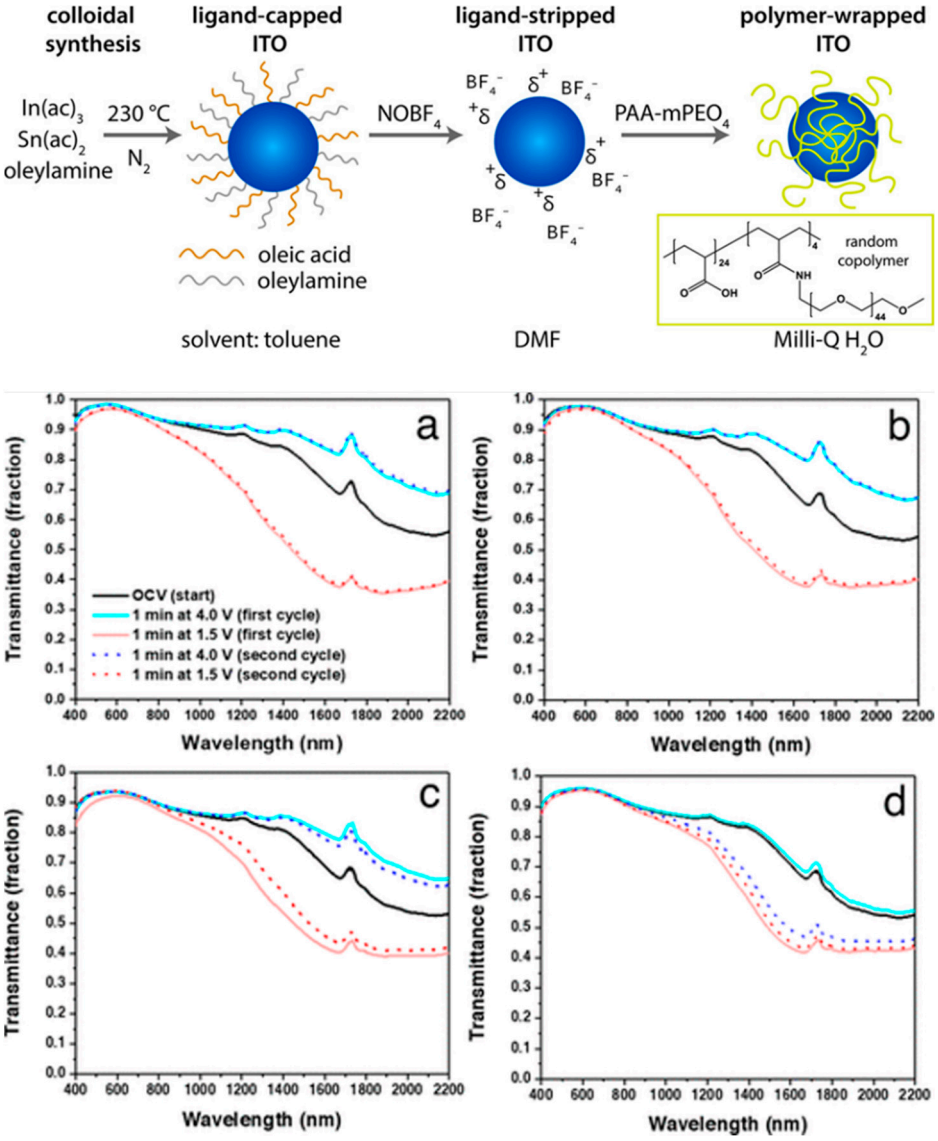


**Figure 17.** Aqueous processing and spray deposition of polymer-wrapped ITO NCs as EC thin films. Top: Illustration of the PAA-mPEO$_4$ wrapping procedure of ITO NCs. Bottom: EC modulation of ITO films spray-coated onto FTO glass from ITO aqueous dispersion in: (**a**) pH 9.1 borate buffer (10% polymer by mass), (**b**) pH 8.5 borate buffer (18% polymer by mass), (**c**) pH 7.9 borate buffer (22% polymer by mass), and (**d**) pH 6.5 Milli-Q water (28% polymer by mass). Reproduced with permission from [203]. Copyright 2023, ACS.

In terms of anodic EC oxides, *IrO*$_2$ [204–206] and *Mn*$_3$*O*$_4$ [207] were also sporadically considered for the spray coating of EC materials, using aqueous solutions of Ir ($IrCl_3$) and Mn ($MnCl_2$) chlorides as precursors and pyrolytic deposition conditions (250 to 520 °C for $IrO_2$, 350 °C for $Mn_3O_4$). Moderate optical contrasts—20%–30%—and CE values—13–26 cm$^2$/C—were obtained with films of various thicknesses—from 100 nm to several µm. Other authors also highlighted the interest in *Co*$_3$*O*$_4$ formulations [208–212], responding anodically but also cathodically as multicolor EC, reporting the spray pyrolysis deposition of corresponding layers of various thicknesses (500–1000 nm) at 300–400 °C from Co chloride or nitrate solutions and obtaining VIS $\Delta T$ values as high as 38%, switching times below 5 s, and CE values up to 47 cm$^2$/C.

EC devices can also integrate passive counter electrode materials instead of actively coloring compounds—such as NiO or $V_2O_5$ in complementarity with $WO_3$, as seen above. To this end, cerium oxide *CeO*$_2$ has been reported as an attractive material allowing for high

optical transparency in the VIS region together with an excellent ability to insert/extract large charge densities and to remain fully transparent regardless of its cationic content ($H^+$, $Li^+$...); however, its low chemical stability in lithium-based electrolytes remains a critical issue for its further large-scale development in EC systems [213–216]. The spray deposition of $CeO_2$ layers was considered in a few publications over the last 20 years, all focusing on the pyrolytic decomposition at 300 to 500 °C of chloride $CeCl_3$ or nitrate $Ce(NO_3)_2$ precursor salts being dissolved in water or in methanol. The first works by B. El Idrissi [217] and P. Patil [218] reported films of 300 to 800 nm thicknesses leading to elevated VIS transparency (generally over 80%) being maintained over several hundreds to thousands of charging/discharging cycles, with ion storage capacities of 20 C/cm$^2$. Consecutive studies further explored the effect of incorporating surfactants or doping with V [219,220], Zr [221], and Ti [222] elements; notably, the use of the last two dopants showed noticeable improvements in the EC performance when counter-electrodes of $CeO_2$-$ZrO_2$ or $CeO_2$-$TiO_2$ (respectively) were combined with $WO_3$ working electrodes, enhancing the CE values of corresponding devices from 42–47 ($CeO_2$ only) to 107 ($CeO_2$-$ZrO_2$) and even 231 cm$^2$/C ($CeO_2$-$TiO_2$).

**Table 4.** Review of spray-coated "other" metal oxide layers in terms of the deposition conditions, resulting thickness, and EC metrics; *N.p.* means "not provided".

| Reference | *Spray Conditions ($T_{dep}$ for Deposition Temperature, t.t. for Thermal Treatment)* | Thickness (nm) | $T_{ble}$ (%) | $T_{col}$ (%) | $\Delta T$ (%) | $t_{ble}$ (s) | $t_{col}$ (s) | CE (cm$^2$/C) | Cycling Runs |
|---|---|---|---|---|---|---|---|---|---|
| | | | | **$MoO_3$** | | | | | |
| **Patil** [187] | $MoO_3$ powder in $NH_4OH$ $T_{dep}$ = 350 °C | 1100 | *N.p.* | *N.p.* | *N.p.* | *N.p.* | *N.p.* | *N.p.* | *N.p.* |
| **Patil** [188] | $MoO_3$ powder in $NH_4OH$ and TiAcAc; $T_{dep}$ = 350 °C | 130–540 | 47 | 31 | 16 | *N.p.* | *N.p.* | 19–37 | 1000 |
| **Sahay** [189] | $MoCl_5$ + ammonium tungstate in methanol; $T_{dep}$ = 390 °C | *N.p.* | 5–25 | 2–17 | 3–8 | 1–5 | 1–25+ | 35–168 | 100 |
| **Unalan** [190] | $MoCl_5$ in $H_2O$ $T_{dep}$ = 300 °C | 100–200 | 42–49 | 21–34 | 15–23 | *N.p.* | *N.p.* | 16–32 | 20 |
| | | | | **$TiO_2$** | | | | | |
| **Patil** [191] | TiAcAc in methanol $T_{dep}$ = 350–450 °C | 200–400 | 65–85 | 50–80 | 5–10 | 3–4 | 4–5 | 3–4 | *N.p.* |
| **Sivakumar** [192] | Titanium isopropoxide in acetylacetone $T_{dep}$ = 200–350 °C with t.t. at 450 °C | 800–1300 | 59–88 | 27–37 | 32–61 | 2 | 3 | 22–101 | 100 |
| **Eshghi** [193] | Titanium isopropoxide in ethanol and acetylacetone $T_{dep}$ = 200 °C with t.t. at 450 °C | 300 | 90–95 | 45–75 | 17–53 | < 1 | 1–2 | 18–92 | *N.p.* |
| **Zelazowska** [194] | TiAcAc (and WAcAc) in dichloromethane and acetylacetone; $T_{dep}$ = 680 °C | 110 | 70 | 15–30 | 40–55 | *N.p.* | *N.p.* | *N.p.* | *N.p.* |
| **Zhao** [195] | $Ti(C_4H_9O)_4$ + $NbCl_5$ in acetylacetone and ethanol; $T_{dep}$ = 320–480 °C | 100–400 | 60–76 | 30–69 | 4–26 | 8–21 | 35–59 | *N.p.* | 1000 |
| **Sivakumar** [196] | Titanium isopropoxide and Ni acetate in ethanol and glycerol $T_{dep}$ = 200 °C with t.t. at 450 °C | 350–600 | 68–89 | 22–61 | 28–46 | 2 | 2–3 | 123–474 | 1000 |
| | | | | **$Nb_2O_5$** | | | | | |
| **Patil** [197] | $Nb_2O_5$ powder in tartaric acid $T_{dep}$ = 300–400 °C | 480 | 78 | 62 | 16 | 5 | 4 | 13 | 1000 |
| **Patil** [198] | $Nb_2O_5$ powder in tartaric acid $T_{dep}$ = 400 °C with t.t. at 500 °C | 450–480 | 77–87 | 62–78 | 8–15 | 4–5 | 3–4 | 10–13 | *N.p.* |
| **Romero** [199] | $NbCl_5$ in $H_2O$ and ethanol and acetic acid $T_{dep}$ = 350–500 °C with t.t. at 500–900 °C | 100–450 | 65 | 25–60 | 5–40 | 6 | 10 | 4–26 | 20 |

**Table 4.** *Cont.*

| Reference | *Spray Conditions ($T_{dep}$ for Deposition Temperature, t.t. for Thermal Treatment)* | Thickness (nm) | $T_{ble}$ (%) | $T_{col}$ (%) | ΔT (%) | $t_{ble}$ (s) | $t_{col}$ (s) | CE ($cm^2$/C) | Cycling Runs |
|---|---|---|---|---|---|---|---|---|---|
| | | | | **$Bi_2O_3$** | | | | | |
| **Bao** [200] | Bi carbonate in $H_2O$ $T_{dep}$ = 500 °C with t.t. at 550 °C | 125–450 | 81 | 10 | 71 | *N.p.* | *N.p.* | 12–18 | 4 |
| | | | | **$SnO_2$** | | | | | |
| **Patil** [201] | $(C_4H_9)_3Sn(OOCCH_3)$ in methanol $T_{dep}$ = 450–500 °C | 400–500 | 78–85 | 68–83 | 2–13 | <1 | <1 | 8–14 | *N.p.* |
| **C.S. Lee** [61] | Sb-doped $SnO_2$ NPs $T_{dep}$ = RT (NPDS) | 800 | 72–78 | 37–54 | 24–43 | ~1 | ~5 | 15 | 10 |
| | | | | **ITO** | | | | | |
| **Maho** [202] | ITO NPs in isopropanol $T_{dep}$ = RT with drying at 100 °C | 70–415 | 53–100 (in NIR) | 42–90 (in NIR) | 10–40 (in NIR) | *N.p.* | *N.p.* | *N.p.* | 10 |
| **Maho** [203] | ITO NPs in $H_2O$ $T_{dep}$ = RT | 130 | 59–75 (in NIR) | 36–42 (in NIR) | 17–39 (in NIR) | *N.p.* | *N.p.* | 535–802 | *N.p.* |
| | | | | **$IrO_2$** | | | | | |
| **Patil** [204] | $IrCl_3$ in $H_2O$ $T_{dep}$ = 250–400 °C | 100–1200 | 25–60 | 20–52 | 2–30 | 2 | 5–6 | 10–26 | *N.p.* |
| **Patil** [205] | $IrCl_3$ in $H_2O$ $T_{dep}$ = 250 °C | 1200–3900 | 37–47 | 27–38 | 3–20 | 2–3 | 2–5 | 10–59 | *N.p.* |
| **Hassanien** [206] | $IrCl_3$ in $H_2O$ $T_{dep}$ = 250–520 °C with t.t. at 600 °C | 100–350 | *N.p.* | *N.p.* | *N.p.* | *N.p.* | *N.p.* | *N.p.* | *N.p.* |
| | | | | **$Mn_3O_4$** | | | | | |
| **Sivakumar** [207] | $MnCl_2$ in $H_2O$ $Td_{ep}$ = 350 °C | 940–1700 | *N.p.* | *N.p.* | 16–23 | *N.p.* | *N.p.* | 4–18 | 100 |
| | | | | **$Co_3O_4$** | | | | | |
| **Patil** [208] | $CoCl_2$ in $H_2O$ $T_{dep}$ = 300 °C | 400 | 25 | 10 | 15 | 2 | 4 | *N.p.* | 1000 |
| **Sivakumar** [209] | $Co(NO_3)_2$ in $H_2O$ $T_{dep}$ = 300–400 °C | 700–1000 | 14–95 | 10–66 | 4–29 | 1–2 | 1–3 | 1–12 | *N.p.* |
| **Sivakumar** [210] | $Co(NO_3)_2{\cdot}6H_2O$ and $Mn(CH_3COO)_2$ in $H_2O$ $T_{dep}$ = 400 °C | 685–850 | 19–61 | 9–26 | 6–35 | 1–4 | 2–3 | 10–29 | *N.p.* |
| **Sivakumar** [211] | $Co(NO_3)_2$ and $Cr(NO_3)_2$ in $H_2O$ $T_{dep}$ = 400 °C | 680–785 | 29–45 | 7–32 | 8–38 | 2–4 | 2–3 | 3–47 | *N.p.* |
| **El Bachiri** [212] | $CoCl_2$ in $H_2O$ $T_{dep}$ = 350 °C | 500 | 40 | 10 | 31 | 2 | 4 | 19 | *N.p.* |
| | | | | **$CeO_2$** | | | | | |
| **El Idrissi** [217] | $CeCl_3$ in $H_2O$ $T_{dep}$ = 300–500 °C + t.t. at 300 °C | 300–800 | 80 ($T_{asdep}$) | *N/A* | *N/A* | *N/A* | *N/A* | *N/A* | 100 |
| **Patil** [218] | $Ce(NO_3)_2$ in methanol $T_{dep}$ = 300–450 °C | 500–790 | 85 ($T_{asdep}$) | *N/A* | *N/A* | *N/A* | *N/A* | *N/A* | 600 |
| **Patil** [219] | $Ce(NO_3)_2$ + $VCl_3$ in methanol $T_{dep}$ not provided | N.p. | 68 | 62 | 6 | *N.p.* | *N.p.* | *N.p.* | *N.p.* |
| **El Habib** [220] | $CeCl_3$ + $VCl_3$ in $H_2O$ $T_{dep}$ = 450 °C | *N.p.* | 50–65 ($T_{asdep}$) | *N/A* | <2 | *N/A* | *N/A* | *N/A* | 10 |
| **Patil** [221] | $Ce(NO_3)_2{\cdot}6H_2O$ and $Zr(NO_3)_2$ in methanol $T_{dep}$ = 400 °C | 540–600 | 86 ($T_{asdep}$) | *N/A* | *N/A* | <1 | *N/A* | *N/A* | 10000 |
| **Patil** [222] | $Ce(NO_3)_3$ and titanium isopropoxide in methanol; $T_{dep}$ = 400 °C | *N.p.* | 75 ($T_{asdep}$) | 72 | 3 | *N/A* | *N/A* | *N/A* | 30000 |

The processing of suitable electrolyte layers to be incorporated in EC device architectures also constitutes a critical and important challenge, with different types of relevant formulations of organic, inorganic, and organic–inorganic hybrid natures being conceivable. Most of them are (gel) polymer-based and are typically wet-deposited onto one

of the two active electrodes (working or counter), before being compressed with the other and laminated together. On the other hand, inorganic electrolyte layers such as transparent lithium phosphorous oxynitride (LiPON) and lithium silicate formulations (aluminosilicates, borosilicates, phosphosilicates) can also be used, typically being intercalated between the working and counter electrode layers in layer-by-layer deposition processes [26,223–225]. The use of metal oxide-based compounds as electrolyte species and of spray coating as a processing methodology in this context, both for (gel) lamination and consecutive film deposition approaches, is only but scarcely reported, with, notably, the patent of R. Cloots et al. [226] related to the 350 °C USP of lithium aluminosilicate LAS $Li_2O$–$Al_2O_3$–$SiO_2$ layers from an aqueous precursor solution mixed with a PEG surfactant. Nevertheless, other metal oxide formulations such as $Li_7La_3Zr_2O_{12}$ [227], $BaCe_{0.72}Zr_{0.2}Y_{0.2}O_3$ [228], or $Mg_{0.5}Ce_{0.2}Zr_{1.8}(PO_4)_3$ [229] have been successfully spray-processed as electrolyte layers in batteries and fuel cells devices and could certainly be exploited further in EC counterparts considering appropriate processing adaptations (to reach a suitable optical transparency).

Finally, the latest literature clearly shows that using spray-coating approaches for the design of advanced, highly-functional EC materials and devices keeps developing, also expanding to emerging formulations beyond the sole category of metal-oxide-based compounds, with micro- and mesoporous metal–organic frameworks (MOFs) and other organometallic materials, organic–halide hybrid perovskites, composite materials, and 2D MXenes. A few very recent studies from 2023 are worth a special mention here—notably, the work of A. Mazel et al. [230] on Zn-based highly oriented surface-anchored metal–organic frameworks (SurMOFs) as spray-coated EC thin films being reversibly switched in a few seconds from orange to dark blue by electrochemical reduction, leading to remarkable 105 $cm^2$/C CE values; in addition, interestingly, the color of the reduced state was shown to be easily changed from dark blue to cyan by modifying the electrolyte composition from LiTFSI-EMIMTFSI to pure EMIMTFSI. Also recently, P.S. Lee and co-workers did consider the spray processing of Fe-based metallo-supramolecular polymers (MSP-Fe) into uniform films exhibiting an excellent EC performance and energy storage property simultaneously, with reported ultrahigh values of CE (1104 $cm^2$/C), fast switching speeds (<2 s), and a large optical contrast (over 72%); large-scale semi-solid state EC systems of a 225 $cm^2$ area could be successfully manufactured by including MSP-Fe films, achieving uniform, fast, and reversible color variations all across the device [231]. Finally, spray coating was originally used by M. Gusatti et al. to prepare novel all-solid-state EC devices free of an ITO transparent conductive electrode, a $WO_3$ active EC layer, and $Li^+$ or any other liquid/gel electrolytes, obtained by spray-depositing a PEDOT:PSS solution on a tris-(8-hydroxyquinoline) aluminum(III) ($Alq_3$) film previously sprayed on a pre-formed Al-coated glass substrate [232]. The fabricated devices demonstrated a reversible and homogeneous color change between light-blue (off) and dark-blue (on) states, with CE values of 175 $cm^2$/C and stability demonstrated over a minimum of 150 cycles.

## 4. Conclusions and Outcomes

From this review of the state of the art, it appears clear that the obtention of EC layers and devices with excellent optical, charging, and transport properties relies on the robust and efficient processing of suitable metal oxide layers, among which $WO_3$, NiO, and $V_2O_5$ are the three main formulations of interest. As screened in this paper, they all show high levels of functionality and efficiency, both optically and electrochemically, leading to qualitative and quantitative figures of merit such as contrasts, kinetics, coloration efficiency, and cycling stability. Nevertheless, important shortcomings remain to be dealt with, notably in terms of precursors and production costs and of more favorable transition schemes from the lab to the industrial scale.

To this end, the proper selection of the fabrication process is one of the most critical issues: clearly, the spray-coating approach can be acknowledged as a versatile and suitable methodology for obtaining extremely homogeneous, adherent, and robust EC metal oxide

films of high functionality and very good performances, offering important advantages such as low operational costs, simple equipment facilities, atmospheric operation, reproducibility, rapid deposition speeds (over 100 nm/s), and a large surface coverage area as well as a high-throughput capacity. As a wet-based technique, it surely allows for an importantly lowered energy consumption compared to the vacuum processes that are mostly used in the current industrial production of EC materials, notably for glazing applications (smart windows). In comparison with other lab-scale wet approaches such as spin or dip coating, it is also one of the most promising film deposition techniques, if not the only one, that can be used first at the laboratory scale for quick and simple trials on small-area substrates but that can in the meantime be considered, and used, for larger-scale developments, with protocols being easily transferable towards industrial production levels and generation of meter-long devices.

However, the production of efficient (metal oxides) EC layers does not have to be based only on strategies of materials design (here, by spray coating) or on characterizations that focus on passing the performance evaluation through standard laboratory spectroscopic and electrochemical tools. One must also consider how the processing conditions are directly and indirectly related to the materials' uniformity, stability under device operating and aging conditions, scalability, as well as recyclability. In this context, spray deposition allows almost uniquely for the progressive adaptation and optimization of all coating parameters, with multiple different micro/nanostructures, crystallinities, surface states, and, ultimately, optical and electronic/electrochemical properties being accessible, directly depending on the fine tuning of spray protocols. As could be established from the present literature screening, these include the properties of the liquid solution feed, especially the nature of precursors (especially those of a corrosive and/or toxic nature, i.e., transitioning from chlorides or nitrate salts to alkoxy derivates such as acetates) and solvents (from hydrophobic alkanes, toluene and chloroform to esters, alcohols, and water), the viscosity, the load, etc. Also the thermal and atmospheric (gas nature and concentration, use of low-vacuum conditions) conditions of layer growth and post-treatment are of high importance, as well as the spray nozzle design, the positioning and movement with respect to the surface, which can lead to roll-to-roll fabrication capacities, the adaptation to various natures and dimensions of substrates, etc.

Still, the specific correlation between how the fundamental properties of the EC metal oxides (and other) materials are being influenced by the spray conditions/parameters and how they will specifically be addressed towards scale-up transfer remains quite rarely considered in most of the reviewed articles, with only a few articles briefly discussing it either as a rapid proof-of-concept final demonstration result or as a perspective work [45,111,113,186,231,233]. In our opinion, this is one of the most important challenges to be addressed in upcoming developments, as such aspects illustrate the critical importance and significance of understanding EC systems from the nano- and microscale in the constitutive individual materials and interfaces, to the process(ability) of assembled devices at a (very) large scale. The latter will be strongly dependent of the synthetic conditions, the processing methods and parameters, the compatibility between components, the functional and economic viability and durability, and the strength towards environmental conditions. These are worth being clearly established and developed in future R&D works, gathering the EC community of chemists, physicists, material scientists, and engineers upon building new foundations for a more robust and efficient large-scale fabrication of EC materials and devices at both academic and industrial levels.

**Author Contributions:** Conceptualization, A.M.; Formal Analysis, A.M., S.N. and F.G.; Writing—Original Draft Preparation, A.M.; Writing—Review and Editing, all authors; Project Administration, A.M., R.C. and A.R.; Funding Acquisition, A.M., R.C. and A.R. All authors have read and agreed to the published version of the manuscript.

**Funding:** The research is funded in France by the University of Bordeaux, with the support of Agence Nationale de la Recherche (A.N.R.) for A. Maho's "Chaire de Professeur Junior", and of Région

Nouvelle-Aquitaine (n° AAPR2023-2022-23944010), and in Belgium by the GREEnMat laboratory – University of Liège, with the support of the Fonds National de la Recherche (F.N.R.S.) under grant n° T.0125.20 (PLASMON_EC).

**Institutional Review Board Statement:** Not applicable.

**Informed Consent Statement:** Not applicable.

**Data Availability Statement:** Not applicable.

**Conflicts of Interest:** The authors declare no conflict of interest.

## List of Common Abbreviations (Alphabetic Order)

| | |
|---|---|
| AACVD | aerosol-assisted chemical vapor deposition |
| APCVD | atmospheric-pressure chemical vapor deposition |
| ATO | antimony-doped tin oxide |
| C | coulomb(s) |
| CE | coloration efficiency |
| CNTs | carbon nanotubes |
| CVD | chemical vapor deposition |
| DMF | N,N-dimethyl formamide |
| DC | direct current (sputtering) |
| EC | electrochromic |
| HTAB | hexadecyl trimetehyleammonium bromide |
| ITO | indium-tin oxide (or tin-doped indium oxide) |
| LSPR | localized surface plasmon resonance |
| MOFs | metal organic frameworks |
| NCs | nanocrystals |
| NIR | near-infrared |
| NPDS | nanoparticle deposition system |
| NPs | nanoparticles |
| OD | optical density |
| PANI | polyaniline |
| PEDOT:PSS | poly(3,4-ethylenedioxythiophene) polystyrene sulfonate |
| PEG | polyethylene glycol |
| PPy | polypyrrole |
| P123 | poly(ethylene glycol)-block-poly(propylene glycol)-block-poly(ethylene glycol) |
| P3HT | poly(3-hexylthiophene-2,5-diyl) |
| Q | charge density |
| RF | radio frequency (sputtering) |
| RT | room temperature |
| R&D | research and development |
| $t_{col}$ | coloration time |
| $t_{ble}$ | bleaching time |
| $T_{asdep}$ | transmittance of as-deposited state |
| $T_{ble}$ | transmittance of bleached state |
| $T_{col}$ | transmittance of colored state |
| $\Delta T$ | contrast—difference in transmittance values of bleached and colored states |
| UV | ultraviolet |
| V | volt(s) |
| VIS | visible |

## References

1. Platt, J.R. Electrochromism, a Possible Change of Color Producible in Dyes by an Electric Field. *J. Chem. Phys.* **1961**, *34*, 862–863. [CrossRef]
2. Deb, S.K. A Novel Electrophotographic System. *Appl. Opt.* **1969**, *8*, 192. [CrossRef]
3. Deb, S.K. Optical and Photoelectric Properties and Colour Centres in Thin Films of Tungsten Oxide. *Philos. Mag.* **1973**, *27*, 801–822. [CrossRef]
4. Lampert, C.M. Electrochromic Materials and Devices for Energy Efficient Windows. *Sol. Energy Mater.* **1984**, *11*, 1–27. [CrossRef]

5. Svensson, J.S.E.M.; Granqvist, C.G. Electrochromic Coatings for "Smart Windows". *Sol. Energy Mater.* **1985**, *12*, 391–402. [CrossRef]
6. Mortimer, R.J.; Rosseinsky, D.R.; Monk, P.M.S. (Eds.) *Electrochromic Materials and Devices*, 1st ed.; Wiley: New York, NY, USA, 2013; ISBN 978-3-527-33610-4.
7. Mortimer, R. Switching Colors with Electricity. *Am. Sci.* **2013**, *101*, 38. [CrossRef]
8. Park, S.-I.; Quan, Y.-J.; Kim, S.-H.; Kim, H.; Kim, S.; Chun, D.-M.; Lee, C.S.; Taya, M.; Chu, W.-S.; Ahn, S.-H. A Review on Fabrication Processes for Electrochromic Devices. *Int. J. Precis. Eng. Manuf.-Green Technol.* **2016**, *3*, 397–421. [CrossRef]
9. Wang, Y.; Runnerstrom, E.L.; Milliron, D.J. Switchable Materials for Smart Windows. *Annu. Rev. Chem. Biomol. Eng.* **2016**, *7*, 283–304. [CrossRef]
10. Granqvist, C.G.; Arvizu, M.A.; Bayrak Pehlivan, İ.; Qu, H.-Y.; Wen, R.-T.; Niklasson, G.A. Electrochromic Materials and Devices for Energy Efficiency and Human Comfort in Buildings: A Critical Review. *Electrochim. Acta* **2018**, *259*, 1170–1182. [CrossRef]
11. Shchegolkov, A.V.; Jang, S.-H.; Shchegolkov, A.V.; Rodionov, Y.V.; Sukhova, A.O.; Lipkin, M.S. A Brief Overview of Electrochromic Materials and Related Devices: A Nanostructured Materials Perspective. *Nanomaterials* **2021**, *11*, 2376. [CrossRef]
12. Guo, J.; Liang, Y.; Zhang, S.; Ma, D.; Yang, T.; Zhang, W.; Li, H.; Cao, S.; Zou, B. Recent Progress in Improving Strategies of Metal Oxide-Based Electrochromic Smart Window. *Green Energy Resour.* **2023**, *1*, 100007. [CrossRef]
13. Hopmann, E.; Zhang, W.; Li, H.; Elezzabi, A.Y. Advances in Electrochromic Device Technology through the Exploitation of Nanophotonic and Nanoplasmonic Effects. *Nanophotonics* **2023**, *12*, 637–657. [CrossRef] [PubMed]
14. Zheng, J.Y.; Sun, Q.; Cui, J.; Yu, X.; Li, S.; Zhang, L.; Jiang, S.; Ma, W.; Ma, R. Review on Recent Progress in $WO_3$-Based Electrochromic Films: Preparation Methods and Performance Enhancement Strategies. *Nanoscale* **2023**, *15*, 63–79. [CrossRef]
15. Kandpal, S.; Ghosh, T.; Rani, C.; Chaudhary, A.; Park, J.; Lee, P.S.; Kumar, R. Multifunctional Electrochromic Devices for Energy Applications. *ACS Energy Lett.* **2023**, *8*, 1870–1886. [CrossRef]
16. Gu, C.; Jia, A.-B.; Zhang, Y.-M.; Zhang, S.X.-A. Emerging Electrochromic Materials and Devices for Future Displays. *Chem. Rev.* **2022**, *122*, 14679–14721. [CrossRef]
17. Beaujuge, P.M.; Reynolds, J.R. Color Control in π-Conjugated Organic Polymers for Use in Electrochromic Devices. *Chem. Rev.* **2010**, *110*, 268–320. [CrossRef]
18. Österholm, A.M.; Nhon, L.; Shen, D.E.; Dejneka, A.M.; Tomlinson, A.L.; Reynolds, J.R. Conquering Residual Light Absorption in the Transmissive States of Organic Electrochromic Materials. *Mater. Horiz.* **2022**, *9*, 252–260. [CrossRef]
19. Welsh, T.A.; Draper, E.R. Water Soluble Organic Electrochromic Materials. *RSC Adv.* **2021**, *11*, 5245–5264. [CrossRef]
20. Liu, Q.; Yang, L.; Ling, W.; Guo, B.; Chen, L.; Wang, J.; Zhang, J.; Wang, W.; Mo, F. Organic Electrochromic Energy Storage Materials and Device Design. *Front. Chem.* **2022**, *10*, 1001425. [CrossRef]
21. Granqvist, C.G. Electrochromics for Smart Windows: Oxide-Based Thin Films and Devices. *Thin Solid Films* **2014**, *564*, 1–38. [CrossRef]
22. Patel, K.J.; Bhatt, G.G.; Ray, J.R.; Suryavanshi, P.; Panchal, C.J. All-Inorganic Solid-State Electrochromic Devices: A Review. *J. Solid State Electrochem.* **2017**, *21*, 337–347. [CrossRef]
23. Xiong, S.; Yin, S.; Wang, Y.; Kong, Z.; Lan, J.; Zhang, R.; Gong, M.; Wu, B.; Chu, J.; Wang, X. Organic/Inorganic Electrochromic Nanocomposites with Various Interfacial Interactions: A Review. *Mater. Sci. Eng. B* **2017**, *221*, 41–53. [CrossRef]
24. Tao, C.; Li, Y.; Wang, J. The Progress of Electrochromic Materials Based on Metal–Organic Frameworks. *Coord. Chem. Rev.* **2023**, *475*, 214891. [CrossRef]
25. Lahav, M.; van der Boom, M.E. Polypyridyl Metallo-Organic Assemblies for Electrochromic Applications. *Adv. Mater.* **2018**, *30*, 1706641. [CrossRef]
26. Ding, Y.; Wang, M.; Mei, Z.; Diao, X. Different Ion-Based Electrolytes for Electrochromic Devices: A Review. *Sol. Energy Mater. Sol. Cells* **2022**, *248*, 112037. [CrossRef]
27. Eh, A.L.; Tan, A.W.M.; Cheng, X.; Magdassi, S.; Lee, P.S. Recent Advances in Flexible Electrochromic Devices: Prerequisites, Challenges, and Prospects. *Energy Technol.* **2018**, *6*, 33–45. [CrossRef]
28. Yang, G.; Zhang, Y.-M.; Cai, Y.; Yang, B.; Gu, C.; Zhang, S.X.-A. Advances in Nanomaterials for Electrochromic Devices. *Chem. Soc. Rev.* **2020**, *49*, 8687–8720. [CrossRef]
29. Rai, V.; Singh, R.S.; Blackwood, D.J.; Zhili, D. A Review on Recent Advances in Electrochromic Devices: A Material Approach. *Adv. Eng. Mater.* **2020**, *22*, 2000082. [CrossRef]
30. Liang, Y.; Cao, S.; Guo, J.; Zeng, R.; Zhao, J.; Zou, B. Dual-Band Electrochromic Smart Window Based on Single-Component Nanocrystals. *ACS Appl. Electron. Mater.* **2022**, *4*, 5109–5118. [CrossRef]
31. Tandon, B.; Lu, H.-C.; Milliron, D.J. Dual-Band Electrochromism: Plasmonic and Polaronic Mechanisms. *J. Phys. Chem. C* **2022**, *126*, 9228–9238. [CrossRef]
32. Bai, T.; Li, W.; Fu, G.; Zhang, Q.; Zhou, K.; Wang, H. Dual-Band Electrochromic Smart Windows towards Building Energy Conservation. *Sol. Energy Mater. Sol. Cells* **2023**, *256*, 112320. [CrossRef]
33. Zhai, Y.; Li, J.; Shen, S.; Zhu, Z.; Mao, S.; Xiao, X.; Zhu, C.; Tang, J.; Lu, X.; Chen, J. Recent Advances on Dual-Band Electrochromic Materials and Devices. *Adv. Funct. Mater.* **2022**, *32*, 2109848. [CrossRef]
34. Gong, H.; Li, W.; Fu, G.; Zhang, Q.; Liu, J.; Jin, Y.; Wang, H. Recent Progress and Advances in Electrochromic Devices Exhibiting Infrared Modulation. *J. Mater. Chem. A* **2022**, *10*, 6269–6290. [CrossRef]

35. Huang, L.; Cao, S.; Liang, Y.; Chen, J.; Yang, T.; Zhao, J.; Zou, B. Advances in multicolor electrochromic devices based on inorganic materials. *J. Mater. Chem. C* **2023**, *11*, 10107–10120. [CrossRef]
36. Bian, C.; Wang, J.; Liu, H.; Yan, Y.; Zhang, P.; Yang, W.; Jia, S.; Guo, X.; Cai, G. Complementary multicolor electrochromic devices with excellent stability based on porous tin oxide nanosheet scaffold. *Nano Res.* **2023**. [CrossRef]
37. Runnerstrom, E.L.; Llordés, A.; Lounis, S.D.; Milliron, D.J. Nanostructured Electrochromic Smart Windows: Traditional Materials and NIR-Selective Plasmonic Nanocrystals. *Chem. Commun.* **2014**, *50*, 10555–10572. [CrossRef]
38. Kriegel, I.; Scotognella, F.; Manna, L. Plasmonic Doped Semiconductor Nanocrystals: Properties, Fabrication, Applications and Perspectives. *Phys. Rep.* **2017**, *674*, 1–52. [CrossRef]
39. Agrawal, A.; Cho, S.H.; Zandi, O.; Ghosh, S.; Johns, R.W.; Milliron, D.J. Localized Surface Plasmon Resonance in Semiconductor Nanocrystals. *Chem. Rev.* **2018**, *118*, 3121–3207. [CrossRef]
40. Padilla, J.; Niklaus, L.; Schott, M.; Posset, U.; Faceira, B.; Mjejri, I.; Rougier, A.; Alesanco, Y.; Viñuales, A.; Shen, D.E.; et al. Quantitative Assessment of the Cycling Stability of Different Electrochromic Materials and Devices. *ACS Appl. Opt. Mater.* **2023**, *1*, 1174–1183. [CrossRef]
41. Gesheva, K.; Ivanova, T.; Bodurov, G.; Szilágyi, I.M.; Justh, N.; Kéri, O.; Boyadjiev, S.; Nagy, D.; Aleksandrova, M. Technologies for Deposition of Transition Metal Oxide Thin Films: Application as Functional Layers in "Smart Windows" and Photocatalytic Systems. *J. Phys. Conf. Ser.* **2016**, *682*, 012011. [CrossRef]
42. Wang, Z.; Kang, Y.; Zhao, S.; Zhu, J. Self-Limiting Assembly Approaches for Nanoadditive Manufacturing of Electronic Thin Films and Devices. *Adv. Mater.* **2020**, *32*, 1806480. [CrossRef]
43. Ukoba, K.O.; Eloka-Eboka, A.C.; Inambao, F.L. Review of Nanostructured NiO Thin Film Deposition Using the Spray Pyrolysis Technique. *Renew. Sustain. Energy Rev.* **2018**, *82*, 2900–2915. [CrossRef]
44. Rahemi Ardekani, S.; Sabour Rouh Aghdam, A.; Nazari, M.; Bayat, A.; Yazdani, E.; Saievar-Iranizad, E. A Comprehensive Review on Ultrasonic Spray Pyrolysis Technique: Mechanism, Main Parameters and Applications in Condensed Matter. *J. Anal. Appl. Pyrolysis* **2019**, *141*, 104631. [CrossRef]
45. Li, X.; Perera, K.; He, J.; Gumyusenge, A.; Mei, J. Solution-Processable Electrochromic Materials and Devices: Roadblocks and Strategies towards Large-Scale Applications. *J. Mater. Chem. C* **2019**, *7*, 12761–12789. [CrossRef]
46. Butt, M.A. Thin-Film Coating Methods: A Successful Marriage of High-Quality and Cost-Effectiveness—A Brief Exploration. *Coatings* **2022**, *12*, 1115. [CrossRef]
47. Coating & Dispensing Technology—KEYENCE. Available online: https://www.keyence.com/ss/products/measure/sealing/coater-type/spray.jsp (accessed on 21 September 2023).
48. Uniform Thin Film Layers of Functional Nanomaterials—Sono-Tek. Available online: https://www.sono-tek.com/industry/alternative-energy-nanomaterials/cnt-nanowires-and-other-nanomaterials/ (accessed on 21 September 2023).
49. Abdellah, A.; Fabel, B.; Lugli, P.; Scarpa, G. Spray Deposition of Organic Semiconducting Thin-Films: Towards the Fabrication of Arbitrary Shaped Organic Electronic Devices. *Org. Electron.* **2010**, *11*, 1031–1038. [CrossRef]
50. Wengeler, L.; Schmitt, M.; Peters, K.; Scharfer, P.; Schabel, W. Comparison of Large Scale Coating Techniques for Organic and Hybrid Films in Polymer Based Solar Cells. *Chem. Eng. Process. Process Intensif.* **2013**, *68*, 38–44. [CrossRef]
51. Eslamian, M. Spray-on Thin Film PV Solar Cells: Advances, Potentials and Challenges. *Coatings* **2014**, *4*, 60–84. [CrossRef]
52. Aziz, F.; Ismail, A.F. Spray Coating Methods for Polymer Solar Cells Fabrication: A Review. *Mater. Sci. Semicond. Process.* **2015**, *39*, 416–425. [CrossRef]
53. Slegers, S.; Linzas, M.; Drijkoningen, J.; D'Haen, J.; Reddy, N.; Deferme, W. Surface Roughness Reduction of Additive Manufactured Products by Applying a Functional Coating Using Ultrasonic Spray Coating. *Coatings* **2017**, *7*, 208. [CrossRef]
54. Sriram, S.R.; Parne, S.R.; Pothukanuri, N.; Edla, D.R. Prospects of Spray Pyrolysis Technique for Gas Sensor Applications—A Comprehensive Review. *J. Anal. Appl. Pyrolysis* **2022**, *164*, 105527. [CrossRef]
55. Parida, B.; Singh, A.; Kalathil Soopy, A.K.; Sangaraju, S.; Sundaray, M.; Mishra, S.; Liu, S.; Najar, A. Recent Developments in Upscalable Printing Techniques for Perovskite Solar Cells. *Adv. Sci.* **2022**, *9*, 2200308. [CrossRef] [PubMed]
56. Ma, S.; Sansoni, S.; Gatti, T.; Fino, P.; Liu, G.; Lamberti, F. Research Progress on Homogeneous Fabrication of Large-Area Perovskite Films by Spray Coating. *Crystals* **2023**, *13*, 216. [CrossRef]
57. Liu, H.; Jiang, W.; Malshe, A. Novel Nanostructured Hydroxyapatite Coating for Dental and Orthopedic Implants. *JOM* **2009**, *61*, 67–69. [CrossRef]
58. Nakaruk, A.; Sorrell, C.C. Conceptual Model for Spray Pyrolysis Mechanism: Fabrication and Annealing of Titania Thin Films. *J. Coat. Technol. Res.* **2010**, *7*, 665–676. [CrossRef]
59. Viguié, J.C.; Spitz, J. Chemical Vapor Deposition at Low Temperatures. *J. Electrochem. Soc.* **1975**, *122*, 585–588. [CrossRef]
60. Siefert, W. Properties of Thin $In_2O_3$ and $SnO_2$ Films Prepared by Corona Spray Pyrolysis, and a Discussion of the Spray Pyrolysis Process. *Thin Solid Films* **1984**, *120*, 275–282. [CrossRef]
61. Kim, H.; Park, Y.; Choi, D.; Ahn, S.-H.; Lee, C.S. Novel Fabrication of an Electrochromic Antimony-Doped Tin Oxide Film Using a Nanoparticle Deposition System. *Appl. Surf. Sci.* **2016**, *377*, 370–375. [CrossRef]
62. Kim, H.; Choi, D.; Kim, K.; Chu, W.; Chun, D.-M.; Lee, C.S. Effect of Particle Size and Amorphous Phase on the Electrochromic Properties of Kinetically Deposited $WO_3$ Films. *Sol. Energy Mater. Sol. Cells* **2018**, *177*, 44–50. [CrossRef]

63. Kim, H.; Kim, K.; Choi, D.; Lee, M.; Chu, W.-S.; Ahn, S.-H.; Chun, D.-M.; Lee, C.S. Microstructural Control of the Electrochromic and Ion Storage Layers on the Performance of an Electrochromic Device Fabricated by the Kinetic Spray Technique. *Int. J. Precis. Eng. Manuf.-Green Technol.* **2018**, *5*, 231–238. [CrossRef]
64. Kim, K.; Choi, D.; Kim, H.; Lee, M.; Chu, W.; Ahn, S.-H.; Chun, D.-M.; Lee, C.S. Investigation of Varying Particle Sizes of Dry-Deposited $WO_3$ Particles in Relation to Performance of Electrochromic Cell. *Int. J. Precis. Eng. Manuf.-Green Technol.* **2018**, *5*, 409–414. [CrossRef]
65. Choi, D.; Son, M.; Im, T.; Ahn, S.-H.; Lee, C.S. Microstructure Control of NiO-Based Ion Storage Layer with Various Sized NiO Particles to Evaluate the Electrochromic Performance. *Mater. Chem. Phys.* **2020**, *249*, 123121. [CrossRef]
66. Donnadieu, A. *Studies of Polycrystalline $WO_3$ and $MoO_3$ Coatings Prepared by Chemical Vapor Deposition*; Lampert, C.M., Granqvist, C.-G., Eds.; Society of Photo-Optical Instrumentation Engineers (SPIE): Hamburg, Germany, 1990; p. 103040C.
67. Bange, K. Colouration of Tungsten Oxide Films: A Model for Optically Active Coatings. *Sol. Energy Mater. Sol. Cells* **1999**, *58*, 1–131. [CrossRef]
68. Niklasson, G.A.; Granqvist, C.G. Electrochromics for Smart Windows: Thin Films of Tungsten Oxide and Nickel Oxide, and Devices Based on These. *J. Mater. Chem.* **2007**, *17*, 127–156. [CrossRef]
69. Deb, S.K. Opportunities and Challenges in Science and Technology of $WO_3$ for Electrochromic and Related Applications. *Sol. Energy Mater. Sol. Cells* **2008**, *92*, 245–258. [CrossRef]
70. Wang, F.; Di Valentin, C.; Pacchioni, G. Semiconductor-to-Metal Transition in $WO_{3-X}$: Nature of the Oxygen Vacancy. *Phys. Rev. B* **2011**, *84*, 073103. [CrossRef]
71. Buch, V.R.; Chawla, A.K.; Rawal, S.K. Review on Electrochromic Property for $WO_3$ Thin Films Using Different Deposition Techniques. *Mater. Today Proc.* **2016**, *3*, 1429–1437. [CrossRef]
72. Craigen, D.; Mackintosh, A.; Hickman, J.; Colbow, K. Spray Deposition and Properties of Electrochromic Tungsten Oxide Films. *J. Electrochem. Soc.* **1986**, *133*, 1529–1530. [CrossRef]
73. Zhang, J.; Wessel, S.A.; Colbow, K. Spray Pyrolysis Elecrochromic $WO_3$ Films: Electrical and X-Ray Diffraction Measurements. *Thin Solid Films* **1990**, *185*, 265–277. [CrossRef]
74. Zhang, J.; Colbow, K. Optical Properties of Pyrolytic Spray Deposited Electrochromic Tungsten Trioxide Films. *Appl. Phys. Lett.* **1991**, *58*, 1013–1014. [CrossRef]
75. Judeinstein, P.; Livage, J. *Electrochromic Properties of Sol-Gel Derived $WO_3$ Coatings*; Mackenzie, J.D., Ulrich, D.R., Eds.; Society of Photo-Optical Instrumentation Engineers (SPIE): San Diego, CA, USA, 1990; p. 344.
76. Gómez, M.; Medina, A.; Estrada, W. Improved Electrochromic Films of $NiO_x$ and $WO_xPy$ Obtained by Spray Pyrolysis. *Sol. Energy Mater. Sol. Cells* **2000**, *64*, 297–309. [CrossRef]
77. Regragui, M.; Addou, M.; Outzourhit, A.; Bernéde, J.C.; El Idrissi, E.; Benseddik, E.; Kachouane, A. Preparation and Characterization of Pyrolytic Spray Deposited Electrochromic Tungsten Trioxide Films. *Thin Solid Films* **2000**, *358*, 40–45. [CrossRef]
78. Regragui, M.; Addou, M.; Outzourhit, A.; El Idrissi, E.; Kachouane, A.; Bougrine, A. Electrochromic Effect in $WO_3$ Thin Films Prepared by Spray Pyrolysis. *Sol. Energy Mater. Sol. Cells* **2003**, *77*, 341–350. [CrossRef]
79. Patil, P.R.; Patil, P.S. Preparation of Mixed Oxide $MoO_3$–$WO_3$ Thin Films by Spray Pyrolysis Technique and Their Characterisation. *Thin Solid Films* **2001**, *382*, 13–22. [CrossRef]
80. Patil, P.S.; Mujawar, S.H.; Inamdar, A.I.; Sadale, S.B. Electrochromic Properties of Spray Deposited $TiO_2$-Doped $WO_3$ Thin Films. *Appl. Surf. Sci.* **2005**, *250*, 117–123. [CrossRef]
81. Bathe, S.R.; Patil, P.S. Titanium Doping Effects in Electrochromic Pulsed Spray Pyrolysed $WO_3$ Thin Films. *Solid State Ion.* **2008**, *179*, 314–323. [CrossRef]
82. Mujawar, S.H.; Inamdar, A.I.; Betty, C.A.; Cerc Korošec, R.; Patil, P.S. Electrochromism in Composite $WO_3$–$Nb_2O_5$ Thin Films Synthesized by Spray Pyrolysis Technique. *J. Appl. Electrochem.* **2011**, *41*, 397–403. [CrossRef]
83. Mujawar, S.; Dhale, B.; Patil, P.S. Electrochromic Properties of Layered $Nb_2O_5$-$WO_3$ Thin Films. *Mater. Today Proc.* **2020**, *23*, 430–436. [CrossRef]
84. Bathe, S.R.; Patil, P.S. Electrochromic Characteristics of Pulsed Spray Pyrolyzed Polycrystalline $WO_3$ Thin Films. *Smart Mater. Struct.* **2008**, *18*, 025004. [CrossRef]
85. Kadam, P.M.; Tarwal, N.L.; Mali, S.S.; Deshmukh, H.P.; Patil, P.S. Enhanced Electrochromic Performance of F-MWCNT-$WO_3$ Composite. *Electrochim. Acta* **2011**, *58*, 556–561. [CrossRef]
86. Kadam, P.M.; Tarwal, N.L.; Shinde, P.S.; Patil, R.S.; Deshmukh, H.P.; Patil, P.S. From Beads-to-Wires-to-Fibers of Tungsten Oxide: Electrochromic Response. *Appl. Phys. A* **2009**, *97*, 323–330. [CrossRef]
87. Sivakumar, R.; Moses Ezhil Raj, A.; Subramanian, B.; Jayachandran, M.; Trivedi, D.C.; Sanjeeviraja, C. Preparation and Characterization of Spray Deposited N-Type $WO_3$ Thin Films for Electrochromic Devices. *Mater. Res. Bull.* **2004**, *39*, 1479–1489. [CrossRef]
88. Zelazowska, E.; Rysiakiewicz-Pasek, E. $WO_3$-Based Electrochromic System with Hybrid Organic–Inorganic Gel Electrolytes. *J. Non-Cryst. Solids* **2008**, *354*, 4500–4505. [CrossRef]
89. Mukherjee, R.; Sahay, P.P. Effect of Precursors on the Microstructural, Optical, Electrical and Electrochromic Properties of $WO_3$ Nanocrystalline Thin Films. *J. Mater. Sci. Mater. Electron.* **2015**, *26*, 6293–6305. [CrossRef]
90. de León, J.M.O.-R.; Acosta, D.R.; Pal, U.; Castañeda, L. Improving Electrochromic Behavior of Spray Pyrolised WO3 Thin Solid Films by Mo Doping. *Electrochim. Acta* **2011**, *56*, 2599–2605. [CrossRef]

91. Kumar, A.; Prajapati, C.S.; Sahay, P.P. Modification in the Microstructural and Electrochromic Properties of Spray-Pyrolysed $WO_3$ Thin Films upon Mo Doping. *J. Sol-Gel Sci. Technol.* **2019**, *90*, 281–295. [CrossRef]
92. Mukherjee, R.; Prajapati, C.S.; Sahay, P.P. Tin-Incorporation Induced Changes in the Microstructural, Optical, and Electrical Behavior of Tungsten Oxide Nanocrystalline Thin Films Grown Via Spray Pyrolysis. *J. Therm. Spray Technol.* **2014**, *23*, 1445–1455. [CrossRef]
93. Acosta, D.R.; Magaña, C.; Hernández, F.; Ortega, J. Electrical, Optical and Electrochromic Properties of Ti:$WO_3$ Thin Films Deposited by the Pulsed Chemical Spray Technique. *Thin Solid Films* **2015**, *594*, 207–214. [CrossRef]
94. Mukherjee, R.; Sahay, P.P. Improved Electrochromic Performance in Sprayed $WO_3$ Thin Films upon Sb Doping. *J. Alloys Compd.* **2016**, *660*, 336–341. [CrossRef]
95. Dalenjan, F.A.; Bagheri-Mohagheghi, M.M.; Shirpay, A. The Study of Structural, Optical and Electrochromic Properties of $WO_3$:Co:Ni Thin Films Deposited by Spray Pyrolysis. *Opt. Quant. Electron.* **2022**, *54*, 711. [CrossRef]
96. Dalenjan, F.A.; Bagheri–Mohagheghi, M.M.; Shirpay, A. The Effect of Cobalt (Co) Concentration on Structural, Optical, and Electrochemical Properties of Tungsten Oxide ($WO_3$) Thin Films Deposited by Spray Pyrolysis. *J. Solid State Electrochem.* **2022**, *26*, 401–408. [CrossRef]
97. Li, C.-P.; Lin, F.; Richards, R.M.; Engtrakul, C.; Dillon, A.C.; Tenent, R.C.; Wolden, C.A. Ultrasonic Spray Deposition of High Performance $WO_3$ Films Using Template-Assisted Sol–Gel Chemistry. *Electrochem. Commun.* **2012**, *25*, 62–65. [CrossRef]
98. Li, C.-P.; Lin, F.; Richards, R.M.; Engtrakul, C.; Tenent, R.C.; Wolden, C.A. The Influence of Sol–Gel Processing on the Electrochromic Properties of Mesoporous $WO_3$ Films Produced by Ultrasonic Spray Deposition. *Sol. Energy Mater. Sol. Cells* **2014**, *121*, 163–170. [CrossRef]
99. Li, C.-P.; Engtrakul, C.; Tenent, R.C.; Wolden, C.A. Scalable Synthesis of Improved Nanocrystalline, Mesoporous Tungsten Oxide Films with Exceptional Electrochromic Performance. *Sol. Energy Mater. Sol. Cells* **2015**, *132*, 6–14. [CrossRef]
100. Bertus, L.M.; Enesca, A.; Duta, A. Influence of Spray Pyrolysis Deposition Parameters on the Optoelectronic Properties of WO3 Thin Films. *Thin Solid Films* **2012**, *520*, 4282–4290. [CrossRef]
101. Bertus, L.M.; Faure, C.; Danine, A.; Labrugere, C.; Campet, G.; Rougier, A.; Duta, A. Synthesis and Characterization of WO3 Thin Films by Surfactant Assisted Spray Pyrolysis for Electrochromic Applications. *Mater. Chem. Phys.* **2013**, *140*, 49–59. [CrossRef]
102. Denayer, J.; Aubry, P.; Bister, G.; Spronck, G.; Colson, P.; Vertruyen, B.; Lardot, V.; Cambier, F.; Henrist, C.; Cloots, R. Improved Coloration Contrast and Electrochromic Efficiency of Tungsten Oxide Films Thanks to a Surfactant-Assisted Ultrasonic Spray Pyrolysis Process. *Sol. Energy Mater. Sol. Cells* **2014**, *130*, 623–628. [CrossRef]
103. Maho, A.; Nicolay, S.; Manceriu, L.; Spronck, G.; Henrist, C.; Cloots, R.; Vertruyen, B.; Colson, P. Comparison of Indium Tin Oxide and Indium Tungsten Oxide as Transparent Conductive Substrates for $WO_3$-Based Electrochromic Devices. *J. Electrochem. Soc.* **2016**, *164*, H25. [CrossRef]
104. Chatzikyriakou, D.; Maho, A.; Cloots, R.; Henrist, C. Ultrasonic Spray Pyrolysis as a Processing Route for Templated Electrochromic Tungsten Oxide Films. *Microporous Mesoporous Mater.* **2017**, *240*, 31–38. [CrossRef]
105. Hu, A.; Jiang, Z.; Kuai, C.; McGuigan, S.; Nordlund, D.; Liu, Y.; Lin, F. Uncovering Phase Transformation, Morphological Evolution, and Nanoscale Color Heterogeneity in Tungsten Oxide Electrochromic Materials. *J. Mater. Chem. A* **2020**, *8*, 20000–20010. [CrossRef]
106. Gesheva, K.A.; Ivanova, T.; Hamelmann, F. Electrically Activated Thin Film Optical Coatings as Functional Layers in Electrochromic Devices. *Sol. Energy Mater. Sol. Cells* **2006**, *90*, 2532–2541. [CrossRef]
107. Li, H.; Chen, J.; Cui, M.; Cai, G.; Lee-Sie Eh, A.; See Lee, P.; Wang, H.; Zhang, Q.; Li, Y. Spray Coated Ultrathin Films from Aqueous Tungsten Molybdenum Oxide Nanoparticle Ink for High Contrast Electrochromic Applications. *J. Mater. Chem. C* **2016**, *4*, 33–38. [CrossRef]
108. Li, H.; McRae, L.; Firby, C.J.; Elezzabi, A.Y. Rechargeable Aqueous Electrochromic Batteries Utilizing Ti-Substituted Tungsten Molybdenum Oxide Based $Zn^{2+}$ Ion Intercalation Cathodes. *Adv. Mater.* **2019**, *31*, 1807065. [CrossRef]
109. Li, H.; McRae, L.; Elezzabi, A.Y. Solution-Processed Interfacial PEDOT:PSS Assembly into Porous Tungsten Molybdenum Oxide Nanocomposite Films for Electrochromic Applications. *ACS Appl. Mater. Interfaces* **2018**, *10*, 10520–10527. [CrossRef]
110. Choi, I.-G.; Choi, D.; Lee, J.-Y.; Lee, M.; Park, S.-I.; Chun, D.-M.; Lee, C.S.; Chu, W.-S. One Million Cycle Durability Test of Electrochromic Devices Using Charge Balance Control. *Int. J. Precis. Eng. Manuf.-Green Technol.* **2020**, *7*, 195–203. [CrossRef]
111. Chang, C.-M.; Chiang, Y.-C.; Cheng, M.-H.; Lin, S.-H.; Jian, W.-B.; Chen, J.-T.; Cheng, Y.-J.; Ma, Y.-R.; Tsukagoshi, K. Fabrication of $WO_3$ Electrochromic Devices Using Electro-Exploding Wire Techniques and Spray Coating. *Sol. Energy Mater. Sol. Cells* **2021**, *223*, 110960. [CrossRef]
112. Hsu, S.-C.; Chao, S.-H.; Wu, N.-J.; Huang, J.-H.; Kang, J.-L.; Weng, H.C.; Liu, T.-Y. Facile Synthesis of Hybrid $WO_3/MoO_x$ Electrochromic Films for Application in Complementary Electrochromic Devices. *J. Alloys Compd.* **2023**, *945*, 169256. [CrossRef]
113. Nguyen, V.-T.; Min, B.K.; Kim, S.K.; Yi, Y.; Choi, C.-G. A Flexible and High-Performance Electrochromic Smart Window Produced by $WO_3/Ti_3C_2T_x$ MXene Hybrids. *J. Mater. Chem. C* **2021**, *9*, 3183–3192. [CrossRef]
114. Pugliese, M.; Scarfiello, R.; Prontera, C.T.; Giannuzzi, R.; Bianco, G.V.; Bruno, G.; Carallo, S.; Mariano, F.; Maggiore, A.; Carbone, L.; et al. Visible Light–Near-Infrared Dual-Band Electrochromic Device. *ACS Sustain. Chem. Eng.* **2023**, *11*, 9601–9612. [CrossRef]
115. Wruck, D.A.; Rubin, M. Structure and Electronic Properties of Electrochromic NiO Films. *J. Electrochem. Soc.* **1993**, *140*, 1097–1104. [CrossRef]

116. Šurca, A.; Orel, B.; Pihlar, B.; Bukovec, P. Optical, Spectroelectrochemical and Structural Properties of Sol-Gel Derived Ni-Oxide Electrochromic Film. *J. Electroanal. Chem.* **1996**, *408*, 83–100. [CrossRef]
117. Boschloo, G.; Hagfeldt, A. Spectroelectrochemistry of Nanostructured NiO. *J. Phys. Chem. B* **2001**, *105*, 3039–3044. [CrossRef]
118. Xia, X.H.; Tu, J.P.; Zhang, J.; Wang, X.L.; Zhang, W.K.; Huang, H. Morphology Effect on the Electrochromic and Electrochemical Performances of NiO Thin Films. *Electrochim. Acta* **2008**, *53*, 5721–5724. [CrossRef]
119. Lampert, C.M.; Omstead, T.R.; Yu, P.C. Chemical and Optical Properties of Electrochromic Nickel Oxide Films. *Sol. Energy Mater.* **1986**, *14*, 161–174. [CrossRef]
120. Arakaki, J.; Reyes, R.; Horn, M.; Estrada, W. Electrochromism in NiOx and WOx Obtained by Spray Pyrolysis. *Sol. Energy Mater. Sol. Cells* **1995**, *37*, 33–41. [CrossRef]
121. Kadam, L.D.; Patil, P.S. Studies on Electrochromic Properties of Nickel Oxide Thin films Prepared by Spray Pyrolysis Technique. *Sol. Energy Mater.* **2001**, *69*, 361–369. [CrossRef]
122. Mahmoud, S.A.; Akl, A.A.; Kamal, H.; Abdel-Hady, K. Opto-Structural, Electrical and Electrochromic Properties of Crystalline Nickel Oxide Thin Films Prepared by Spray Pyrolysis. *Phys. B Condens. Matter* **2002**, *311*, 366–375. [CrossRef]
123. Wang, S.-Y.; Wang, W.; Wang, W.-Z.; Du, Y.-W. Preparation and Characterization of Highly Oriented NiO(200) Films by a Pulse Ultrasonic Spray Pyrolysis Method. *Mater. Sci. Eng. B* **2002**, *90*, 133–137. [CrossRef]
124. Kamal, H.; Elmaghraby, E.K.; Ali, S.A.; Abdel-Hady, K. The Electrochromic Behavior of Nickel Oxide Films Sprayed at Different Preparative Conditions. *Thin Solid Films* **2005**, *483*, 330–339. [CrossRef]
125. Lin, S.-H.; Chen, F.-R.; Kai, J.-J. Electrochromic Properties of Nano-Structured Nickel Oxide Thin Film Prepared by Spray Pyrolysis Method. *Appl. Surf. Sci.* **2008**, *254*, 2017–2022. [CrossRef]
126. Romero, R.; Martin, F.; Ramos-Barrado, J.R.; Leinen, D. Synthesis and Characterization of Nanostructured Nickel Oxide Thin Films Prepared with Chemical Spray Pyrolysis. *Thin Solid Films* **2010**, *518*, 4499–4502. [CrossRef]
127. Ismail, R.A.; Ghafori, S.; Kadhim, G.A. Preparation and Characterization of Nanostructured Nickel Oxide Thin Films by Spray Pyrolysis. *Appl. Nanosci.* **2013**, *3*, 509–514. [CrossRef]
128. Sharma, R.; Acharya, A.D.; Shrivastava, S.B.; Shripathi, T.; Ganesan, V. Preparation and Characterization of Transparent NiO Thin Films Deposited by Spray Pyrolysis Technique. *Optik* **2014**, *125*, 6751–6756. [CrossRef]
129. Gowthami, V.; Meenakshi, M.; Perumal, P.; Sivakuma, R.; Sanjeeviraja, C. Preparation of Rod Shaped Nickel Oxide Thin Films by a Novel and Cost Effective Nebulizer Technique. *Mater. Sci. Semicond. Process.* **2014**, *27*, 1042–1049. [CrossRef]
130. Barir, R.; Benhaoua, B.; Benhamida, S.; Rahal, A.; Sahraoui, T.; Gheriani, R. Effect of Precursor Concentration on Structural Optical and Electrical Properties of NiO Thin Films Prepared by Spray Pyrolysis. *J. Nanomater.* **2017**, *2017*, 5204639. [CrossRef]
131. Gomaa, M.M.; Yazdi, G.R.; Schmidt, S.; Boshta, M.; Khranovskyy, V.; Eriksson, F.; Farag, B.S.; Osman, M.B.S.; Yakimova, R. Effect of Precursor Solutions on the Structural and Optical Properties of Sprayed NiO Thin Films. *Mater. Sci. Semicond. Process.* **2017**, *64*, 32–38. [CrossRef]
132. Chtouki, T.; Soumahoro, L.; Kulyk, B.; Bougharraf, H.; Kabouchi, B.; Erguig, H.; Sahraoui, B. Comparison of Structural, Morphological, Linear and Nonlinear Optical Properties of NiO Thin Films Elaborated by Spin-Coating and Spray Pyrolysis. *Optik* **2017**, *128*, 8–13. [CrossRef]
133. Ravi Dhas, C.; Santhoshi Monica, S.E.; Venkatesh, R.; Sivakumar, R.; Nathanael, A.J.; Vignesh, R.; Arivukarasan, D.; Gnana Malar, K.C.M.; Keerthana, S. Correlation of Annealing Temperature on Physico-Chemical Properties and Electrochromic Performance of Nebulizer Spray-Coated NiO Films. *Inorg. Nano-Metal Chem.* **2023**, *53*, 178–190. [CrossRef]
134. Obaida, M.; Fathi, A.M.; Moussa, I.; Afify, H.H. Characterization and Electrochromic Properties of NiO Thin Films Prepared Using a Green Aqueous Solution by Pulsed Spray Pyrolysis Technique. *J. Mater. Res.* **2022**, *37*, 2282–2292. [CrossRef]
135. Chen, Z.; Dedova, T.; Acik, I.O.; Danilson, M.; Krunks, M. Nickel Oxide Films by Chemical Spray: Effect of Deposition Temperature and Solvent Type on Structural, Optical, and Surface Properties. *Appl. Surf. Sci.* **2021**, *548*, 149118. [CrossRef]
136. Garduño, I.A.; Alonso, J.C.; Bizarro, M.; Ortega, R.; Rodríguez-Fernández, L.; Ortiz, A. Optical and Electrical Properties of Lithium Doped Nickel Oxide Films Deposited by Spray Pyrolysis onto Alumina Substrates. *J. Cryst. Growth* **2010**, *312*, 3276–3281. [CrossRef]
137. Loyola Poul Raj, I.; Valanarasu, S.; Rimal Isaac, R.S.; Ramudu, M.; Bitla, Y.; Ganesh, V.; Yahia, I.S. The Role of Silver Doping in Tuning the Optical Absorption, Energy Gap, Photoluminescence Properties of NiO Thin Films for UV Photosensor Applications. *Optik* **2022**, *254*, 168634. [CrossRef]
138. Sathisha, D.; Naik, K.G. *Synthesis and Characterization of Cobalt Doped Nickel Oxide Thin Films by Spray Pyrolysis Method*; AIP Conference Proceedings: Bikaner, India, 2018; p. 100021.
139. Martinez-Luevanos, A.; Oliva, J.; Garcia, C.R.; Avalos-Belmontes, F.; Garcia-Lobato, M.A. Effect of Cobalt on the Electrochromic Properties of NiO Films Deposited by Spray Pyrolysis. *Appl. Phys. A* **2017**, *123*, 349. [CrossRef]
140. Sharma, R.; Acharya, A.D.; Moghe, S.; Shrivastava, S.B.; Gangrade, M.; Shripathi, T.; Ganesan, V. Effect of Cobalt Doping on Microstructural and Optical Properties of Nickel Oxide Thin Films. *Mater. Sci. Semicond. Process.* **2014**, *23*, 42–49. [CrossRef]
141. Moghe, S.; Acharya, A.D.; Panda, R.; Shrivastava, S.B.; Gangrade, M.; Shripathi, T.; Ganesan, V. Effect of Copper Doping on the Change in the Optical Absorption Behaviour in NiO Thin Films. *Renew. Energy* **2012**, *46*, 43–48. [CrossRef]
142. Mani Menaka, S.; Umadevi, G.; Manickam, M. Effect of Copper Concentration on the Physical Properties of Copper Doped NiO Thin Films Deposited by Spray Pyrolysis. *Mater. Chem. Phys.* **2017**, *191*, 181–187. [CrossRef]

143. Monica, S.E.S.; Dhas, C.R.; Venkatesh, R.; Sivakumar, R.; Vignesh, R.; Ferby, V.A. Nebulizer Sprayed Nickel-Manganese (Ni-Mn) Mixed Metal Oxide Nanocomposite Coatings for High-Performance Electrochromic Device Applications. *J. Solid State Electrochem.* **2022**, *26*, 1271–1290. [CrossRef]
144. Brioual, B.; Ghannam, H.; Rossi, Z.; Aouni, A.; El-Habib, A.; Diani, M.; Addou, M.; Matassa, R.; Nottola, S.; Jbilou, M. Effect of In-Doping on Electrochromic Behavior of NiO Thin Films. *Materialia* **2023**, *30*, 101832. [CrossRef]
145. Mrabet, C.; Ben Amor, M.; Boukhachem, A.; Amlouk, M.; Manoubi, T. Physical Properties of La-Doped NiO Sprayed Thin Films for Optoelectronic and Sensor Applications. *Ceram. Int.* **2016**, *42*, 5963–5978. [CrossRef]
146. Tenent, R.C.; Gillaspie, D.T.; Miedaner, A.; Parilla, P.A.; Curtis, C.J.; Dillon, A.C. Fast-Switching Electrochromic Li+-Doped NiO Films by Ultrasonic Spray Deposition. *J. Electrochem. Soc.* **2010**, *157*, H318. [CrossRef]
147. Kumar, A.; Sahay, P.P. Lithium Doping in Spray-Pyrolyzed NiO Thin Films: Results on Their Microstructural, Optical and Electrochromic Properties. *Appl. Phys. A* **2021**, *127*, 286. [CrossRef]
148. Denayer, J.; Bister, G.; Simonis, P.; Colson, P.; Maho, A.; Aubry, P.; Vertruyen, B.; Henrist, C.; Lardot, V.; Cambier, F.; et al. Surfactant-Assisted Ultrasonic Spray Pyrolysis of Nickel Oxide and Lithium-Doped Nickel Oxide Thin Films, toward Electrochromic Applications. *Appl. Surf. Sci.* **2014**, *321*, 61–69. [CrossRef]
149. Manceriu, L.M.; Colson, P.; Maho, A.; Eppe, G.; Nguyen, N.D.; Labrugere, C.; Rougier, A.; Cloots, R.; Henrist, C. Straightforward Prediction of the $Ni_{1-x}O$ Layers Stoichiometry by Using Optical and Electrochemical Measurements. *J. Phys. D Appl. Phys.* **2017**, *50*, 225501. [CrossRef]
150. Carrillo-Delgado, C.; Arano-Martínez, J.A.; Vidales-Hurtado, M.A.; Torres-Torres, D.; Martínez-González, C.L.; Torres-Torres, C. Electrically Induced Directional Self-Focusing in Electrochromic NiO Thin Solid Films. *J. Mater. Sci. Mater. Electron.* **2023**, *34*, 953. [CrossRef]
151. Garcia-Lobato, M.A.; Garcia, C.R.; Mtz-Enriquez, A.I.; Lopez-Badillo, C.M.; Garcias-Morales, C.; Muzquiz-Ramos, E.M.; Cruz-Ortiz, B.R. Enhanced Electrochromic Performance of NiO-MWCNTs Thin Films Deposited by Electrostatic Spray Deposition. *Mater. Res. Bull.* **2019**, *114*, 95–100. [CrossRef]
152. Berlanga-Rodriguez, A.; Avalos-Belmontes, F.; Arvizu, M.A.; Garcia, C.R.; Rodríguez-Varela, F.J.; Oyervides-Muñoz, E.; Garcia-Lobato, M.A. Influence of the Diameter of Multi-Walled Carbon Nanotubes on the Electrochromic Performance of NiO Thin Films. *Mater. Lett.* **2021**, *289*, 129403. [CrossRef]
153. Wang, J.; Zhu, R.; Gao, Y.; Jia, Y.; Cai, G. Unveiling the Multistep Electrochemical Desorption Mechanism of Cubic NiO Films for Transmissive-to-Black Electrochromic Energy Storage Devices. *J. Phys. Chem. Lett.* **2023**, *14*, 2284–2291. [CrossRef]
154. Marrani, A.G.; Novelli, V.; Sheehan, S.; Dowling, D.P.; Dini, D. Probing the Redox States at the Surface of Electroactive Nanoporous NiO Thin Films. *ACS Appl. Mater. Interfaces* **2014**, *6*, 143–152. [CrossRef]
155. Awais, M.; Dowling, D.P.; Decker, F.; Dini, D. Electrochemical Characterization of Nanoporous Nickel Oxide Thin Films Spray-Deposited onto Indium-Doped Tin Oxide for Solar Conversion Scopes. *Adv. Condens. Matter Phys.* **2015**, *2015*, 1–18. [CrossRef]
156. Cogan, S.F.; Nguyen, N.M.; Perrotti, S.J.; Rauh, R.D. Optical Properties of Electrochromic Vanadium Pentoxide. *J. Appl. Phys.* **1989**, *66*, 1333–1337. [CrossRef]
157. Šurca, A.; Orel, B.; Dražič, G.; Pihlar, B. Ex Situ and In Situ Infrared Spectroelectrochemical Investigations of $V_2O_5$ Crystalline Films. *J. Electrochem. Soc.* **1999**, *146*, 232–242. [CrossRef]
158. Beke, S. A Review of the Growth of $V_2O_5$ Films from 1885 to 2010. *Thin Solid Films* **2011**, *519*, 1761–1771. [CrossRef]
159. Mjejri, I.; Manceriu, L.M.; Gaudon, M.; Rougier, A.; Sediri, F. Nano-Vanadium Pentoxide Films for Electrochromic Displays. *Solid State Ion.* **2016**, *292*, 8–14. [CrossRef]
160. Le, T.K.; Pham, P.V.; Dong, C.-L.; Bahlawane, N.; Vernardou, D.; Mjejri, I.; Rougier, A.; Kim, S.W. Recent Advances in Vanadium Pentoxide ($V_2O_5$) towards Related Applications in Chromogenics and beyond: Fundamentals, Progress, and Perspectives. *J. Mater. Chem. C* **2022**, *10*, 4019–4071. [CrossRef]
161. Bouzidi, A.; Benramdane, N.; Nakrela, A.; Mathieu, C.; Khelifa, B.; Desfeux, R.; Da Costa, A. First Synthesis of Vanadium Oxide Thin Films by Spray Pyrolysis Technique. *Mater. Sci. Eng. B* **2002**, *95*, 141–147. [CrossRef]
162. Boudaoud, L.; Benramdane, N.; Desfeux, R.; Khelifa, B.; Mathieu, C. Structural and Optical Properties of $MoO_3$ and $V_2O_5$ Thin Films Prepared by Spray Pyrolysis. *Catal. Today* **2006**, *113*, 230–234. [CrossRef]
163. Patil, C.E.; Tarwal, N.L.; Shinde, P.S.; Deshmukh, H.P.; Patil, P.S. Synthesis of Electrochromic Vanadium Oxide by Pulsed Spray Pyrolysis Technique and Its Properties. *J. Phys. D Appl. Phys.* **2009**, *42*, 025404. [CrossRef]
164. Patil, C.E.; Jadhav, P.R.; Tarwal, N.L.; Deshmukh, H.P.; Karanjkar, M.M.; Patil, P.S. Electrochromic Performance of Mixed $V_2O_5$–$MoO_3$ Thin Films Synthesized by Pulsed Spray Pyrolysis Technique. *Mater. Chem. Phys.* **2011**, *126*, 711–716. [CrossRef]
165. Patil, C.E.; Jadhav, P.R.; Tarwal, N.L.; Deshmukh, H.P.; Karanjakar, M.M.; Wali, A.A.; Patil, P.S. Electrochromic Properties of Vanadium Oxide Thin Films Prepared by PSPT: Effect of Substrate Temperature. *AIP Conf. Proc.* **2013**, *1536*, 517–518. [CrossRef]
166. Patil, C.E.; Tarwal, N.L.; Jadhav, P.R.; Shinde, P.S.; Deshmukh, H.P.; Karanjkar, M.M.; Moholkar, A.V.; Gang, M.G.; Kim, J.H.; Patil, P.S. Electrochromic Performance of the Mixed $V_2O_5$–$WO_3$ Thin Films Synthesized by Pulsed Spray Pyrolysis Technique. *Curr. Appl. Phys.* **2014**, *14*, 389–395. [CrossRef]
167. Hwang, K.S.; Kang, B.A.; Kim, S.D.; Hwangbo, S.; Kim, J.T. Amorphous Vanadium Pentoxide Thin Films Prepared by Electrostatic Spraying-Pyrolysis Deposition. *Ceram. Int.* **2012**, *38*, S645–S647. [CrossRef]

168. Wei, Y.; Li, M.; Zheng, J.; Xu, C. Structural Characterization and Electrical and Optical Properties of $V_2O_5$ Films Prepared via Ultrasonic Spraying. *Thin Solid Films* **2013**, *534*, 446–451. [CrossRef]
169. Abd–Alghafour, N.M.; Ahmed, N.M.; Hassan, Z.; Mohammad, S.M. Influence of Solution Deposition Rate on Properties of $V_2O_5$ Thin Films Deposited by Spray Pyrolysis Technique. *AIP Conf. Proc.* **2016**, *1756*, 090010.
170. Margoni, M.M.; Mathuri, S.; Ramamurthi, K.; Babu, R.R.; Sethuraman, K. Sprayed Vanadium Pentoxide Thin Films: Influence of Substrate Temperature and Role of $HNO_3$ on the Structural, Optical, Morphological and Electrical Properties. *Appl. Surf. Sci.* **2017**, *418*, 280–290. [CrossRef]
171. Darroudi, N.; Eshghi, H. Effects of Nozzle-to-Substrate Distance and Annealing Atmospheres on $V_2O_5$ Thin Films Prepared by Spray Pyrolysis Technique. *Mater. Sci. Eng. B* **2020**, *262*, 114726. [CrossRef]
172. Mouratis, K.; Tudose, V.; Romanitan, C.; Pachiu, C.; Tutunaru, O.; Suchea, M.; Couris, S.; Vernardou, D.; Emmanouel, K. Electrochromic Performance of $V_2O_5$ Thin Films Grown by Spray Pyrolysis. *Materials* **2020**, *13*, 3859. [CrossRef] [PubMed]
173. Mouratis, K.; Tudose, I.V.; Bouranta, A.; Pachiu, C.; Romanitan, C.; Tutunaru, O.; Couris, S.; Koudoumas, E.; Suchea, M. Annealing Effect on the Properties of Electrochromic $V_2O_5$ Thin Films Grown by Spray Deposition Technique. *Nanomaterials* **2020**, *10*, 2397. [CrossRef] [PubMed]
174. Zhang, S.; Chen, S.; Luo, Y.; Yan, B.; Gu, Y.; Yang, F.; Cao, Y. Large-Scale Preparation of Solution-Processable One-Dimensional $V_2O_5$ Nanobelts with Ultrahigh Aspect Ratio for Bifunctional Multicolor Electrochromic and Supercapacitor Applications. *J. Alloys Compds* **2020**, *842*, 155882. [CrossRef]
175. Khmissi, H.; Mahmoud, S.A.; Akl, A.A. Investigation of Thermal Annealing Effect on the Microstructure, Morphology, Linear and Non-Linear Optical Properties of Spray Deposited Nanosized $V_2O_5$ Thin Films. *Optik* **2021**, *227*, 165979. [CrossRef]
176. Tutel, Y.; Durukan, M.B.; Koc, S.; Koylan, S.; Cakmak, H.; Kocak, Y.; Hekmat, F.; Ozensoy, E.; Ozbay, E.; Udum, Y.A.; et al. Multichromic Vanadium Pentoxide Thin Films Through Ultrasonic Spray Deposition. *J. Electrochem. Soc.* **2021**, *168*, 106511. [CrossRef]
177. Romanitan, C.; Tudose, I.V.; Mouratis, K.; Popescu, M.C.; Pachiu, C.; Couris, S.; Koudoumas, E.; Suchea, M. Structural Investigations in Electrochromic Vanadium Pentoxide Thin Films. *Phys. Status Solidi* **2022**, *219*, 2100431. [CrossRef]
178. Mousavi, M.; Kompany, A.; Shahtahmasebi, N.; Bagheri-Mohagheghi, M.-M. Effect of S-Doping on Structural, Optical and Electrochemical Properties of Vanadium Oxide Thin Films Prepared by Spray Pyrolysis. *Phys. Scr.* **2013**, *88*, 065701. [CrossRef]
179. Abyazisani, M.; Bagheri-Mohagheghi, M.M.; Benam, M.R. Study of Structural and Optical Properties of Nanostructured V2O5 Thin Films Doped with Fluorine. *Mater. Sci. Semicond. Process.* **2015**, *31*, 693–699. [CrossRef]
180. Kovendhan, M.; Paul Joseph, D.; Manimuthu, P.; Sendilkumar, A.; Karthick, S.N.; Sambasivam, S.; Vijayarangamuthu, K.; Kim, H.J.; Choi, B.C.; Asokan, K.; et al. Prototype Electrochromic Device and Dye Sensitized Solar Cell Using Spray Deposited Undoped and 'Li' Doped $V_2O_5$ Thin Film Electrodes. *Curr. Appl. Phys.* **2015**, *15*, 622–631. [CrossRef]
181. Tabatabai Yazdi, S.; Pilevar Shahri, R.; Shafei, S. First Synthesis of In-Doped Vanadium Pentoxide Thin Films and Their Structural, Optical and Electrical Characterization. *Mater. Sci. Eng. B* **2021**, *263*, 114755. [CrossRef]
182. Mrigal, A.; Temsamani, R.; Addou, M.; Hssein, M.; El Jouad, M. Electrochromic Properties of Mo-Doped $V_2O_5$ Thin Films Deposited by Spray Pyrolysis Process. *Eur. Phys. J. Appl. Phys.* **2019**, *86*, 20301. [CrossRef]
183. Gandasiri, R.; Sreelatha, C.J.; Nagaraju, P.; Vijayakumar, Y. Effect of Annealing Temperature on Micro-Structural, Optical and Electrical Characterization of Nanostructured $V_2O_5$ Thin Films Prepared by Spray Pyrolysis Technique. *Phys. B Condens. Matter* **2019**, *572*, 220–224. [CrossRef]
184. Hsiao, Y.-S.; Chang-Jian, C.-W.; Syu, W.-L.; Yen, S.-C.; Huang, J.-H.; Weng, H.-C.; Lu, C.-Z.; Hsu, S.-C. Enhanced Electrochromic Performance of Carbon-Coated $V_2O_5$ Derived from a Metal–Organic Framework. *Appl. Surf. Sci.* **2021**, *542*, 148498. [CrossRef]
185. Li, H.; Liang, H.; Li, R.; Lu, Z.; Hou, C.; Zhang, Q.; Li, Y.; Li, K.; Wang, H. Ultrafast, Stable Electrochromics Enabled by Hierarchical Assembly of $V_2O_5$@C Microrod Network. *ACS Appl. Mater. Interfaces* **2022**, *14*, 48037–48044. [CrossRef]
186. Kim, J.; Lee, K.H.; Lee, S.; Park, S.; Chen, H.; Kim, S.K.; Yim, S.; Song, W.; Lee, S.S.; Yoon, D.H.; et al. Minimized Optical Scattering of MXene-Derived 2D $V_2O_5$ Nanosheet-Based Electrochromic Device with High Multicolor Contrast and Accuracy. *Chem. Eng. J.* **2023**, *453*, 139973. [CrossRef]
187. Patil, P.S.; Patil, R.S. Studies on Spray Pyrolyzed Molybdenum Trioxide Thin Films. *Bull. Mater. Sci.* **1995**, *18*, 911–916. [CrossRef]
188. Mahajan, S.S.; Mujawar, S.H.; Shinde, P.S.; Inamdar, A.I.; Patil, P.S. Structural, Morphological, Optical and Electrochromic Properties of Ti-Doped $MoO_3$ Thin Films. *Sol. Energy Mater. Sol. Cells* **2009**, *93*, 183–187. [CrossRef]
189. Kumar, A.; Prajapati, C.S.; Sahay, P.P. Results on the Microstructural, Optical and Electrochromic Properties of Spray-Deposited $MoO_3$ Thin Films by the Influence of W Doping. *Mater. Sci. Semicond. Process.* **2019**, *104*, 104668. [CrossRef]
190. Turel, O.; Hacioglu, S.O.; Coskun, S.; Toppare, L.; Unalan, H.E. Sequential Deposition of Electrochromic $MoO_3$ Thin Films with High Coloration Efficiency and Stability. *J. Electrochem. Soc.* **2017**, *164*, E565. [CrossRef]
191. Shinde, P.S.; Deshmukh, H.P.; Mujawar, S.H.; Inamdar, A.I.; Patil, P.S. Spray Deposited Titanium Oxide Thin Films as Passive Counter Electrodes. *Electrochim. Acta* **2007**, *52*, 3114–3120. [CrossRef]
192. Dhandayuthapani, T.; Sivakumar, R.; Ilangovan, R.; Gopalakrishnan, C.; Sanjeeviraja, C.; Sivanantharaja, A.; Hari Krishna, R. Efficient Electrochromic Performance of Anatase $TiO_2$ Thin Films Prepared by Nebulized Spray Deposition Method. *J. Solid State Electrochem.* **2018**, *22*, 1825–1838. [CrossRef]
193. Enayati-Taloobaghi, H.; Eshghi, H. Achievement of High Electrochromic Performance of $TiO_2$ Thin Films Prepared via Spray Pyrolysis Method, Influence of Annealing Process. *Mater. Res. Bull.* **2023**, *167*, 112416. [CrossRef]

194. Zelazowska, E.; Rysiakiewicz-Pasek, E. Thin $TiO_2$ Films for an Electrochromic System. *Opt. Mater.* **2009**, *31*, 1802–1804. [CrossRef]
195. Liu, R.; Ren, Y.; Cai, H.; Zhang, C.; Wang, J.; Zhao, G.; Zhang, S. Fabrication of Electrochromic $TiO_2$:Nb Films by Ultrasonic Spray Pyrolysis. *Opt. Mater.* **2022**, *127*, 112315. [CrossRef]
196. Dhandayuthapani, T.; Sivakumar, R.; Ilangovan, R.; Sanjeeviraja, C.; Jeyadheepan, K.; Gopalakrishnan, C.; Sivaprakash, P.; Arumugam, S. Brown Coloration and Electrochromic Properties of Nickel Doped $TiO_2$ Thin Films Deposited by Nebulized Spray Pyrolysis Technique. *Thin Solid Films* **2020**, *694*, 137754. [CrossRef]
197. Mujawar, S.H.; Inamdar, A.I.; Patil, S.B.; Patil, P.S. Electrochromic Properties of Spray-Deposited Niobium Oxide Thin Films. *Solid State Ion.* **2006**, *177*, 3333–3338. [CrossRef]
198. Mujawar, S.H.; Inamdar, A.I.; Betty, C.A.; Ganesan, V.; Patil, P.S. Effect of Post Annealing Treatment on Electrochromic Properties of Spray Deposited Niobium Oxide Thin Films. *Electrochim. Acta* **2007**, *52*, 4899–4906. [CrossRef]
199. Romero, R.; Dalchiele, E.A.; Martín, F.; Leinen, D.; Ramos-Barrado, J.R. Electrochromic Behaviour of $Nb_2O_5$ Thin Films with Different Morphologies Obtained by Spray Pyrolysis. *Sol. Energy Mater. Sol. Cells* **2009**, *93*, 222–229. [CrossRef]
200. Fan, H.; Yan, W.; Ding, Y.; Bao, Z. Using Flame-Assisted Printing to Fabricate Large Nanostructured Oxide Thin Film for Electrochromic Applications. *Nanosc. Res. Lett.* **2020**, *15*, 218. [CrossRef]
201. Patil, P.S.; Sadale, S.B.; Mujawar, S.H.; Shinde, P.S.; Chigare, P.S. Synthesis of Electrochromic Tin Oxide Thin Films with Faster Response by Spray Pyrolysis. *Appl. Surf. Sci.* **2007**, *253*, 8560–8567. [CrossRef]
202. Maho, A.; Comeron Lamela, L.; Henrist, C.; Henrard, L.; Tizei, L.H.G.; Kociak, M.; Stéphan, O.; Heo, S.; Milliron, D.J.; Vertruyen, B.; et al. Solvothermally-Synthesized Tin-Doped Indium Oxide Plasmonic Nanocrystals Spray-Deposited onto Glass as near-Infrared Electrochromic Films. *Sol. Energy Mater. Sol. Cells* **2019**, *200*, 110014. [CrossRef]
203. Maho, A.; Saez Cabezas, C.A.; Meyertons, K.A.; Reimnitz, L.C.; Sahu, S.; Helms, B.A.; Milliron, D.J. Aqueous Processing and Spray Deposition of Polymer-Wrapped Tin-Doped Indium Oxide Nanocrystals as Electrochromic Thin Films. *Chem. Mater.* **2020**, *32*, 8401–8411. [CrossRef]
204. Patil, P.S.; Kawar, R.K.; Sadale, S.B. Effect of Substrate Temperature on Electrochromic Properties of Spray-Deposited Ir-Oxide Thin Films. *Appl. Surf. Sci.* **2005**, *249*, 367–374. [CrossRef]
205. Patil, P.S.; Mujawar, S.H.; Sadale, S.B.; Deshmukh, H.P.; Inamdar, A.I. Effect of Film Thickness on Electrochromic Activity of Spray Deposited Iridium Oxide Thin Films. *Mater. Chem. Phys.* **2006**, *99*, 309–313. [CrossRef]
206. Hassanien, A.S.; Akl, A. Crystal Imperfections and Mott Parameters of Sprayed Nanostructure $IrO_2$ Thin Films. *Phys. B Condens. Matter* **2015**, *473*, 11–19. [CrossRef]
207. Vignesh, R.; Sivakumar, R.; Slimani, Y.; Sanjeeviraja, C. Molarity Influenced Interesting Electrochromic Optical Modulation Peak Shift in Nebulized Spray Deposited $Mn_3O_4$ Films. *J. Electrochem. Soc.* **2023**, *170*, 063506. [CrossRef]
208. Patil, P.S.; Kadam, L.D.; Lokhande, C.D. Studies on Electrochromism of Spray Pyrolyzed Cobalt Oxide Thin Films. *Sol. Energy Mater. Sol. Cells* **1998**, *53*, 229–234. [CrossRef]
209. Dhas, C.R.; Venkatesh, R.; Sivakumar, R.; Raj, A.M.E.; Sanjeeviraja, C. Fast Electrochromic Response of Porous-Structured Cobalt Oxide ($Co_3O_4$) Thin Films by Novel Nebulizer Spray Pyrolysis Technique. *Ionics* **2016**, *22*, 1911–1926. [CrossRef]
210. Venkatesh, R.; Dhas, C.R.; Sivakumar, R.; Dhandayuthapani, T.; Sudhagar, P.; Sanjeeviraja, C.; Raj, A.M.E. Analysis of Optical Dispersion Parameters and Electrochromic Properties of Manganese-Doped $Co_3O_4$ Dendrite Structured Thin Films. *J. Phys. Chem. Solids* **2018**, *122*, 118–129. [CrossRef]
211. Ravi Dhas, C.; Venkatesh, R.; Sivakumar, R.; Dhandayuthapani, T.; Subramanian, B.; Sanjeeviraja, C.; Moses Ezhil Raj, A. Electrochromic Performance of Chromium-Doped $Co_3O_4$ Nanocrystalline Thin Films Prepared by Nebulizer Spray Technique. *J. Alloys Compd.* **2019**, *784*, 49–59. [CrossRef]
212. El Bachiri, A.; Soussi, L.; Karzazi, O.; Louardi, A.; Rmili, A.; Erguig, H.; El Idrissi, B. Electrochromic and Photoluminescence Properties of Cobalt Oxide Thin Films Prepared by Spray Pyrolysis. *Spectrosc. Lett.* **2019**, *52*, 66–73. [CrossRef]
213. Özer, N. Optical Properties and Electrochromic Characterization of Sol–Gel Deposited Ceria Films. *Sol. Energy Mater. Sol. Cells* **2001**, *68*, 391–400. [CrossRef]
214. Masetti, E.; Varsano, F.; Decker, F.; Krasilnikova, A. Sputter Deposited Cerium–Vanadium Oxide: Optical Characterization and Electrochromic Behavior. *Electrochim. Acta* **2001**, *46*, 2085–2090. [CrossRef]
215. Avellaneda, C.O.; Bulhões, L.O.S.; Pawlicka, A. The $CeO_2$–$TiO_2$–$ZrO_2$ Sol–Gel Film: A Counter-Electrode for Electrochromic Devices. *Thin Solid Films* **2005**, *471*, 100–104. [CrossRef]
216. Verma, A.; Samanta, S.B.; Mehra, N.C.; Bakhshi, A.K.; Agnihotry, S.A. Sol–Gel Derived Nanocrystalline $CeO_2$–$TiO_2$ Coatings for Electrochromic Windows. *Sol. Energy Mater. Sol. Cells* **2005**, *86*, 85–103. [CrossRef]
217. El Idrissi, B.; Addou, M.; Outzourhit, A.; Regragui, M.; Bougrine, A.; Kachouane, A. Sprayed $CeO_2$ Thin Films for Electrochromic Applications. *Sol. Energy Mater. Sol. Cells* **2001**, *69*, 1–8. [CrossRef]
218. Bhosale, A.K.; Tarwal, N.L.; Shinde, P.S.; Kadam, P.M.; Patil, R.S.; Barman, S.R.; Patil, P.S. Effective Utilization of Spray Pyrolyzed $CeO_2$ as Optically Passive Counter Electrode for Enhancing Optical Modulation of $WO_3$. *Solid State Ion.* **2009**, *180*, 1324–1331. [CrossRef]
219. Dalavi, D.S.; Bhosale, A.K.; Desai, R.S.; Patil, P.S. Energy Efficient Electrochromic Smart Windows Based on Highly Stable $CeO_2$-$V_2O_5$ Optically Passive Counter Electrode. *Mater. Today Proc.* **2021**, *43*, 2702–2706. [CrossRef]
220. El-Habib, A.; Addou, M.; Aouni, A.; Zimou, J.; Diani, M.; Ftouhi, H.; Jouad, Z.E. Physical Properties and Electrochemical Behavior of Thin Layers of Vanadium Doped Cerium Dioxide. *Surf. Interfaces* **2021**, *23*, 100906. [CrossRef]

221. Bhosale, A.K.; Shinde, P.S.; Tarwal, N.L.; Pawar, R.C.; Kadam, P.M.; Patil, P.S. Synthesis and Characterization of Highly Stable Optically Passive $CeO_2$–$ZrO_2$ Counter Electrode. *Electrochim. Acta* **2010**, *55*, 1900–1906. [CrossRef]
222. Bhosale, A.K.; Kulal, S.R.; Gurame, V.M.; Patil, P.S. Spray Deposited $CeO_2$–$TiO_2$ Counter Electrode for Electrochromic Devices. *Bull. Mater. Sci.* **2015**, *38*, 483–491. [CrossRef]
223. Thakur, V.K.; Ding, G.; Ma, J.; Lee, P.S.; Lu, X. Hybrid Materials and Polymer Electrolytes for Electrochromic Device Applications. *Adv. Mater.* **2012**, *24*, 4071–4096. [CrossRef]
224. Yoo, S.J.; Lim, J.W.; Sung, Y.-E. Improved Electrochromic Devices with an Inorganic Solid Electrolyte Protective Layer. *Sol. Energy Mater. Sol. Cells* **2006**, *90*, 477–484. [CrossRef]
225. Nguyen, C.A.; Argun, A.A.; Hammond, P.T.; Lu, X.; Lee, P.S. Layer-by-Layer Assembled Solid Polymer Electrolyte for Electrochromic Devices. *Chem. Mater.* **2011**, *23*, 2142–2149. [CrossRef]
226. Cloots, R.; Henrist, C.; Denayer, J.; Maho, A.; Cambier, F.; Lardot, V.; Bister, G.; Aubry, P. Improved Process of Ultrasonic Spray Pyrolysis Deposition of One or More Electrochromic and/or Electrolytic Films on a Substrate. WO2016113050A1, 21 July 2016.
227. Djenadic, R.; Botros, M.; Benel, C.; Clemens, O.; Indris, S.; Choudhary, A.; Bergfeldt, T.; Hahn, H. Nebulized Spray Pyrolysis of Al-Doped $Li_7La_3Zr_2O_{12}$ Solid Electrolyte for Battery Applications. *Solid State Ion.* **2014**, *263*, 49–56. [CrossRef]
228. Fan, L.; Xie, H.; Su, P.-C. Spray Coating of Dense Proton-Conducting $BaCe_{0.7}Zr_{0.1}Y_{0.2}O_3$ Electrolyte for Low Temperature Solid Oxide Fuel Cells. *Int. J. Hydrog. Energy* **2016**, *41*, 6516–6525. [CrossRef]
229. Liang, B.; Keshishian, V.; Liu, S.; Yi, E.; Jia, D.; Zhou, Y.; Kieffer, J.; Ye, B.; Laine, R.M. Processing Liquid-Feed Flame Spray Pyrolysis Synthesized $Mg_{0.5}Ce_{0.2}Zr_{1.8}(PO_4)_3$ Nanopowders to Free Standing Thin Films and Pellets as Potential Electrolytes in All-Solid-State Mg Batteries. *Electrochim. Acta* **2018**, *272*, 144–153. [CrossRef]
230. Mazel, A.; Rocco, L.; Penin, N.; Rougier, A. Oriented Surface-Anchored Metal–Organic Frameworks (SurMOFs) as Electrochromic Thin Films. *Adv. Opt. Mater.* **2023**, *11*, 2202939. [CrossRef]
231. Liu, S.; Wei, C.; Wang, H.; Yang, W.; Zhang, J.; Wang, Z.; Zhao, W.; Lee, P.S.; Cai, G. Processable Nanoarchitectonics of Two-Dimensional Metallo-Supramolecular Polymer for Electrochromic Energy Storage Devices with High Coloration Efficiency and Stability. *Nano Energy* **2023**, *110*, 108337. [CrossRef]
232. Gusatti, M.; Souza, D.A.R.; Ribeiro, S.J.L.; Nalin, M. An Electrolyte-Free Electrochromic Device Using Aluminum as Counter Electrode Material. *Sol. Energy Mater. Sol. Cells* **2023**, *260*, 112494. [CrossRef]
233. Li, H.; Li, J.; Hou, C.; Ho, D.; Zhang, Q.; Li, Y.; Wang, H. Solution-Processed Porous Tungsten Molybdenum Oxide Electrodes for Energy Storage Smart Windows. *Adv. Mater. Technol.* **2017**, *2*, 1700047. [CrossRef]